

**NASA
Technical
Paper
2157**

June 1983

NASA
TP
2157
c.1

0067713



TECH LIBRARY KAFB, NM

Effect of Tail-Fin Span on Stability and Control Characteristics of a Canard-Controlled Missile at Supersonic Mach Numbers

A. B. Blair, Jr.,
Jerry M. Allen,
and Gloria Hernandez

LOAN COPY: RETURN TO
AFWL TECHNICAL LIBRARY
KIRTLAND AFB, N.M. 87117

NASA

25

25th Anniversary
1958-1983





0067713

NASA
Technical
Paper
2157

1983

Effect of Tail-Fin Span on Stability and Control Characteristics of a Canard-Controlled Missile at Supersonic Mach Numbers

A. B. Blair, Jr.,
Jerry M. Allen,
and Gloria Hernandez
Langley Research Center
Hampton, Virginia



National Aeronautics
and Space Administration
**Scientific and Technical
Information Branch**

SUMMARY

An experimental wind-tunnel investigation has been conducted at Mach numbers from 1.60 to 3.50 to obtain the longitudinal and lateral-directional aerodynamic characteristics of a circular, cruciform, canard-controlled missile with variations in tail-fin span. In addition, comparisons were made with the experimental aerodynamic characteristics using three missile aeroprediction programs: MISSILE1, MISSILE2, and NSWCDM. The results of the investigation indicate that for the test Mach number range, canard roll control at low angles of attack is feasible on tail-fin configurations with tail-to-canard span ratios of less than or equal to 0.75. The canards are effective pitch and yaw control devices on each tail-fin span configuration tested. Programs MISSILE1 and MISSILE2 provide very good predictions of longitudinal aerodynamic characteristics and fair predictions of lateral-directional aerodynamic characteristics at low angles of attack, with MISSILE2 predictions generally in better agreement with test data. Program NSWCDM provides good longitudinal and lateral-directional aerodynamic predictions that improve with increases in tail-fin span. Estimates of rolling-moment coefficient are in good agreement with test data at low angles of attack. Programs MISSILE1, MISSILE2, and NSWCDM appear to be acceptable engineering design tools for aeroprediction and, in general, make reasonable estimates of the test data; however, these programs need to be modified in order to better predict the lateral-directional aerodynamic characteristics at higher angles of attack (greater than 12°).

INTRODUCTION

It is well documented that missile configurations utilizing forward-control surfaces experience the problem of induced rolling moments at supersonic Mach numbers. (See refs. 1 to 3.) For these forward-controlled configurations, the need is either to reduce or eliminate the induced rolling moments or to provide an efficient system for their control.

A preliminary analytical study (ref. 4) for a class of canard-controlled-missile configurations similar to the Sidewinder missile has indicated that aerodynamic improvements can be made with the implementation of a canard roll-control system. Such a system requires a reduction in tail-fin span and eliminates the need for roll-eroners which are currently being used to produce airframe damping in roll. In an effort to complement and verify the predictions from this study, a cooperative NASA/Motorola missile research program was established.

This joint research program consisted of a parametric supersonic wind-tunnel investigation of a canard-controlled missile with systematic variations in tail-fin span for the purpose of establishing a comprehensive experimental aerodynamic data base. The present paper presents the results of that investigation. A summary of the significant findings, along with limited comparisons of experimental and analytical aerodynamic characteristics, has been reported in references 5 to 7. The present study includes tail-fin span optimizations for stability, longitudinal and directional control, induced roll and roll control, and the effects of missile roll orientation. In addition, three missile aerodynamic prediction programs are evaluated by comparison with the test data. The prediction programs are described in detail in references 8 to 12 and include MISSILE1, MISSILE2, and NSWCDM.

The tests were conducted in the Langley Unitary Plan Wind Tunnel at Mach numbers from 1.60 to 3.50 for a Reynolds number of 6.6×10^6 per meter (2.0×10^6 per foot). The nominal angle-of-attack range was from -4° to 18° at model roll angles of 0° , 26.6° , and 45° .

SYMBOLS

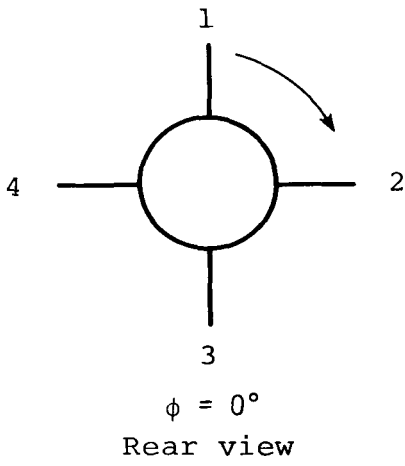
The aerodynamic coefficient data are referred to the body-axis system which is fixed in the vertical-horizontal planes regardless of the model roll angle. The moment reference center is located aft of the model nose at 45.0 percent of the body length.

Values are given in both SI and U.S. Customary Units. The measurements and calculations were made in U.S. Customary Units. Factors relating the two systems are given in reference 13.

A	reference area (based on body diameter), 14.081313 cm^2 (2.182608 in^2)
AR	aspect ratio of aerodynamic surface based on total exposed planform area
b_t/b_c	ratio of exposed tail span to exposed canard span (body excluded)
C_A	axial-force coefficient, Axial force/qA
$C_{A,c}$	chamber axial-force coefficient, Chamber axial force/qA
C_{BM}	coefficient of canard root bending moment, Canard root bending moment/qAd (see fig. 18)
C_{HM}	coefficient of canard hinge moment, Canard hinge moment/qAd (see fig. 18)
C_l	rolling-moment coefficient, Rolling moment/qAd
$C_{l\delta}$	roll-control effectiveness of two canards at $\alpha = 0^\circ$, $\Delta C_l/\Delta\delta_{roll}$, per degree of deflection
C_m	pitching-moment coefficient, Pitching moment/qAd
$C_{m\delta}$	pitch-control effectiveness of two canards at $\alpha = 0^\circ$, $\Delta C_m/\Delta\delta_{pitch}$, per degree of deflection
C_N	normal-force coefficient, Normal force/qA
C_{NF}	coefficient of canard normal force, Canard normal force/qA (see fig. 18)
C_n	yawing-moment coefficient, Yawing moment/qAd
$C_{n\delta}$	yaw-control effectiveness of two canards at $\alpha = 0^\circ$, $\Delta C_n/\Delta\delta_{yaw}$, per degree of deflection
C_y	side-force coefficient, Side force/qA
d	reference body diameter, 4.234 cm (1.667 in.)

l	model length, 102.319 cm (40.283 in.)
M	free-stream Mach number
q	free-stream dynamic pressure
x_{ac}/l	aerodynamic-center location as fraction of model length, measured from nose apex
α	angle of attack, deg
δ_i	angular control deflection of canard panel where subscript i denotes panel 1, 2, 3, or 4 shown in sketch A
δ_{pitch}	pitch-control deflection of canards 2 and 4 (sketch A), positive leading edge up, $(\delta_2 + \delta_4)/2$, deg
δ_{roll}	roll-control deflection (aileron); total differential angle of canards 2 and 4 (sketch A), positive aileron providing clockwise model rotation when viewed from rear; $\delta_4 - \delta_2$, deg
δ_{yaw}	yaw-control deflection of canards 1 and 3 (sketch A), positive for leading edge right when viewed from the rear, $(\delta_1 + \delta_3)/2$, deg
ϕ	model roll angle; positive for clockwise roll when viewed from rear (for $\phi = 0^\circ$, canards and tail fins are in vertical and horizontal planes), deg

Canard panels



Subscripts:

AB afterbody viscous crossflow
o evaluated at $\alpha = 0^\circ$
VSE side-edge vortex

APPARATUS AND TESTS

Wind Tunnel

Tests were conducted in both the low and high Mach number test sections of the Langley Unitary Plan Wind Tunnel, which is a variable-pressure continuous-flow tunnel. The test sections are approximately 2.13 m (7 ft) long and 1.22 m (4 ft) square. The nozzles leading to the test sections consist of asymmetric sliding blocks which permit continuous variations in Mach number from about 1.5 to 2.9 in the low Mach number test section and from about 2.3 to 4.7 in the high Mach number test section. (See ref. 14 for more complete details about the tunnel.)

Model

Dimensional details of the model are shown in figure 1, and photographs of the model are shown in figure 2. The model had a pointed tangent ogive nose of fineness ratio 2.25, a smooth circular high-fineness-ratio body with no launch straps or hanger lugs, and cruciform canards and aft tail fins. The model configurations were basically variations of the Sidewinder missile that included reduced-aspect-ratio canards and four sets of interchangeable tail fins with the same root chords. The tail fins approximated greater, equal, and reduced-span configurations of the Sidewinder tail-fin planforms without rollerons (table I). Canard deflections included pitch-, roll-, and yaw-control settings.

Tests were performed at the following tunnel conditions:

Mach number	Stagnation temperature		Stagnation pressure (absolute)		Reynolds number	
	K	°F	kPa	lbf/ft ²	Per meter	Per foot
1.60	325	125	51.7	1079	6.6×10^6	2.0×10^6
1.75			54.3	1133		
2.00			60.0	1253		
2.50			76.6	1600		
3.00			99.7	2083		
3.50			129.4	2703		

The dew point temperature measured at stagnation pressure was maintained below 239 K (-30°F) to assure negligible condensation effects. All tests were performed with boundary-layer transition strips 1.02 cm (0.40 in.) aft of the leading edges which were measured streamwise on both sides of the canards and tail fins and located 3.05 cm (1.20 in.) aft of the body nose. The transition strips were approximately 0.157 cm (0.062 in.) wide and were composed of No. 50 sand grains sprinkled in acrylic plastic for the tests at $M = 1.60$ to $M = 2.00$. For the tests at higher Mach numbers, transition strips were composed of individual grains of No. 40 sand grains with a nominal height of 0.046 cm (0.018 in.) and were spaced about 0.183 cm (0.072 in.) between centers measured perpendicular to the airstream (ref. 15).

Measurements and Corrections

Aerodynamic forces and moments on the model were measured by means of a six-component electrical strain-gage balance which was housed within the model. The balance was attached to a sting which was, in turn, rigidly fastened to the model support system. Balance-chamber pressure was measured by means of a pressure orifice located in the balance chamber. The model base was feathered to the outer diameter so that no base area existed. In addition, limited tests were made in which canard panel 2 was instrumented to measure canard normal force, hinge moment, and root bending moment. (See sketch A in Symbols.)

Model angle of attack has been corrected for deflection of the balance and sting due to aerodynamic loads and tunnel-flow misalignment. The axial-force coefficient data have been adjusted to correspond to free-stream static pressure acting over the model base. Typical measured values of chamber axial-force coefficient are presented in figure 3.

PRESENTATION OF RESULTS

The results of this investigation are shown in the following figures:

Figure

Experimental data:

Longitudinal aerodynamic characteristics:

Effect of tail-fin span at

$\phi = 0^\circ$	4
$\phi = 45^\circ$	5

Effect of tail-fin span on pitch control at $\phi = 0^\circ$	6
--	---

Summary of each tail-fin configuration	7
--	---

Lateral-directional aerodynamic characteristics:

Effect of tail-fin span on roll control at

$\phi = 0^\circ$	8
$\phi = 26.57^\circ$	9
$\phi = 45^\circ$	10

Effect of tail-fin span on yaw control at $\phi = 0^\circ$	11
--	----

Effect of tail-fin span for an asymmetric roll orientation at $\phi = 26.57^\circ$	12
---	----

Summary of canard control effectiveness of each tail-fin configuration at $\phi = 0^\circ$	13
---	----

Comparison of experimental data and theory:

Longitudinal aerodynamic characteristics of each tail-fin configuration at	
$\phi = 0^\circ$	14
$\phi = 45^\circ$	15
Pitch-control characteristics of each tail-fin configuration at	
$\phi = 0^\circ$	16
Summary of canard pitch-control effectiveness of each tail-fin configuration at $\phi = 0^\circ$	17
Longitudinal aerodynamic characteristics at $\phi = 0^\circ$ for	
Canard alone in presence of body (one panel)	18
Tail alone in presence of body (two tail-fin panels)	19
Complete model with $b_t/b_c = 0.47$ and 1.25	20
Lateral-directional aerodynamic characteristics of each tail-fin configuration for	
Roll control at $\phi = 0^\circ$	21
Yaw control at $\phi = 0^\circ$	22
Asymmetric roll orientation at $\phi = 26.57^\circ$	23
Summary of canard control effectiveness of each tail-fin configuration for	
Roll control	24
Yaw control	25
Schlieren photographs $b_t/b_c = 0.47, 0.75$, and 1.07 at $\phi = 0^\circ$; $\delta_{yaw} = -5^\circ$	26

EXPERIMENTAL RESULTS

Longitudinal Aerodynamic Characteristics

The effects of tail-fin span on the longitudinal aerodynamic characteristics of the model at roll angles of 0° and 45° are presented in figures 4 and 5, respectively. As would be expected, there is an increase in normal-force-coefficient slope ($C_{N\alpha}$), stability level ($-C_{m\alpha}$), and axial-force coefficient with an increase in tail-fin span.

When lower stability levels are required to attain more maneuverability (e.g., Relaxed Static Stability Concept), the reduced tail-span configurations may be ideal candidates.

Pitch-control characteristics for each tail-fin configuration are presented in figure 6. A comparison of figure 6 with figure 4 ($\delta_{pitch} = 0^\circ$) indicates that the canards are effective in producing pitching moments accompanied by small reductions in normal-force coefficient ($\alpha = 0^\circ$) with increases in tail-fin span. These effects are due to the canard downwash field which induces greater tail loads as tail span increases, thus reducing the total model normal-force coefficient. The net effect is a favorable canard-tail interference that produces a pitching-moment couple on the model in the direction of the desired maneuver.

The summary of longitudinal aerodynamic characteristics of each tail-fin configuration that includes a cross plot of b_t/b_c is presented in figure 7. The data for $M = 1.75$ are taken from unpublished NASA data. In general, with increases in tail span, there are increases in $C_{m\delta}$ and $C_{A,o}$ and a rearward movement of

aerodynamic-center locations. As would be expected for the complete model, the tail configurations of larger span (e.g., $b_t/b_c \geq 1.07$) have less travel in aerodynamic center throughout the test Mach number range.

Lateral-Directional Aerodynamic Characteristics

The effects of tail-fin span on the canard roll-control characteristics of the model at $\phi = 0^\circ$, 26.57° , and 45° are presented in figures 8 to 10. Limited tail-off data are also shown. The canards are effective roll-control devices throughout the test Mach number and model angle-of-attack and roll-angle ranges for the reduced-tail-span configurations (e.g., $b_t/b_c \leq 0.75$). In general, there is a reduction of canard roll control with increases in tail span at low angles of attack. The complex flow fields produced by the deflected canard panels pass very close to the tail fins and induce rolling moments of opposite direction to those created by the canards. For tail-span configurations with $b_t/b_c > 1.07$, this induced roll is large enough to counteract the canard roll, in effect producing a total model rolling moment which is negligible, or, in some cases opposite to that desired (roll reversal). However, for $\phi = 0^\circ$, increases in roll control occur with increases in tail-fin span at the higher angles of attack.

The effects of tail-fin span on yaw-control characteristics of the model at $\phi = 0^\circ$ are presented in figure 11. In general, for $b_t/b_c \leq 1.07$, increases in tail span at low angles of attack produce increases in canard yaw control and induced rolling-moment coefficients. For values of b_t/b_c greater than 1.07, the data indicate that a reduction in yaw control occurs.

The effects of tail-fin span on lateral-directional aerodynamic characteristics of the model at $\phi = 26.57^\circ$ for zero control settings are shown in figure 12. The magnitude of induced rolling-moment coefficient, and yawing-moment coefficient due to model roll asymmetry increases at the low Mach numbers with increases in tail-fin span.

A summary of canard control effectiveness of each tail-fin configuration at $\alpha = 0^\circ$ is presented in figure 13. In general, there is an increase in $C_{m\delta}$ and $C_{n\delta}$ with increases in tail span ($b_t/b_c \leq 1.07$) that represents favorable canard downwash and sidewash tail loadings on the larger tail-fin span configurations. For a constant tail-span configuration there is the expected decrease in effectiveness with increases in Mach number. For the test Mach number range, the data indicate that canard roll control at low angles of attack is feasible on reduced tail-fin span configurations ($b_t/b_c \leq 0.75$).

COMPARISON OF EXPERIMENTAL DATA AND THEORY

Theoretical Methods

In references 5 to 7, two different classes of missile aeroprediction programs for circular bodies were exercised by comparisons with test data. In an effort to expand and complement these data comparisons for missile configurations in the Sidewinder class, test data and theory comparisons are presented in this paper. The

aeroprediction programs applied were developed by Nielsen Engineering and Research, Inc. (NEAR) under government contract and are described in detail in references 8 to 12.

The first class of programs is essentially preliminary design programs that obtain forces and moments to provide rapid engineering predictions. (See refs. 8 and 9.) These programs use data bases augmented by analysis and include MISSILE1 and MISSILE2 applicable to missile configurations with axisymmetric bodies. Program MISSILE2 is a modified version of MISSILE1 with the major change being the incorporation of a vortex-cloud model for the prediction of afterbody vorticity.

The second class of aeroprediction programs consists of the DEMON series which is a more sophisticated research tool than programs MISSILE1 and MISSILE2. The DEMON programs use supersonic panel methods and give detailed pressure loadings along with forces and moments (ref. 10). Included in the DEMON series is a simplified version NSWCDM (derived from DEMON2) designed as a semiproduction missile aeroprediction program specialized to supersonic missile configurations with axisymmetric bodies. However, unlike DEMON2 which could only provide isolated component loads, program NSWCDM is automated to give overall forces and moments for the entire missile configuration. For these reasons, program NSWCDM is used in this paper.

Both classes of aeroprediction programs provide estimates of static longitudinal and lateral-directional aerodynamic characteristics at high angles of attack and arbitrary roll angles; they also track the vortices from canard or wing sections to the tail sections using the same vortex method (refs. 11 and 12). A summary of the major characteristics of these programs (NSWCDM, MISSILE1, and MISSILE2) is presented in the appendix. Regions of Mach number and aspect ratio of canard and tail-fin validity for the current MISSILE1 and MISSILE2 data bases are presented in figure A1 in the appendix.

Longitudinal Aerodynamic Characteristics

Comparisons of experimental and analytical longitudinal aerodynamic characteristics of each tail-fin configuration at model roll angles of 0° and 45° at $M = 2.50$ are presented in figures 14 and 15, respectively. (Note that when both MISSILE codes predict identical values, only predictions from one code is shown.) In general, there is good agreement between test data and the predictions of both programs MISSILE1 and MISSILE2, with better agreement occurring for the larger tail spans. For the tail configuration $b_t/b_c = 1.25$ (fig. 15(d)), MISSILE1 and MISSILE2 predictions diverge at the higher angles of attack probably because of different afterbody vorticity models. Program NSWCDM provides accurate predictions for tail configurations $b_t/b_c > 1.07$ but underpredicts both normal-force and pitching-moment coefficients for the $b_t/b_c \leq 0.75$ span (longer tip chords) configurations at the higher angles of attack.

Pitch-control comparisons for each tail-fin configuration at $\phi = 0^\circ$ are presented in figure 16. Again, the codes are in good agreement with the measured values except for NSWCDM which underestimates pitching-moment coefficient for the smaller span configurations and overestimates it for tail configuration $b_t/b_c = 1.25$ at the higher angles of attack.

A summary comparison of experimental and analytical canard pitch-control effectiveness of each tail-fin configuration at $\phi = 0^\circ$ is shown in figure 17. The test value of $C_{m\delta}$ for $M = 1.75$ was obtained from unpublished NASA data. In general,

the code estimates are reasonably accurate for the test Mach number range, an exception being for MISSILE1 which underestimates $C_{m\delta}$ for configurations $b_t/b_c \geq 1.07$.

In an attempt to isolate and/or improve the load predictions of program NSWCDM that were underestimated for tail configurations $b_t/b_c \leq 0.75$, missile-component loading contributions were evaluated. The measured load data for canard panel 2 alone in the presence of the body are presented in figure 18. Program NSWCDM estimates are in good agreement with the test data at $M = 2.50$, but this program overpredicts the measured values at the higher angles of attack at $M = 3.50$. In general, program MISSILE2 underpredicts the panel loads at the higher angles of attack for both Mach numbers. It might be pointed out that $M = 3.50$ falls outside the valid Mach number range for both prediction codes. (See the appendix.)

Comparisons between test data and load predictions for two tail-fin panels in the presence of the body are presented in figure 19. It should be noted that these test data were not obtained from direct tail-panel measured loads; rather, the test data shown are the difference in normal-force coefficients between the body-tail and the body-alone configurations and include body upwash and carryover effects. The predictions also include these interference effects. In the upper part of figure 19, program NSWCDM underpredicts the normal-force coefficients for the $b_t/b_c = 0.47$ and 0.75 tail panels which have the longer tip chords. It is believed that for these longer tip-chord panels, especially at higher angles of attack, nonlinear side-edge suction loading becomes a primary source of normal force. Adding the estimated normal-force coefficient increment produced by the side-edge vortex does bring the high-angle-of-attack predictions up to the test-data level of the reduced span tails; however, there is a slight overprediction for the larger tail spans. It appears that the overall panel load predictions of NSWCDM would be improved by including side-edge effects for the reduced-span longer-tip-chord fins. In the lower part of figure 19, program MISSILE2 predictions are in very good agreement with test data.

Comparisons of test data with predictions from program NSWCDM for the complete model with tail configurations $b_t/b_c = 0.47$ and 1.25 at $M = 2.50$ are shown in figure 20. In addition to the missile component loadings already discussed, non-linear afterbody loads due to crossflow drag were also estimated. A simple algebraic equation derived from crossflow theory was used to obtain the normal-force coefficient increment produced by the afterbody crossflow separation. Adding the estimated normal-force coefficient increments due to both the side-edge vortex and afterbody viscous crossflow separation bring the predictions within reasonable agreement to the measured data for tail-fin configuration $b_t/b_c = 0.47$. However, with the addition of these increments, NSWCDM overpredicts the test data of tail-fin configuration $b_t/b_c = 1.25$, especially pitching-moment coefficient. These increments are presently being incorporated in an updated version of NSWCDM that will be called program LRCDM2.

Lateral-Directional Aerodynamic Characteristics

Roll control.- A comparison of experimental and analytical roll-control characteristics of each tail-fin configuration at $M = 2.50$ for $\phi = 0^\circ$ is presented in figure 21. The predictions from program NSWCDM are in good agreement with test data at the lower angles of attack ($\alpha \leq 8^\circ$), especially for tail configuration $b_t/b_c = 0.47$. However, the predictions diverged from test data at the higher angles of attack. In general, the overall agreement of program NSWCDM with test data is much better than that produced by either programs MISSILE1 or MISSILE2. Both MISSILE codes underpredict roll control and give similar predictions up to angles of attack

of about 10° , where they diverge from each other. This divergence trend, which is also exhibited by the yawing-moment coefficient estimates, begins at the angle of attack where both programs start predicting afterbody vorticity. For angles of attack above 10° , these trends reflect the effects of different afterbody vorticity models contained in each program. (See ref. 11 for a brief description of the vortex models.) Since the tail-fins-off predictions from all three computer programs are in excellent agreement with limited tail-fins-off test data (flagged symbols in fig. 21(d)), it appears that improvements are needed in all three codes to predict more accurately the tail-fin loadings.

Yaw control.- A comparison of experimental and analytical yaw-control characteristics of each tail-fin configuration at $M = 2.50$ for $\phi = 0^\circ$ is presented in figure 22. In general, program NSWCDM predictions are in good agreement with test data, the yaw control and induced rolling-moment predictions becoming excellent with increases in tail span for angles of attack up to about 12° . Of the MISSILE codes, MISSILE2 reflects the same prediction trends as program NSWCDM except MISSILE2 underpredicts the low-angle-of-attack induced rolling moments. The erratic behavior of MISSILE1 predictions at the higher angles of attack for tail configuration $b_t/b_c = 0.47$ may be due to the afterbody vorticity model that this code uses. MISSILE1 underpredicts yaw control and induced rolling moment for the larger tail spans at the lower angles of attack.

Asymmetric roll orientation.- Comparisons of test data and predictions of the lateral-directional aerodynamic characteristics of selected tail-fin configurations at $M = 1.75$ for $\phi = 26.57^\circ$ are presented in figure 23. The prediction trends of program NSWCDM generally follow those of the test data. The estimates of the MISSILE codes overpredict the measured data at the higher angles of attack.

Roll-control and yaw-control effectiveness.- Summary comparisons of test data and analytical canard roll- and yaw-control effectiveness of each tail-fin configuration at $\phi = 0^\circ$ and $\alpha = 0^\circ$ are presented in figures 24 and 25, respectively. For the test Mach number range, the predictions of roll-control effectiveness from program NSWCDM (fig. 24) are in very good agreement with the test data and reflect the roll reversal trends of tail configurations $b_t/b_c \geq 1.07$. In general, canard roll-control effectiveness is underpredicted by both MISSILE codes and for tail configurations $b_t/b_c > 1.07$ is underpredicted even more at the lower Mach numbers. MISSILE1 code estimates are a little better than MISSILE2 estimates for tail configurations $b_t/b_c > 0.75$. Predictions of canard yaw-control effectiveness from all of the codes (fig. 25) are in good agreement with test data.

Schlieren photographs.- In an attempt to visualize canard-generated flow fields, schlieren photographs of tail configurations $b_t/b_c \leq 1.07$ with canard yaw control at $M = 1.75$ are shown in figure 26. In general, this figure shows that the most dominant feature at $\alpha = 0^\circ$ results from the vortex originating at the tips of the vertical canards which are loaded due to the yaw control. For tail configurations $b_t/b_c < 0.75$ in particular, these canard tip vortices clear the tail fins, whereas for tail configuration $b_t/b_c = 1.07$, there is evidence of vortex flow impingement on the tail fins. (See fig. 26(c).) It is believed that this impingement reduces the beneficial canard downwash and sidewash induced tail-fin loadings that help to produce model pitch and yawing moments. For each tail-fin configuration, vortices emanating from both tips of the vertical and horizontal canards pass very close to the tail fins as the angle of attack increases. These canard vortices, which include downwash and sidewash, result in the loading and unloading of individual tail fins with changes in angle of attack. In the lower portion of figure 26(a), predicted tip vortex trajectories of the canard are superimposed on the test-data vortices of tail

configuration $b_t/b_c = 0.47$. From the side view, these MISSILE1 predictions are shown to be in excellent agreement with the test data. Since all three prediction codes presented in this paper use the same vortex tracking method, MISSILE1 may be an indicator of their accuracies; however, the prediction methods of determining the influences on tail-fin loadings produced by the canard generated flow fields are in need of improvement, as illustrated by the comparisons made in figure 21(d).

CONCLUSIONS

An experimental wind-tunnel investigation has been conducted at Mach numbers from 1.60 to 3.50 to obtain the longitudinal and lateral-directional aerodynamic characteristics of a circular, cruciform, canard-controlled missile with variations in tail-fin span. In addition, comparisons were made with the experimental aerodynamic characteristics using three missile aeroprediction programs: MISSILE1, MISSILE2, and NSWCDM. The results of the investigation are as follows:

1. For the test Mach number range, the data indicate that canard roll control at low angles of attack is feasible on tail-fin configurations with tail-to-canard span ratios less than or equal to 0.75.
2. The canards are effective pitch and yaw control devices on each tail-fin span configuration tested.
3. Programs MISSILE1 and MISSILE2 provide very good predictions of longitudinal aerodynamic characteristics and fair predictions of lateral-directional aerodynamic characteristics at low angles of attack, with MISSILE2 predictions generally in better agreement with test data.
4. Program NSWCDM provides good longitudinal and lateral-directional aerodynamic predictions that improve with increases in tail-fin span. Estimates of rolling-moment coefficient are in good agreement with test data at low angles of attack.
5. Programs MISSILE1, MISSILE2, and NSWCDM appear to be acceptable engineering design tools for aeroprediction and, in general, make reasonable estimates of the test data; however, these programs need to be modified in order to better predict the lateral-directional aerodynamic characteristics at higher angles of attack (greater than 12°).

Langley Research Center
National Aeronautics and Space Administration
Hampton, VA 23665
May 2, 1983

APPENDIX

AEROPREDICTION PROGRAMS

This appendix summarizes major characteristics of the analytical programs.

NSWCDM

The aeroprediction program NSWCDM calculates detailed aerodynamic loadings and pressure distributions acting on missile configurations including monoplane, cruciform, and interdigitated lifting surfaces mounted on bodies with circular cross sections. Calculations are based on paneling methods in which supersonic linear theory solutions are used. Vortex strengths and positions are calculated by empirical and vortex tracking methods. The Mach number range is from 1.3 to about 3.0. The angle of attack is up to 20° with a variable model roll angle.

MISSILE1 and MISSILE2

The aeroprediction programs MISSILE1 and MISSILE2 predict static longitudinal, directional, and lateral aerodynamic characteristics of cruciform missile configurations with circular bodies. Prediction techniques manipulate empirical aerodynamic data retrieved from a data base. External vortex influences are computed and superimposed on the missile. Vortex strengths and positions are calculated by empirical and vortex tracking methods. The Mach number range is from 0.8 to 3.0 and angle of attack is up to 45° with a variable model roll angle. For the current data base, there is a restriction in fin aspect ratio with Mach number. Mach number and aspect-ratio regions of validity are presented in figure A1.

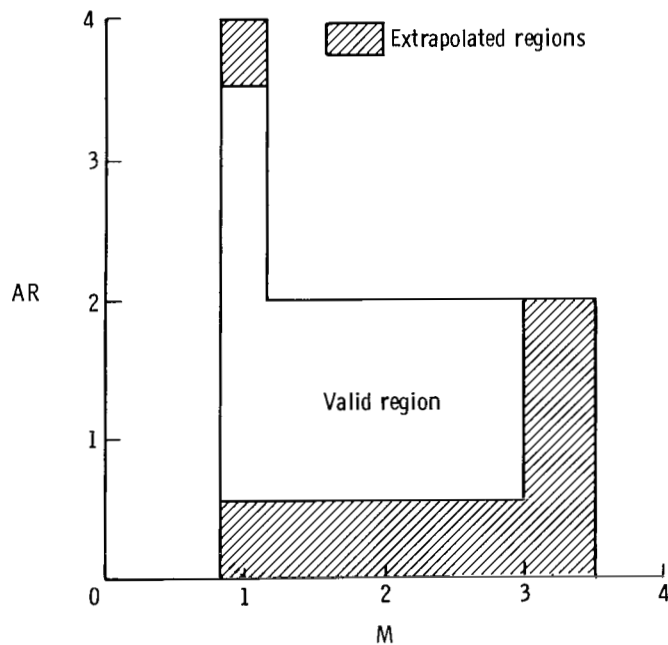


Figure A1.- Mach number and fin aspect ratio regions of validity for current MISSILE1 and MISSILE2 data bases.

REFERENCES

1. Corlett, William A.; and Howell, Dorothy T.: Aerodynamic Characteristics at Mach 0.60 to 4.63 of Two Cruciform Missile Models, One Having Trapezoidal Wings With Canard Controls and the Other Having Delta Wings With Tail Controls. NASA TM X-2780, 1973.
2. Blair, A. B., Jr.: Aerodynamic Characteristics of a Tandem-Canard Missile at Mach Numbers From 1.83 to 4.63. NASA TM X-3040, 1974.
3. Burt, James R., Jr.: The Effectiveness of Canards for Roll Control. Tech. Rep. RD-77-8, U.S. Army, Nov. 1976. (Available from DTIC as AD A037 077.)
4. Rapp, G. H.: Performance Improvements With Sidewinder Missile Airframe Variants. AIAA Paper 79-0091, Jan. 1979.
5. Blair, A. B., Jr.; and Rapp, G. H.: Experimental and Analytical Comparison of Aerodynamic Characteristics of a Forward-Control Missile. AIAA-80-0374, Jan. 1980.
6. Allen, Jerry M.: Comparison of Analytical and Experimental Supersonic Aerodynamic Characteristics of a Forward Control Missile. AIAA-81-0398, Jan. 1981.
7. Allen, Jerry M.; and Blair, A. B., Jr.: Comparison of Analytical and Experimental Supersonic Aerodynamic Characteristics of a Forward Control Missile. J. Spacecr. & Rockets, vol. 19, no. 2, Mar.-Apr. 1982, pp. 155-159.
8. Nielsen, Jack N.; Hemsch, Michael J.; and Smith, Charles A.: A Preliminary Method for Calculating the Aerodynamic Characteristics of Cruciform Missiles to High Angles of Attack Including Effects of Roll Angle and Control Deflections. ONR-CR215-226-4F, U.S. Navy, Nov. 1, 1977. (Available from DTIC as AD A054 349.)
9. Smith, C. A.; and Nielsen, J. N.: Final Report - Prediction of Aerodynamic Characteristics of Cruciform Missiles to High Angles of Attack Utilizing a Distributed Vortex Wake. NEAR TR 208 (Contract N60921-79-C-A049), Nielsen Eng. & Res., Inc., Jan. 1980.
10. Dillenius, M. F. E.; and Smith, C. A.: Final Report - Program NSWCDM, Aerodynamic Prediction Program for Cruciform Canard-Axisymmetric Body-Cruciform Tail Missiles at Supersonic Speeds. NEAR TR 217 (Contract No. N70921-79-C-A365), Nielsen Eng. & Res., Inc., Apr. 1980.
11. Hemsch, Michael J.; and Nielsen, Jack N.: Status Report on Triservice Data Base Extension of PROGRAM MISSILE. Proceedings of the Twelfth Navy Symposium on Aeroballistics - Volume I, U.S. Navy, May 1981, pp. I-107 - I-115.
12. Dillenius, M. F. E.; Hemsch, M. J.; Sawyer, W. C.; Allen, J. M.; and Blair, A. B., Jr.: Comprehensive Missile Aerodynamics Programs for Preliminary Design. AIAA-82-0375, Jan. 1982.
13. Standard for Metric Practice. E 380-79, American Soc. Testing & Mater., c.1980.

14. Jackson, Charlie M., Jr.; Corlett, William A.; and Monta, William J.: Description and Calibration of the Langley Unitary Plan Wind Tunnel. NASA TP-1905, 1981.
15. Stallings, Robert L., Jr.; and Lamb, Milton: Effects of Roughness Size on the Position of Boundary-Layer Transition and on the Aerodynamic Characteristics of a 55° Swept Delta Wing at Supersonic Speeds. NASA TP-1027, 1977.

TABLE I.- GEOMETRIC CHARACTERISTICS OF CANARD AND TAIL-FIN CONFIGURATIONS

TF-4 canard:

Exposed root chord, cm (in.)	11.123 (4.379)
Tip chord, cm (in.)	3.338 (1.314)
Exposed taper ratio	0.300
Exposed span, cm (in.)	14.463 (5.694)
Exposed planform area, ^a cm ² (in ²)	104.561 (16.207)
Maximum thickness, cm (in.)	0.508 (0.200)
Exposed aspect ratio	2.00
Leading-edge sweep, deg	47.1
Hinge line, percent root chord	57.0

Tails fins:

Configuration $b_t/b_c = 0.47$:

Exposed root chord, cm (in.)	21.590 (8.500)
Tip chord, cm (in.)	18.204 (7.167)
Exposed taper ratio	0.843
Exposed span, cm (in.)	6.772 (2.666)
Exposed planform area, ^a cm ² (in ²)	134.735 (20.884)
Thickness, cm (in.)	0.231 (0.091)
Exposed aspect ratio	0.34
Leading-edge sweep, deg	45.0

Configuration $b_t/b_c = 0.75$:

Exposed root chord, cm (in.)	21.590 (8.500)
Tip chord, cm (in.)	16.167 (6.365)
Exposed taper ratio	0.749
Exposed span, cm (in.)	10.846 (4.270)
Exposed planform area, ^a cm ² (in ²)	204.748 (31.736)
Thickness, cm (in.)	0.231 (0.091)
Exposed aspect ratio	0.58
Leading-edge sweep, deg	45.0

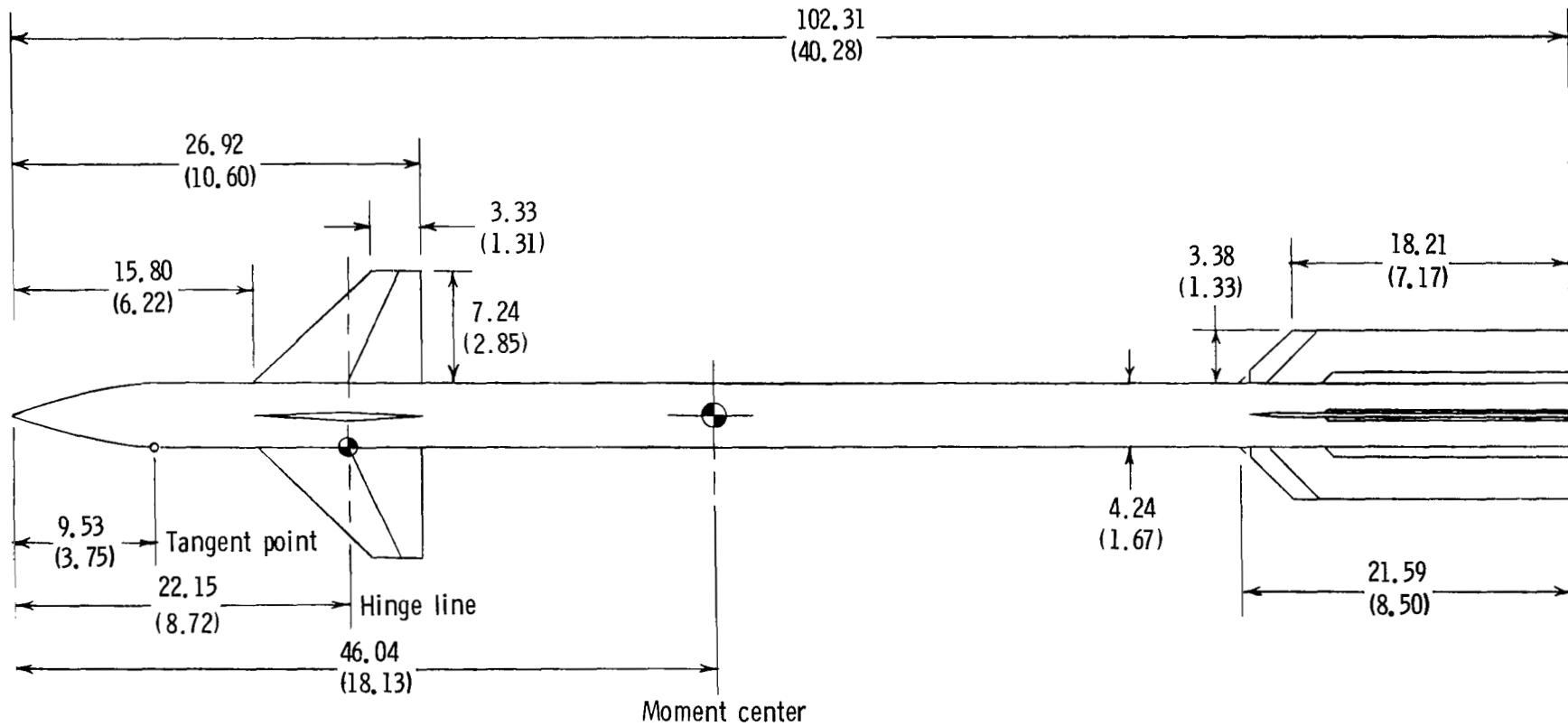
Configuration $b_t/b_c = 1.07$:

Exposed root chord, cm (in.)	21.590 (8.500)
Tip chord, cm (in.)	13.863 (5.458)
Exposed taper ratio	0.642
Exposed span, cm (in.)	15.453 (6.084)
Exposed planform area, ^a cm ² (in ²)	273.935 (42.460)
Thickness, cm (in.)	0.231 (0.091)
Exposed aspect ratio	0.87
Leading-edge sweep, deg	45.0

Configuration $b_t/b_c = 1.25$:

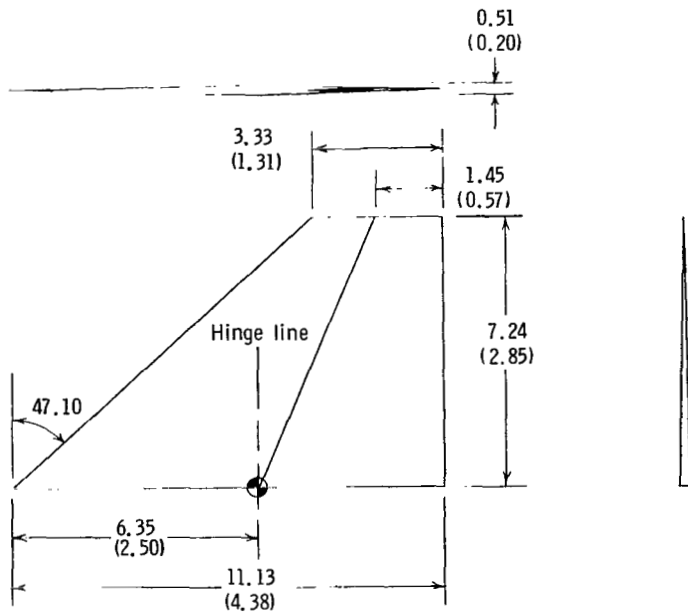
Exposed root chord, cm (in.)	21.590 (8.500)
Tip chord, cm (in.)	12.550 (4.941)
Exposed taper ratio	0.581
Exposed span, cm (in.)	18.080 (7.1118)
Exposed planform area, ^a cm ² (in ²)	308.625 (47.837)
Thickness, cm (in.)	0.231 (0.091)
Exposed aspect ratio	1.06
Leading-edge sweep, deg	45.0

^aExposed planform area is the area formed when two exposed panels of the canard or tail fin are joined together.



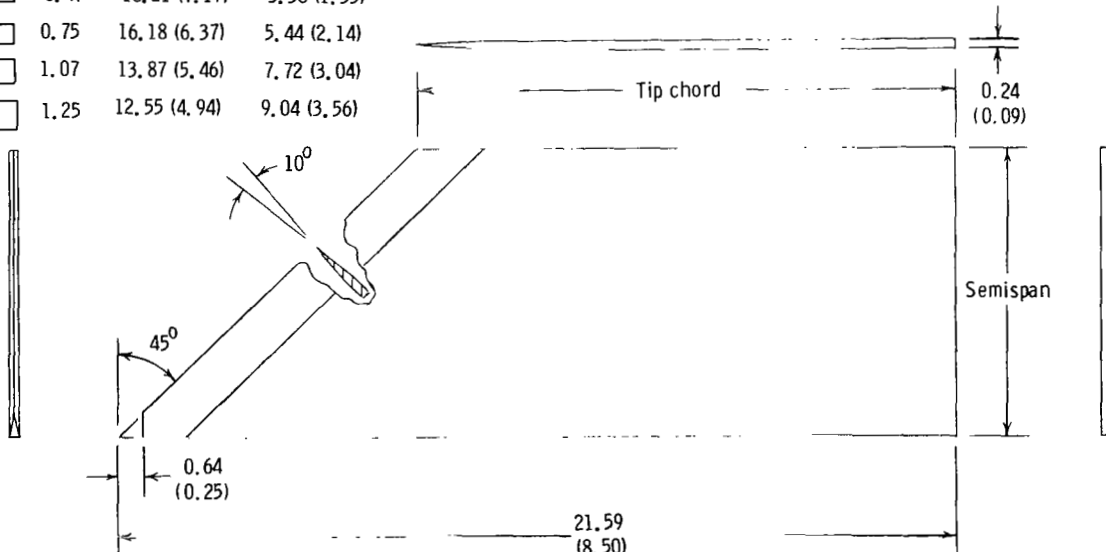
(a) Complete model with tail fins $b_t/b_C = 0.47$.

Figure 1.- Model details. All dimensions are given in centimeters (inches) unless otherwise indicated.



TF-4 canard

Tail	b_t/b_c	Tip chord	Semispan
—	0.47	18.21 (7.17)	3.38 (1.33)
—	0.75	16.18 (6.37)	5.44 (2.14)
—	1.07	13.87 (5.46)	7.72 (3.04)
—	1.25	12.55 (4.94)	9.04 (3.56)



Tail fins

(b) Canard and tail fins.

Figure 1.- Concluded.

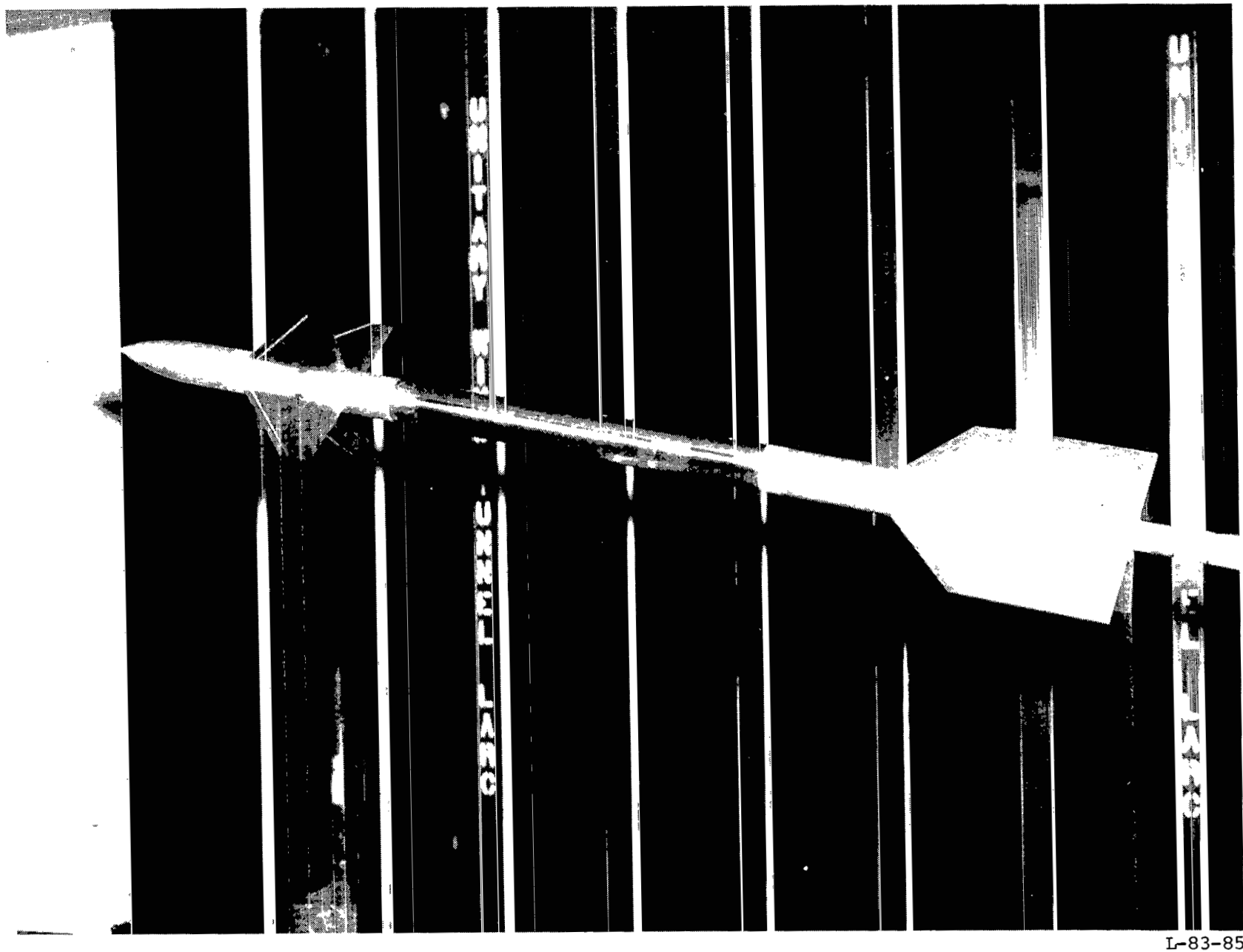


Figure 2.- Model with tail fins $b_t/b_c = 1.07$.

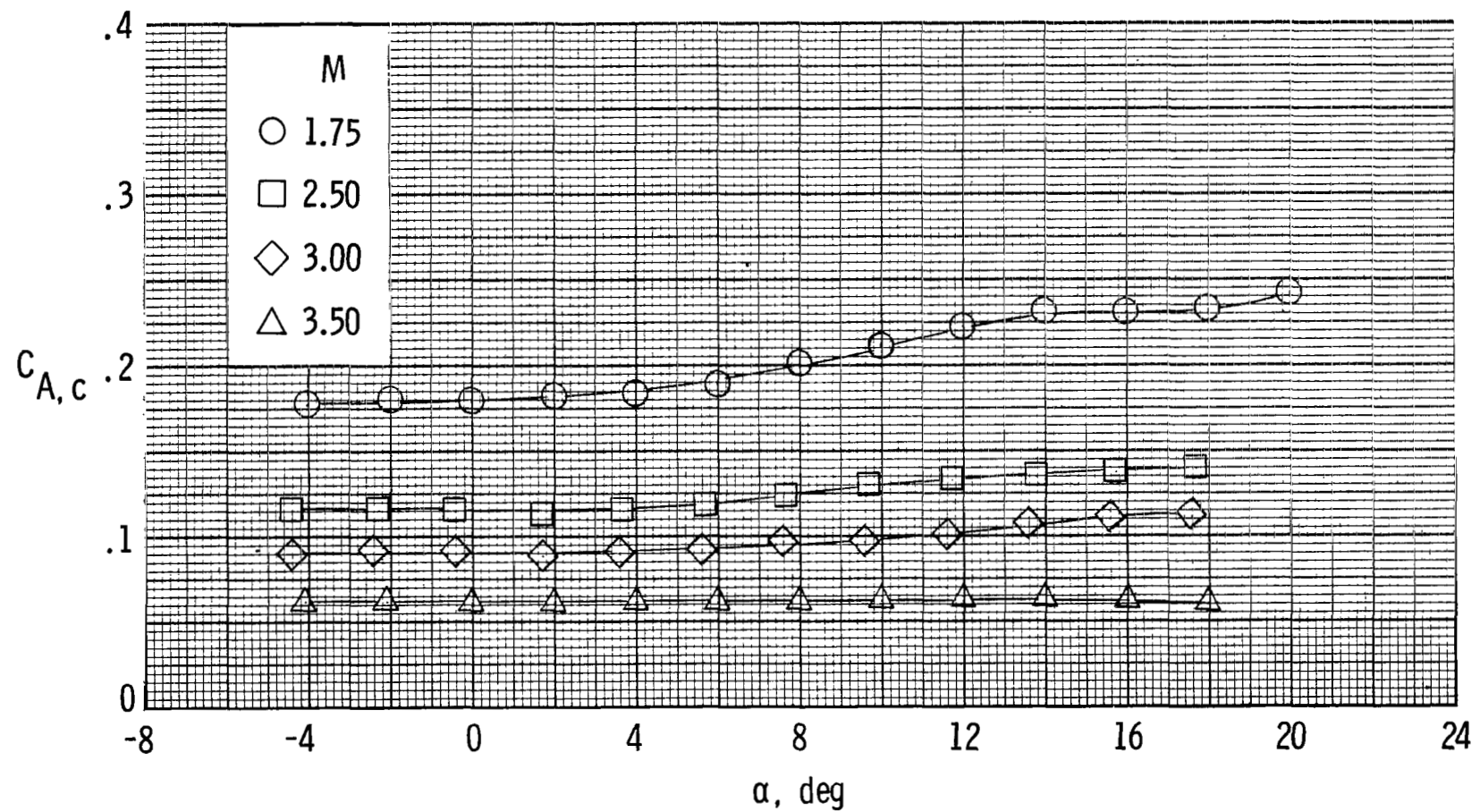
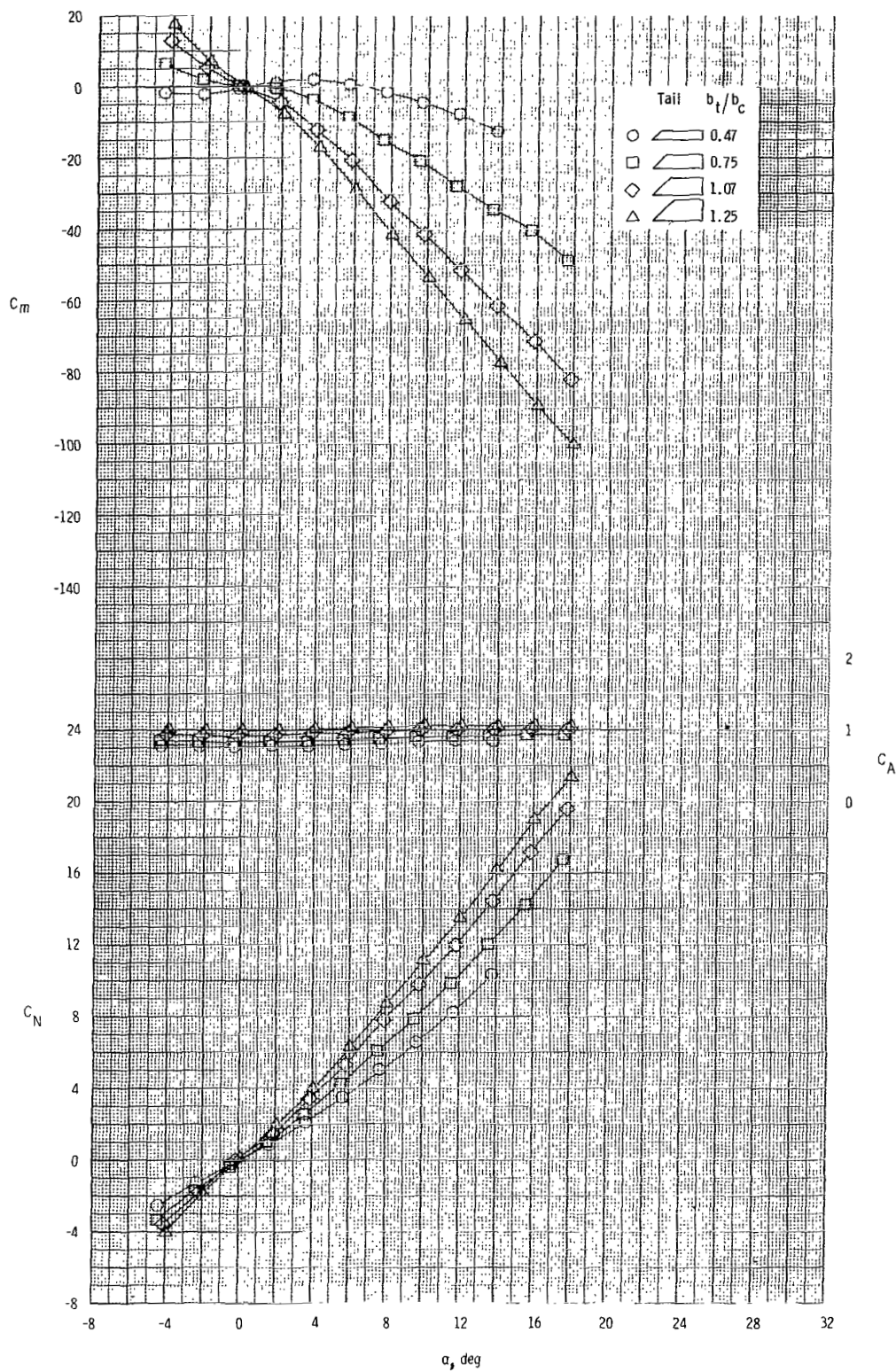
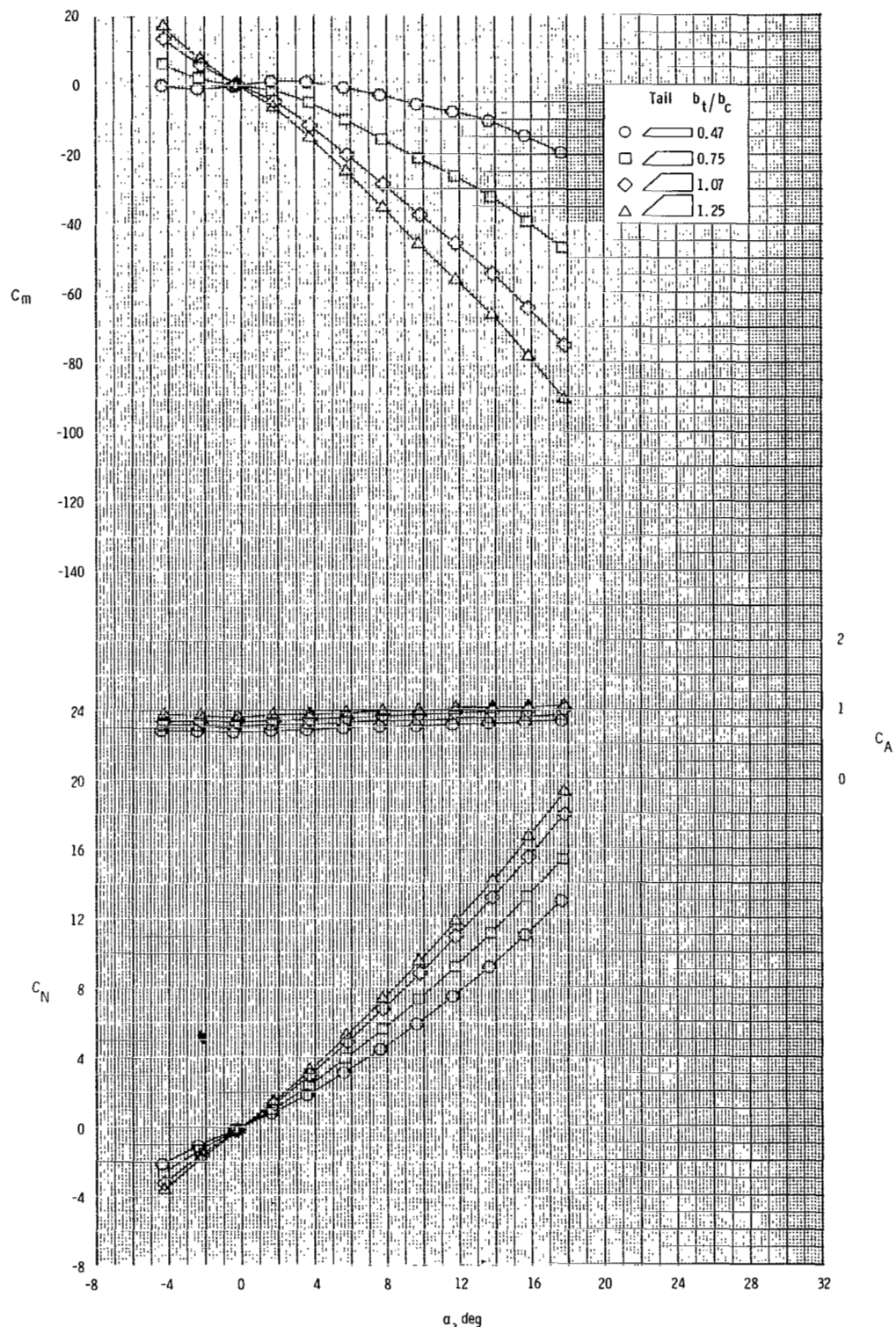


Figure 3.- Typical variation of measured balance-chamber axial-force coefficient with angle of attack. Complete model with tail-fin configuration $b_t/b_c = 0.47$ and zero control deflection.



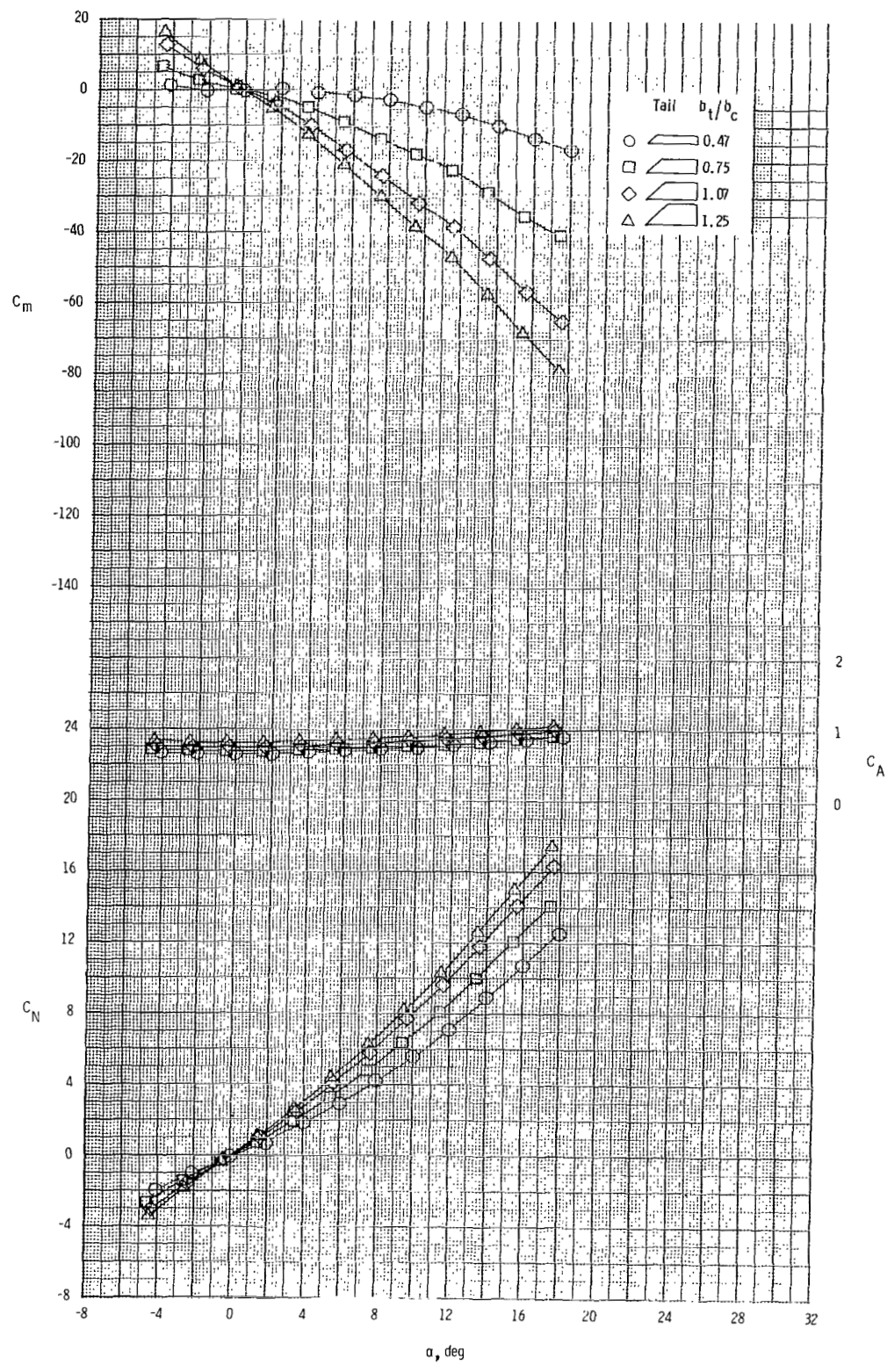
(a) $M = 2.50.$

Figure 4.- Effects of tail-fin span on longitudinal aerodynamic characteristics at $\phi = 0^\circ$.



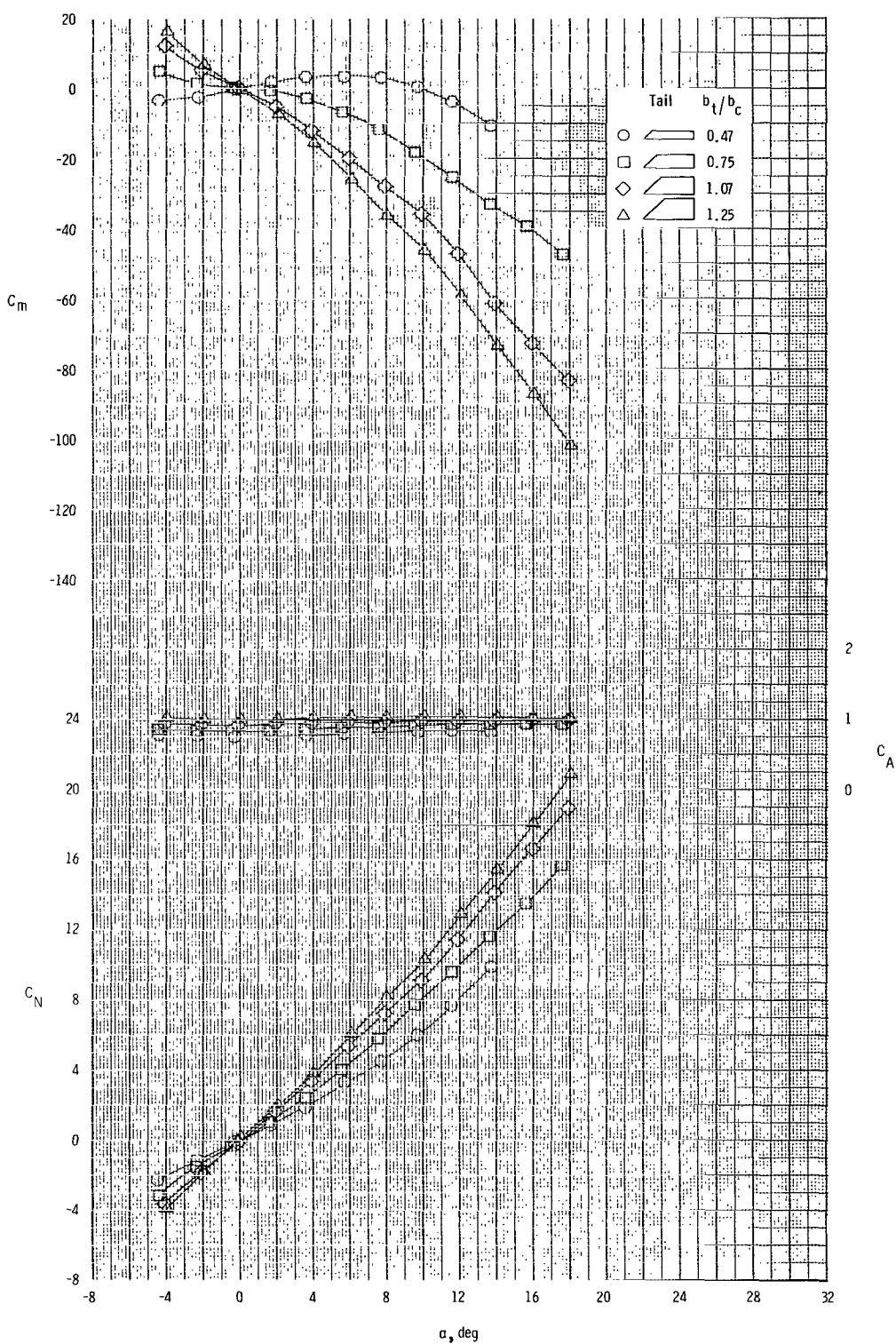
(b) $M = 3.00.$

Figure 4.- Continued.



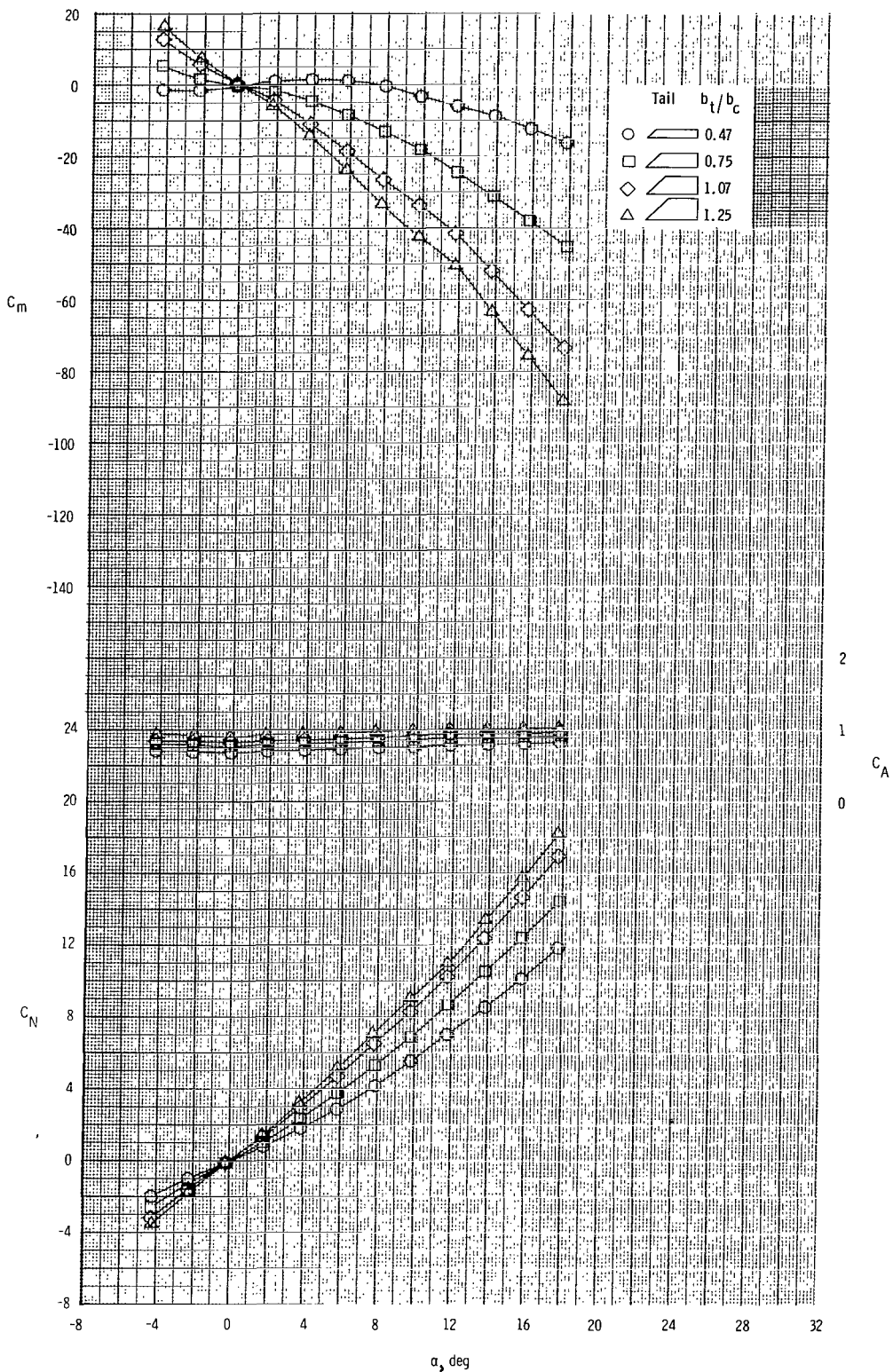
(c) $M = 3.50.$

Figure 4.- Concluded.



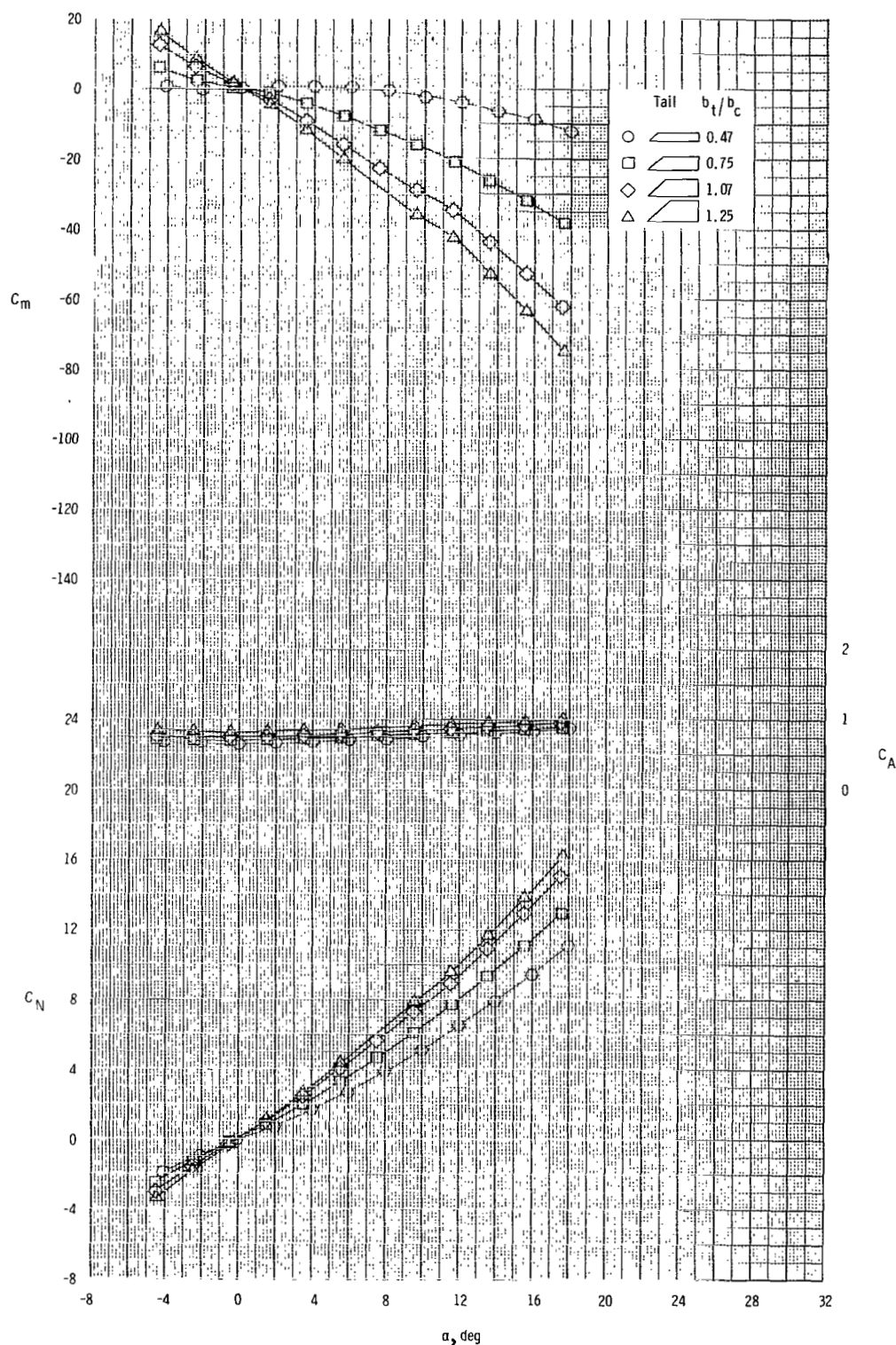
(a) $M = 2.50$.

Figure 5.- Effects of tail-fin span on longitudinal aerodynamic characteristics at $\phi = 45^\circ$.



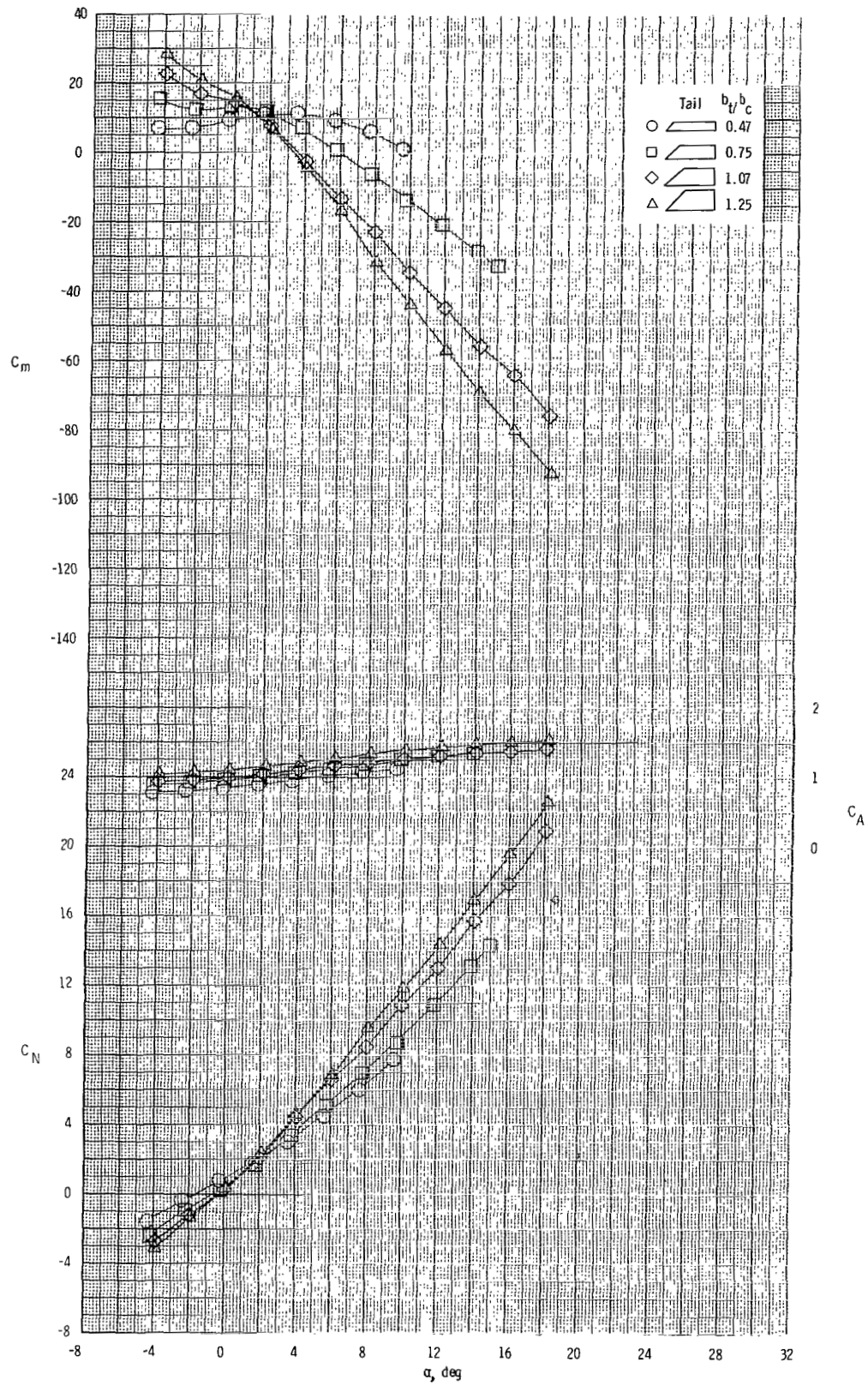
(b) $M = 3.00.$

Figure 5.- Continued.



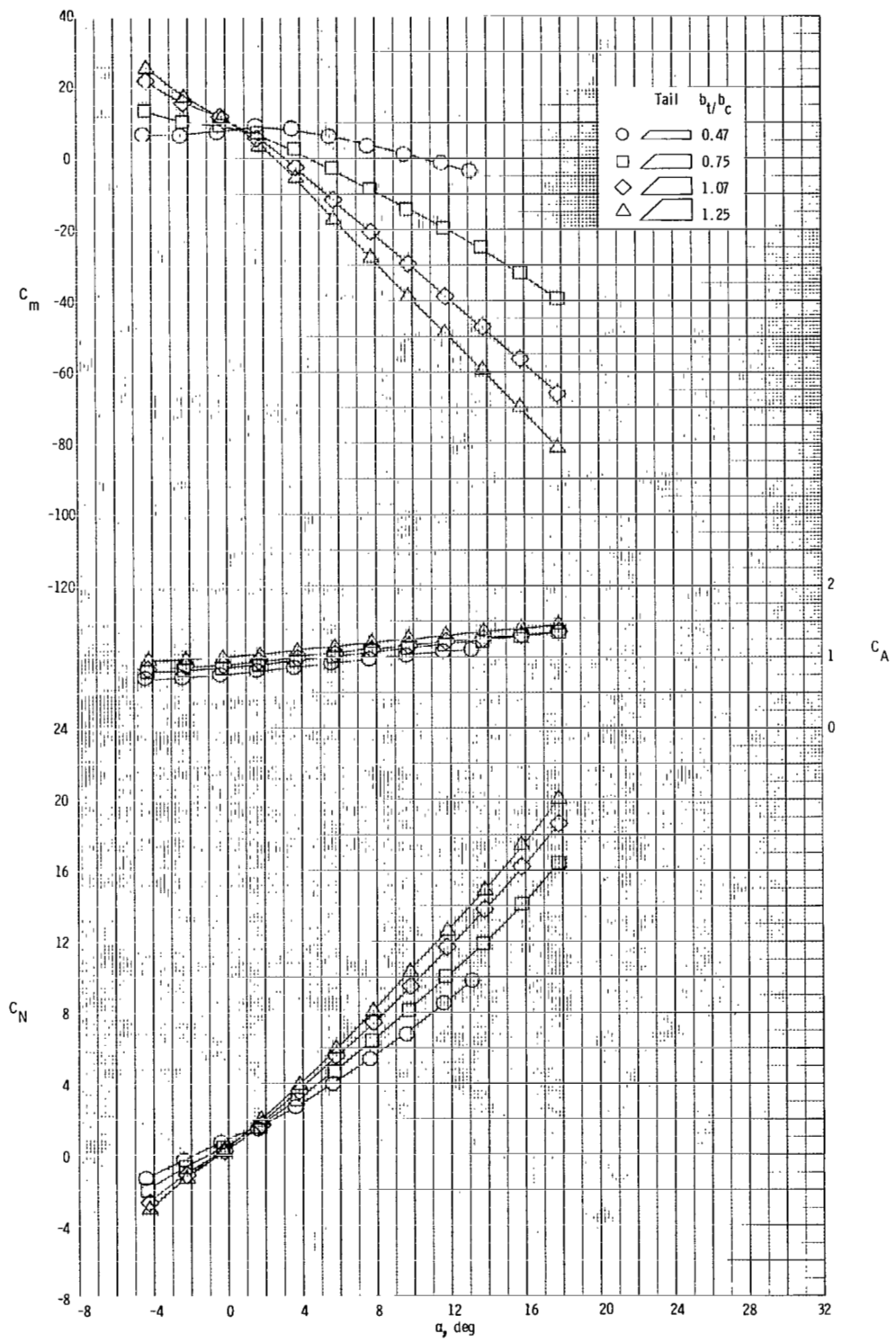
(c) $M = 3.50.$

Figure 5.- Concluded.



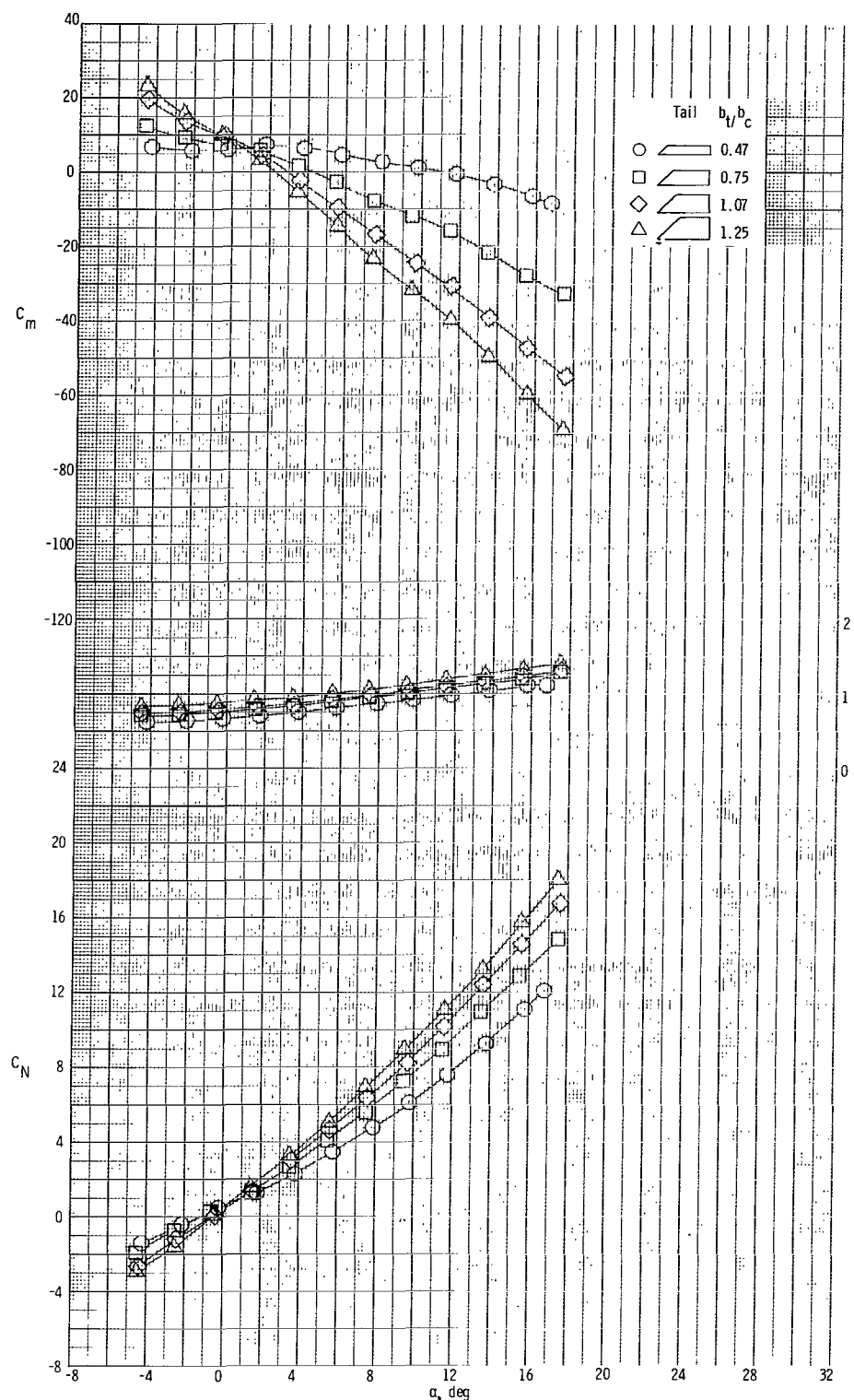
(a) $M = 2.50.$

Figure 6.- Effects of tail-fin span on pitch-control characteristics at $\phi = 0^\circ.$
 $\delta_{pitch} = 5^\circ.$



(b) $M = 3.00$.

Figure 6.- Continued.



(c) $M = 3.50.$

Figure 6.- Concluded.

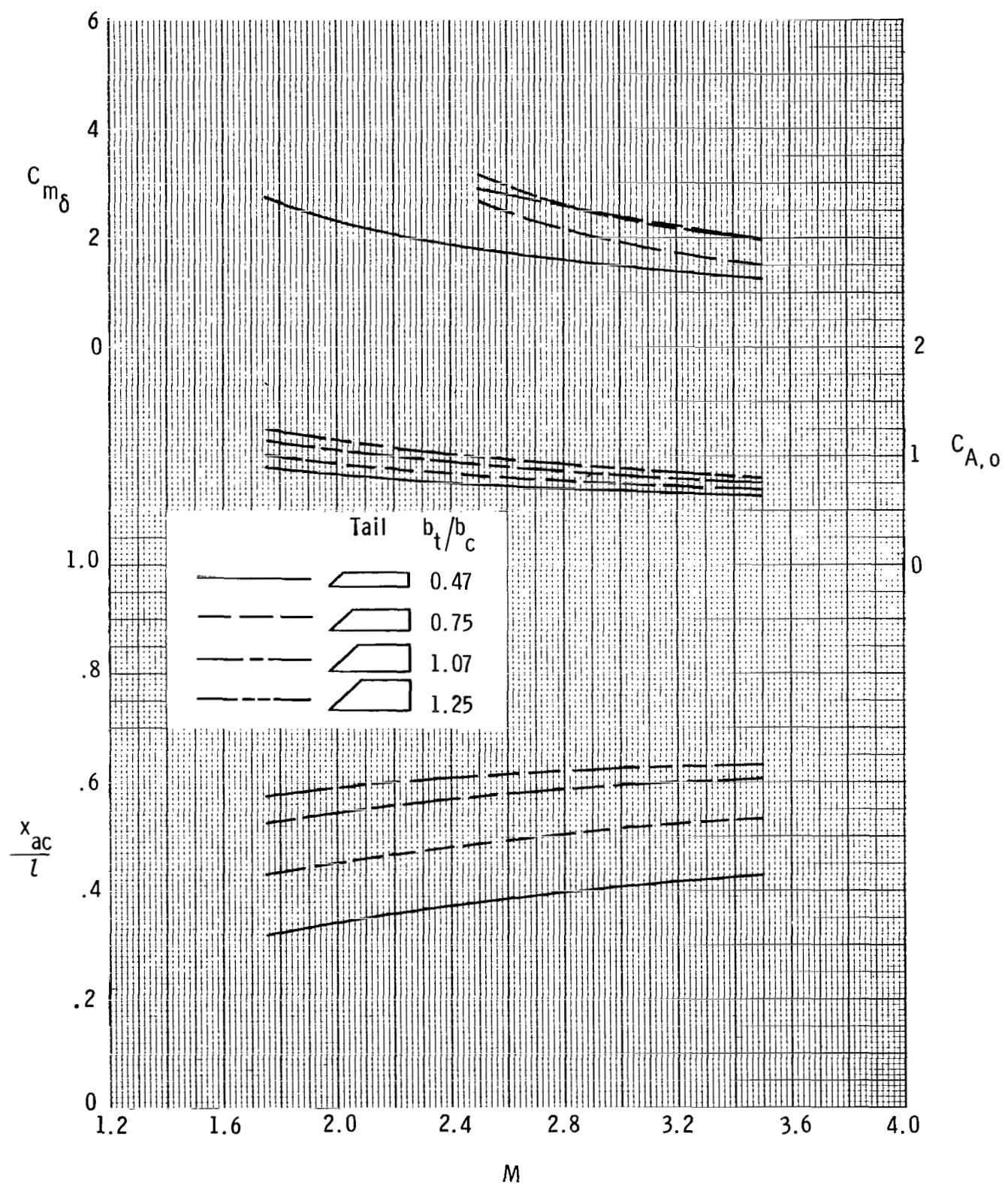


Figure 7.- Summary of longitudinal aerodynamic characteristics. $\phi = 0^\circ$.

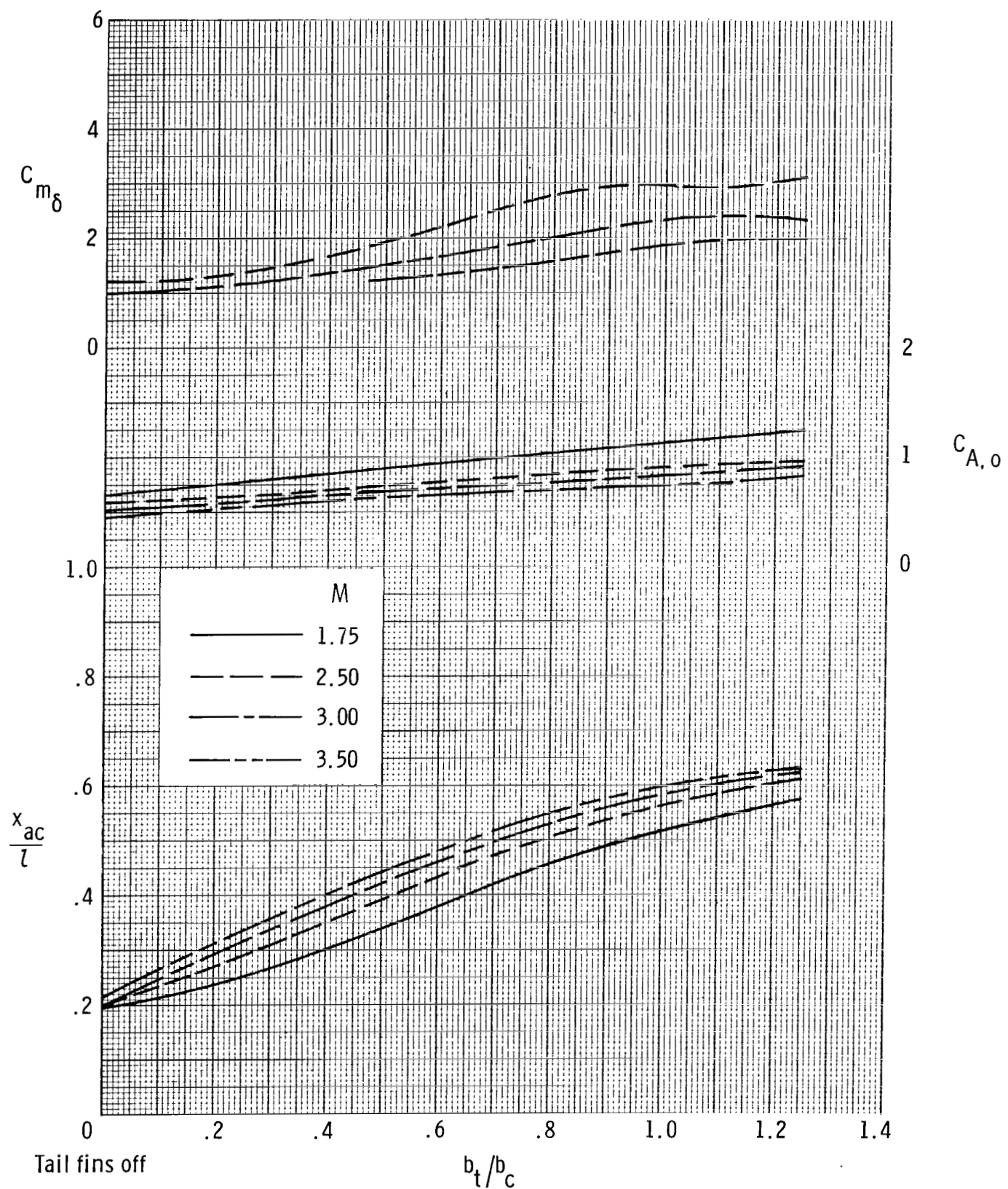
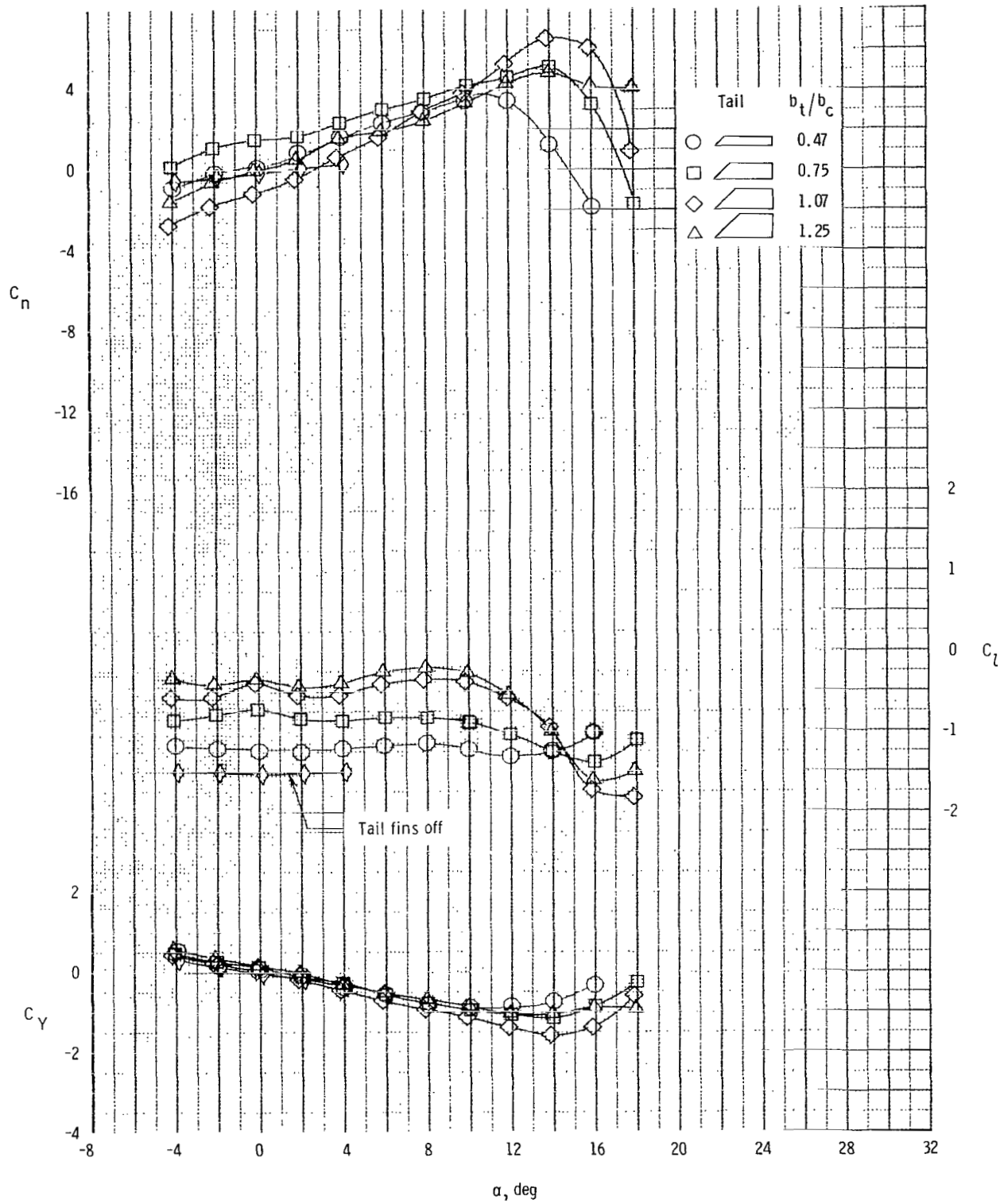
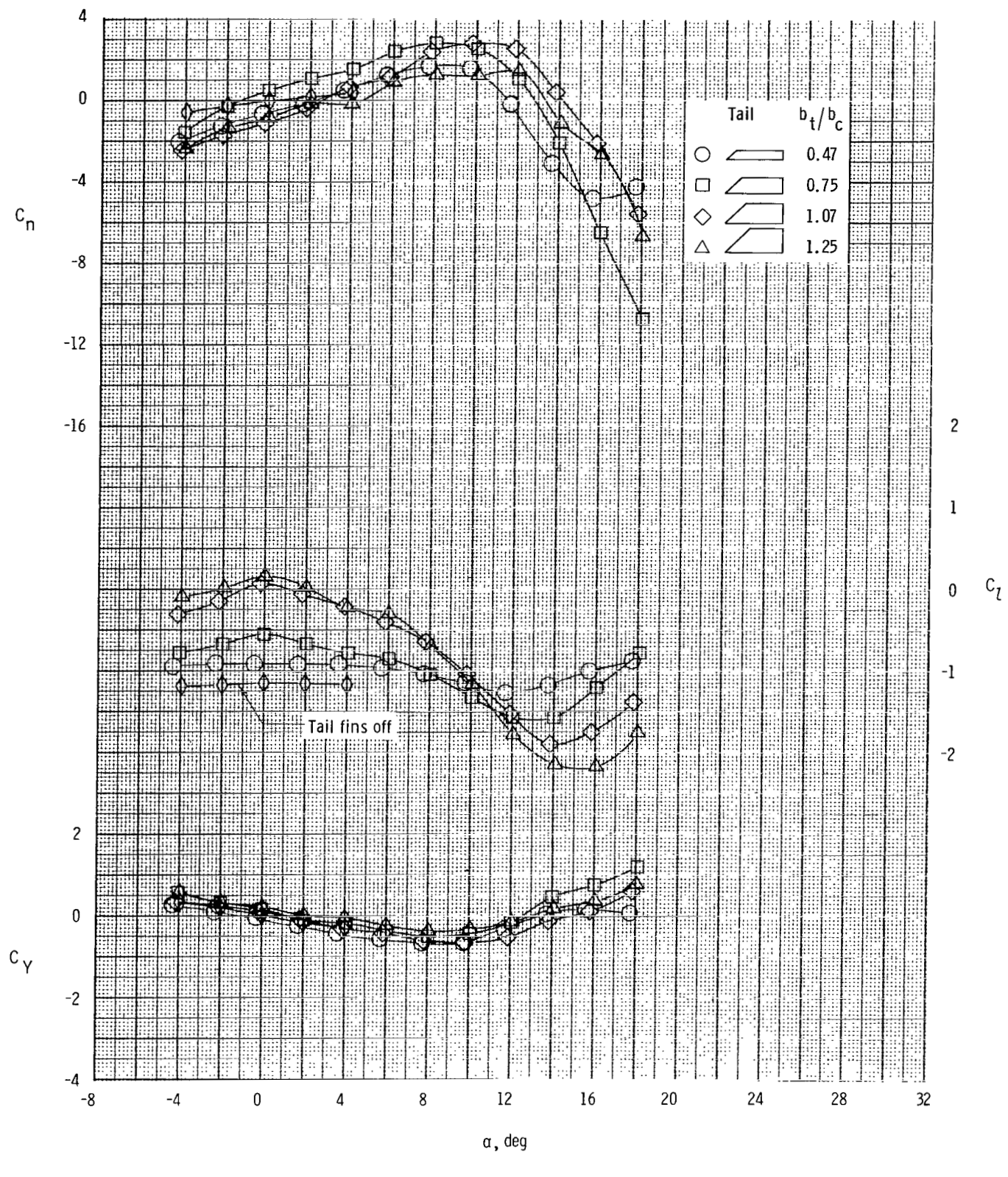


Figure 7.- Concluded.



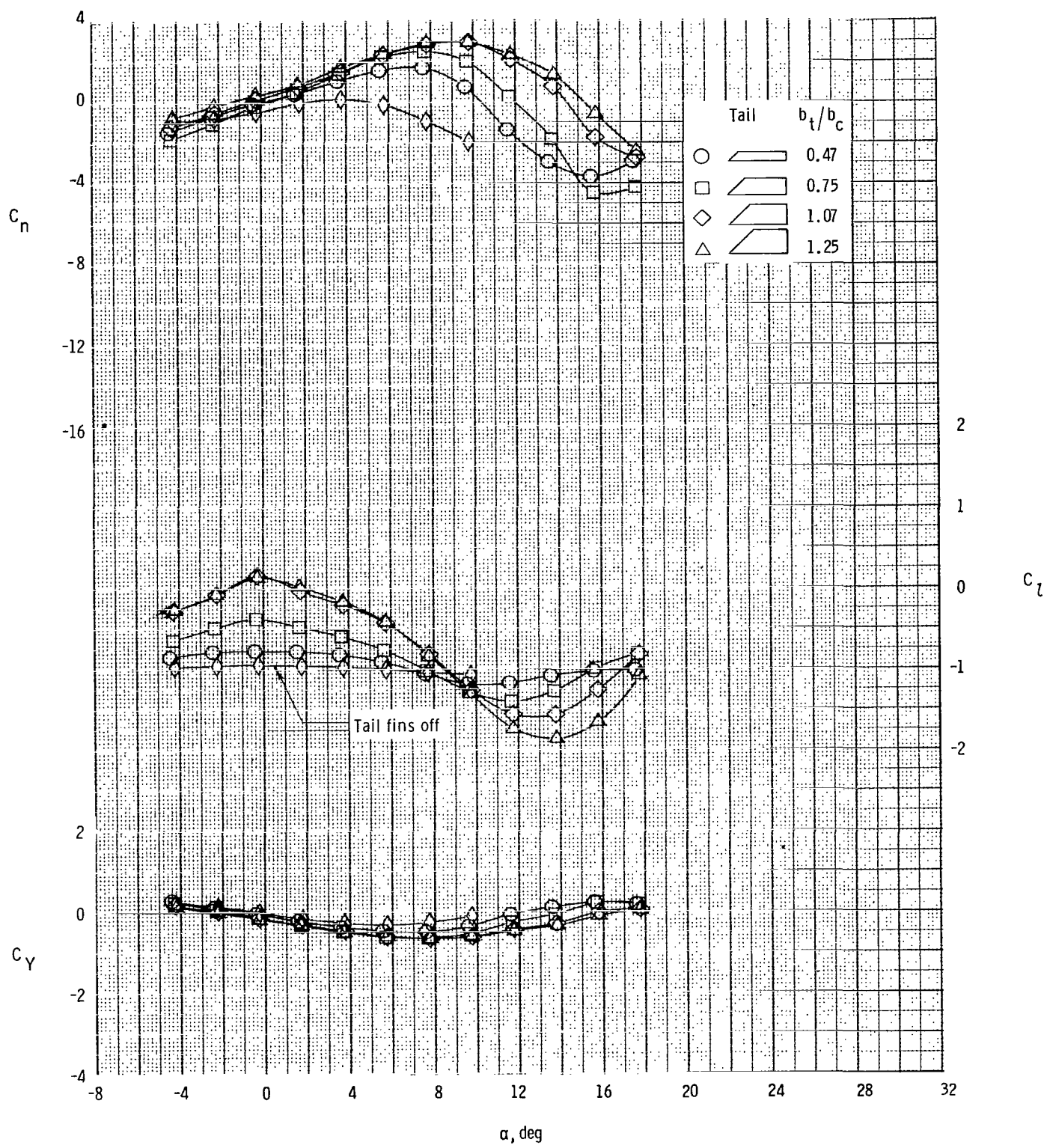
(a) $M = 1.75$.

Figure 8.- Effects of tail-fin span on roll-control characteristics at $\phi = 0^\circ$.
 $\delta_{\text{roll}} = -10^\circ$.



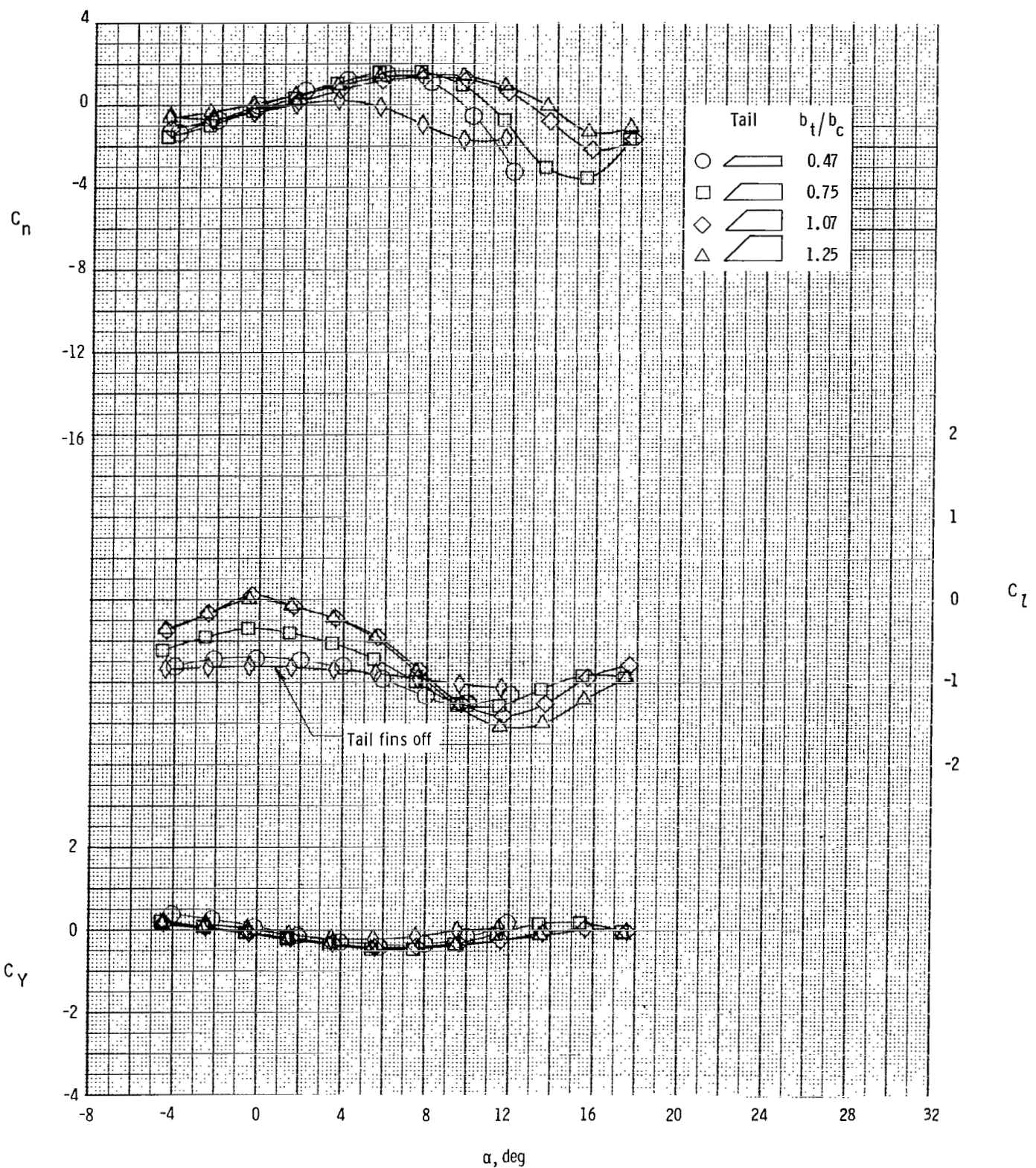
(b) $M = 2.50.$

Figure 8.- Continued.



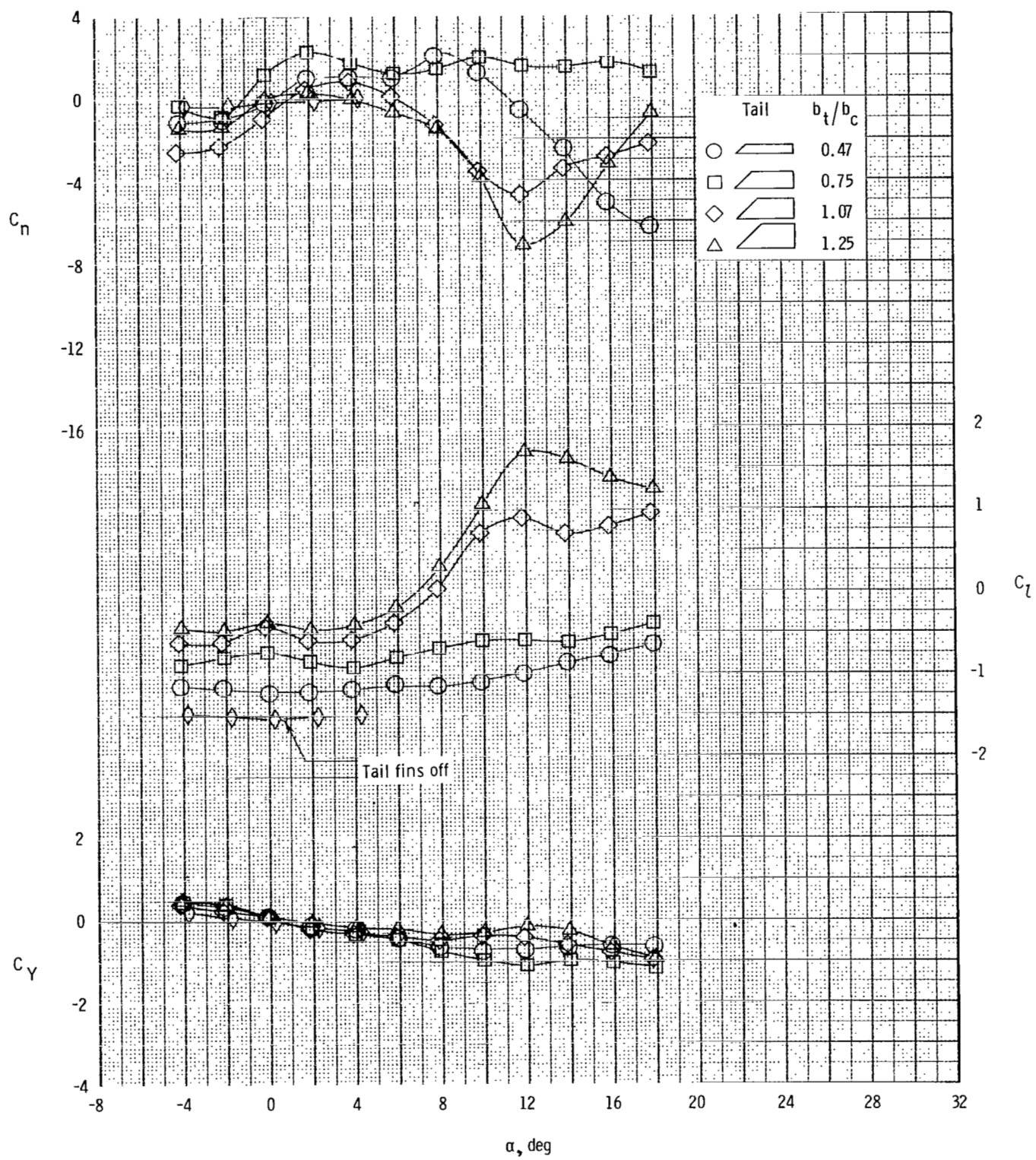
(c) $M = 3.00.$

Figure 8.- Continued.



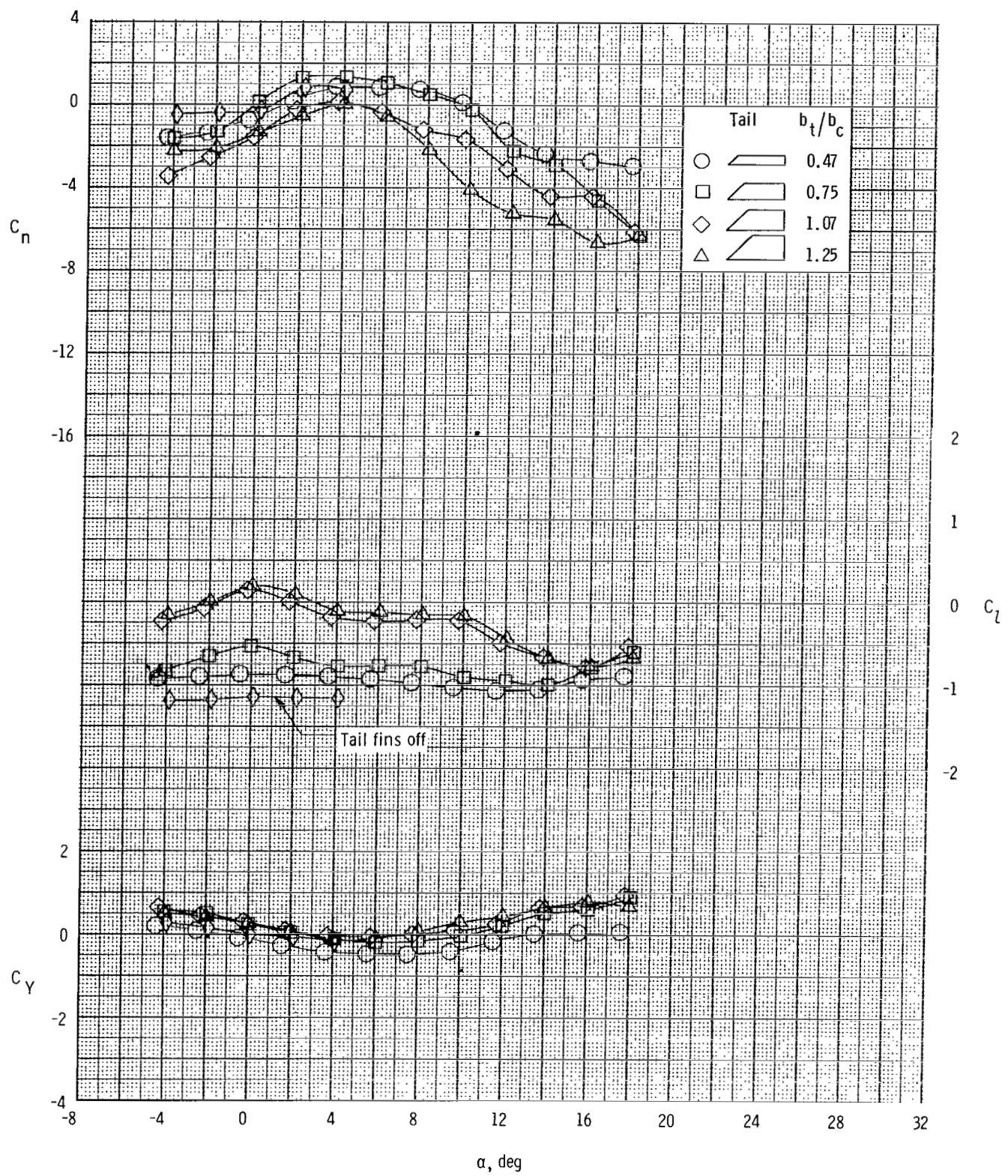
(d) $M = 3.50.$

Figure 8.- Concluded.



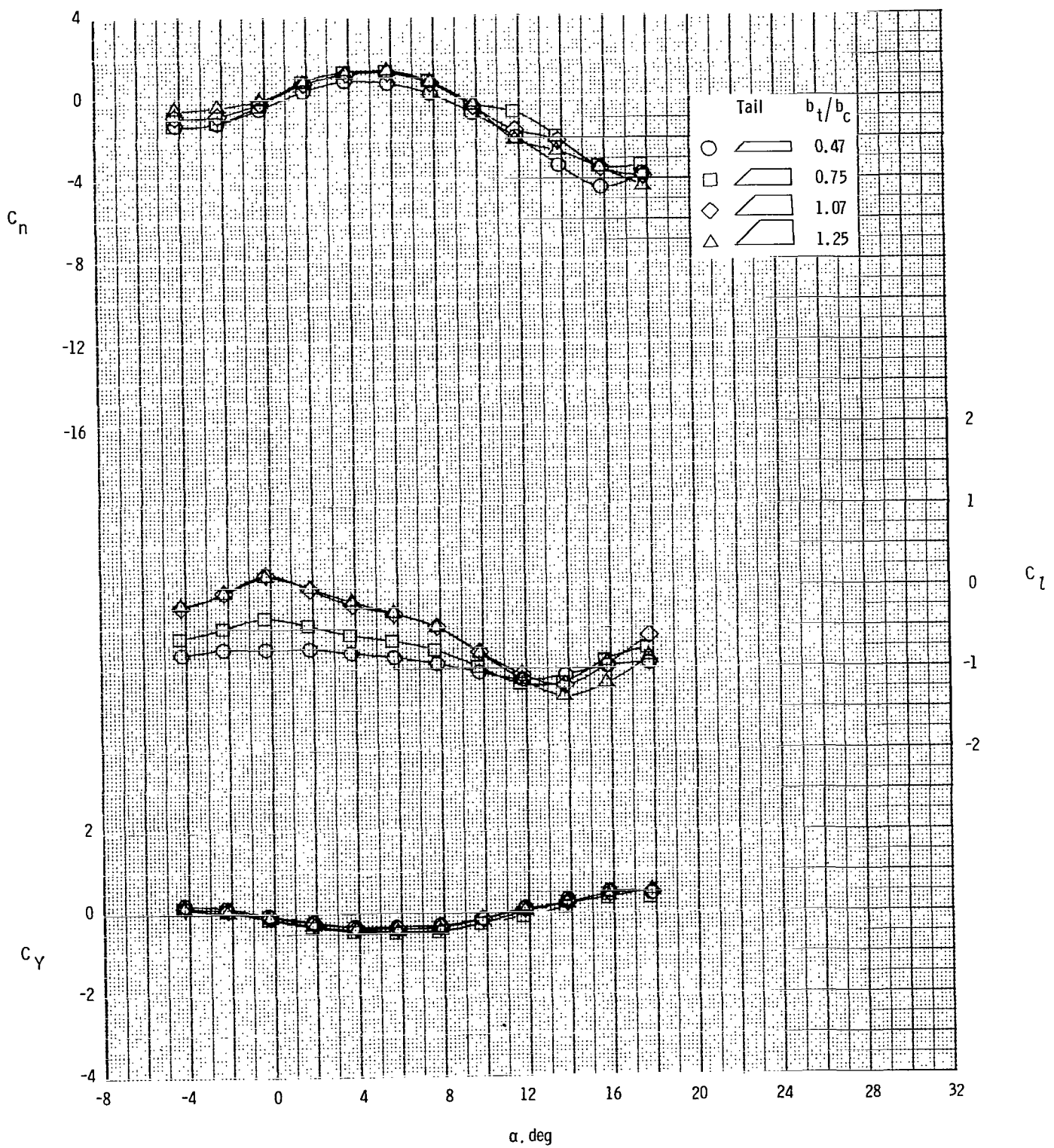
(a) $M = 1.75$.

Figure 9.- Effects of tail-fin span on roll-control characteristics at $\phi = 26.57^\circ$.
 $\delta_{\text{roll}} = -10^\circ$.



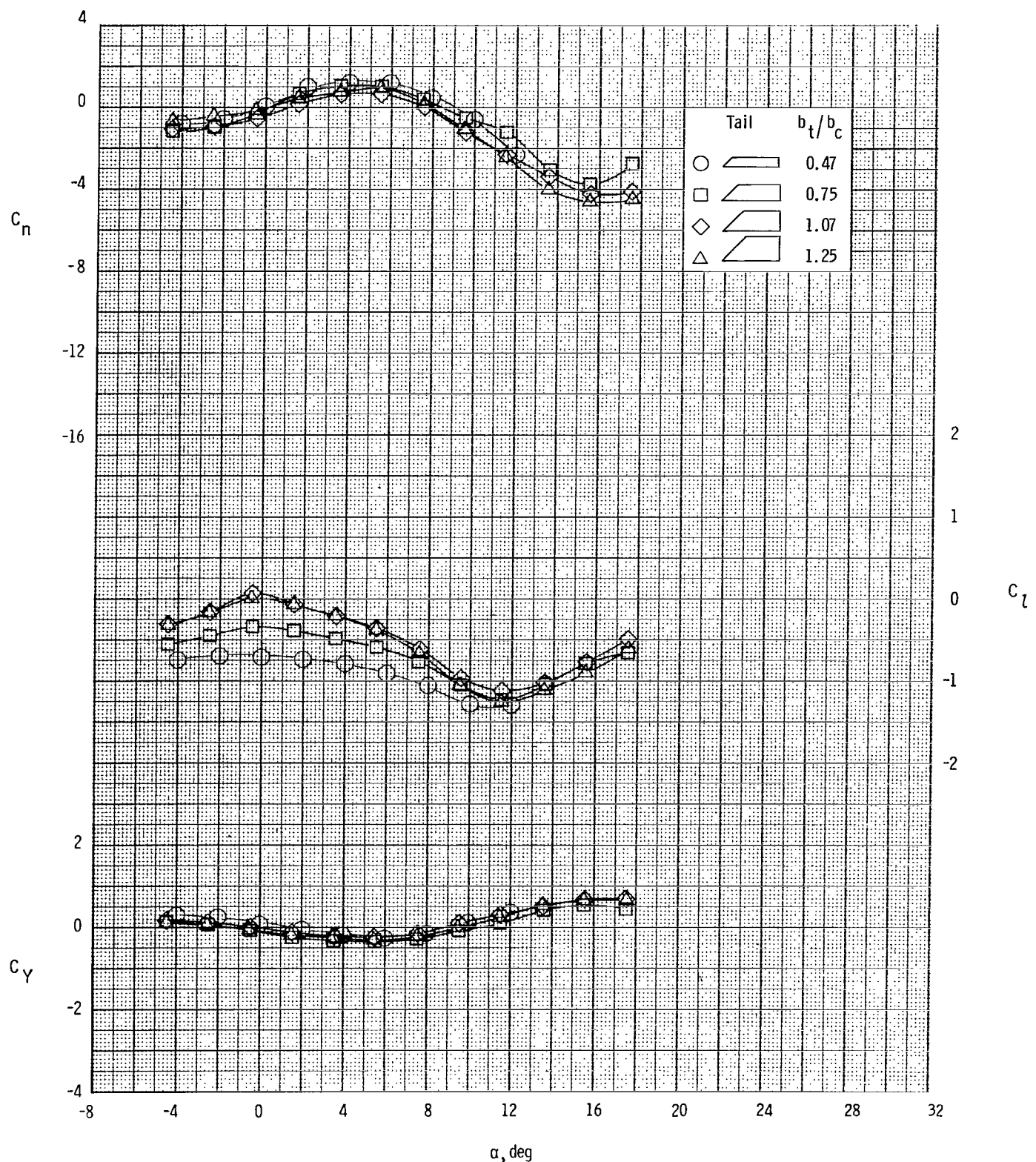
(b) $M = 2.50.$

Figure 9.- Continued.



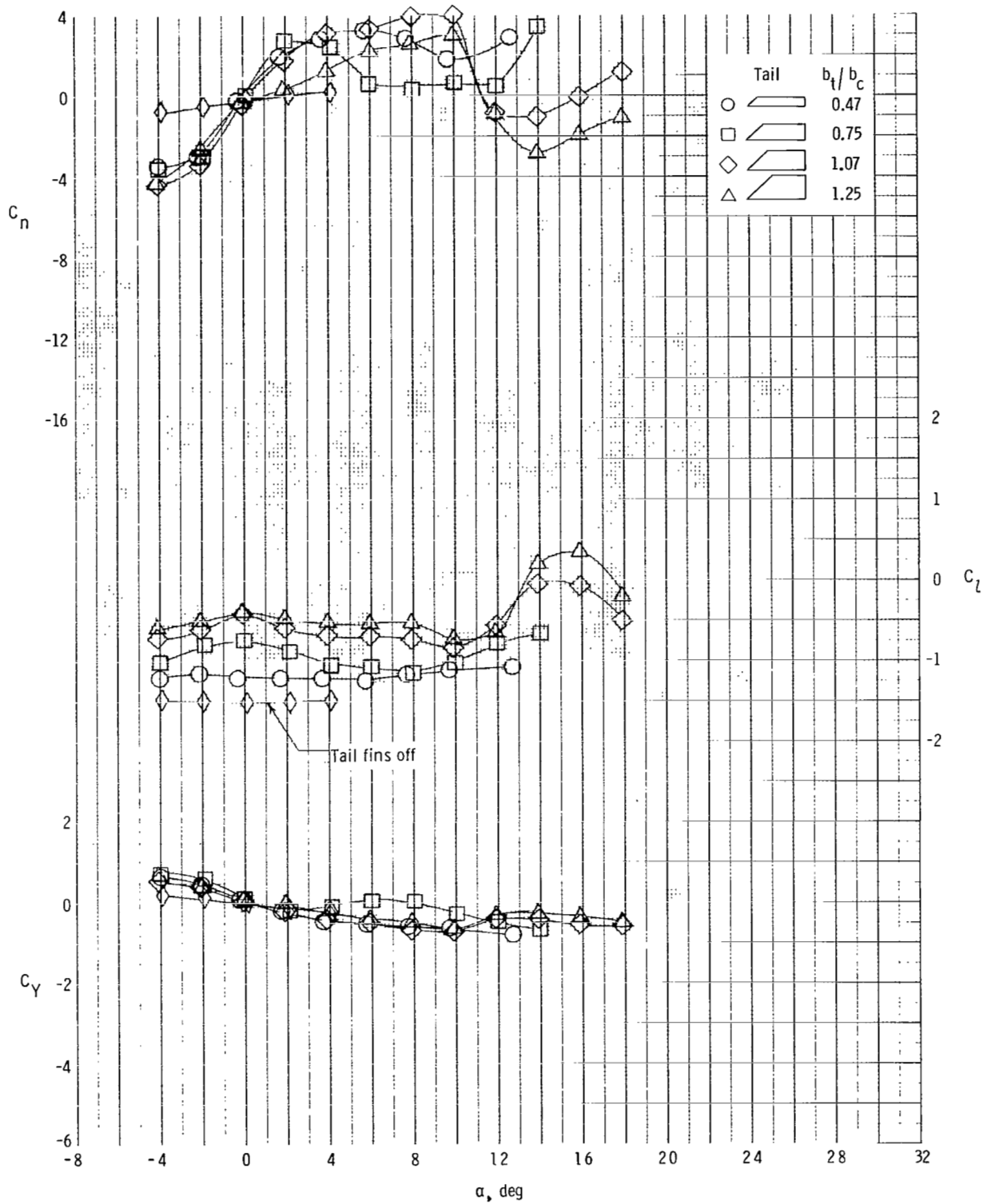
(c) $M = 3.00.$

Figure 9.- Continued.



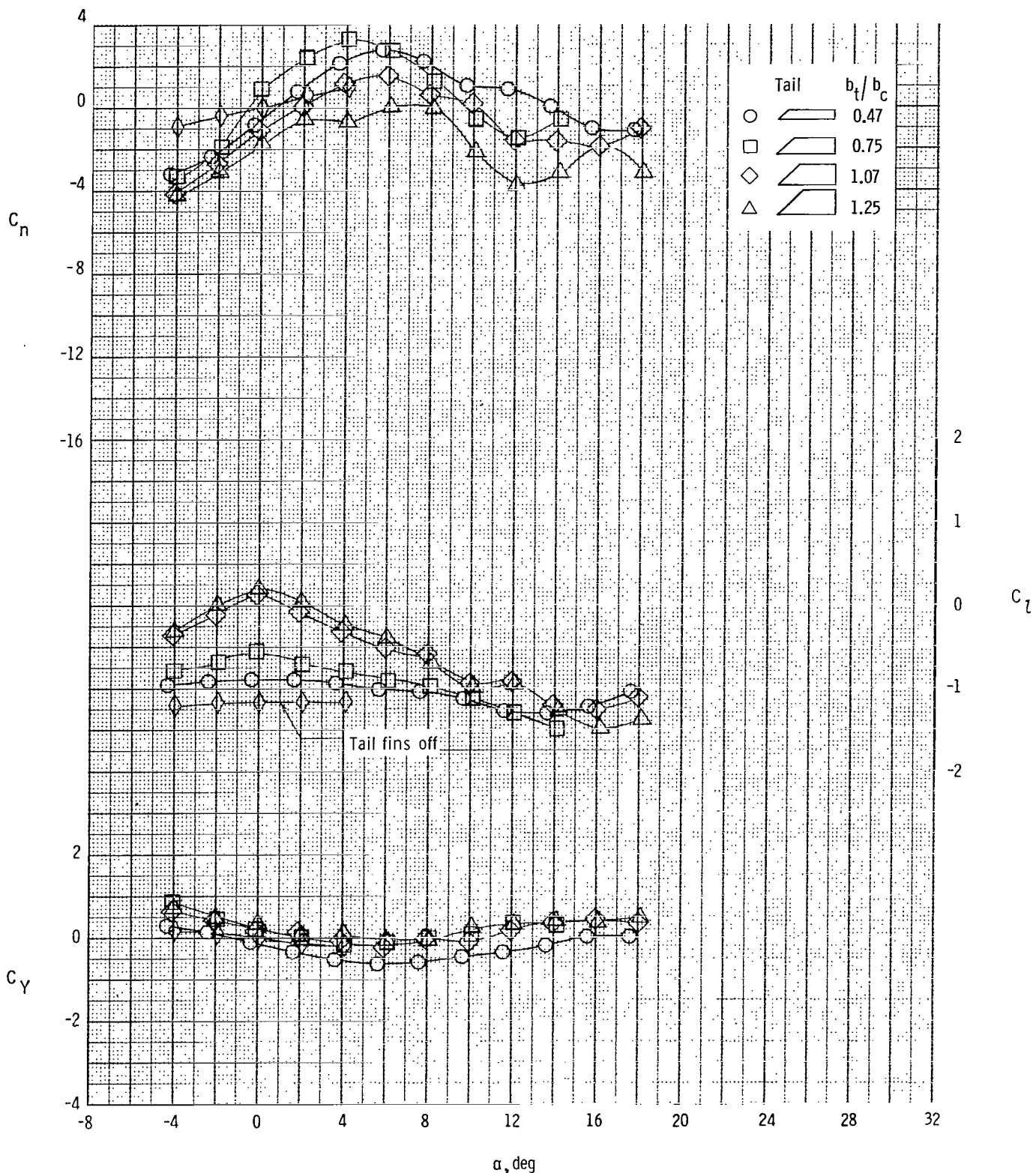
(d) $M = 3.50.$

Figure 9.- Concluded.



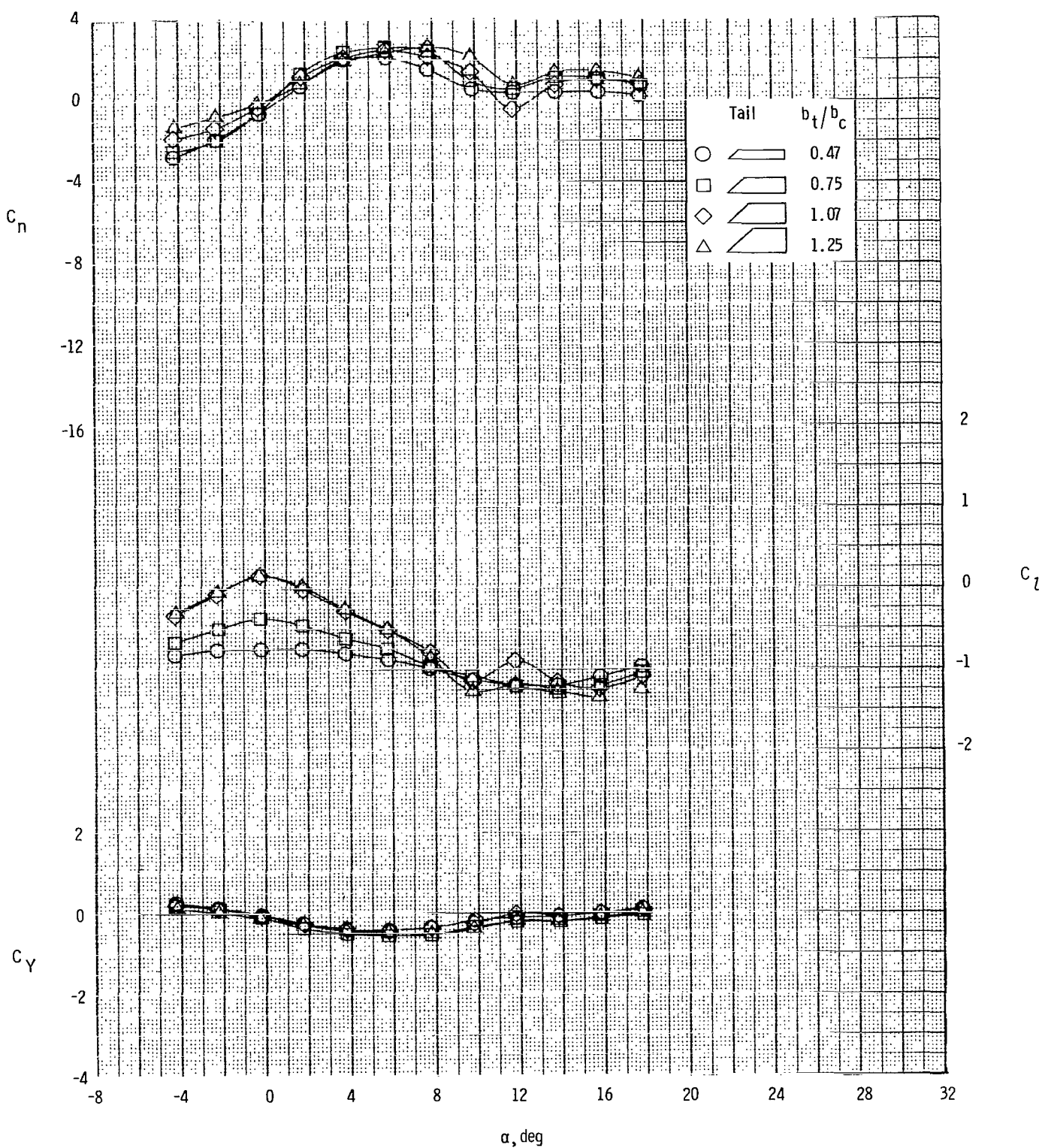
(a) $M = 1.75$.

Figure 10.- Effects of tail-fin span on roll-control characteristics at $\phi = 45^\circ$.
 $\delta_{\text{roll}} = -10^\circ$.



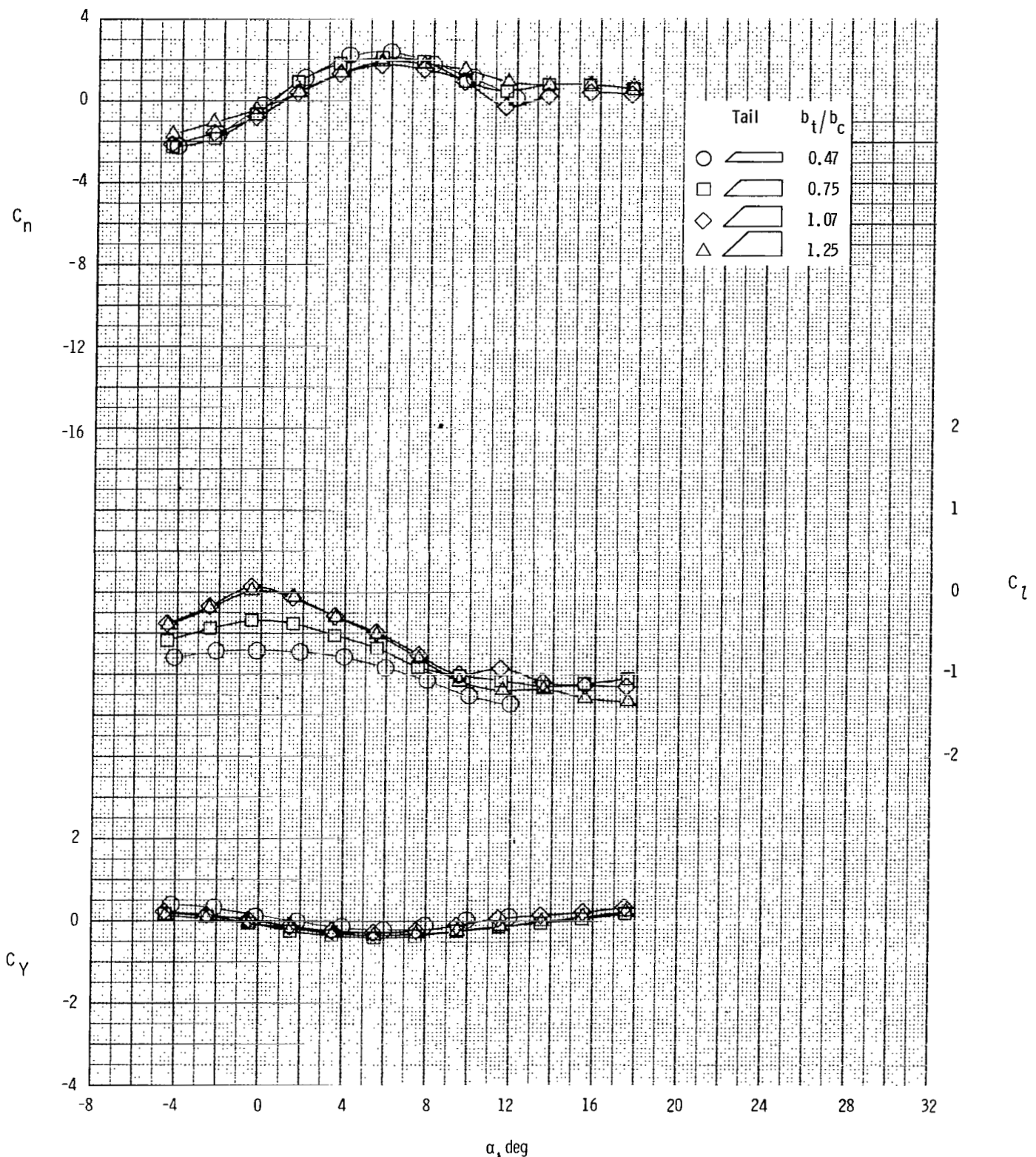
(b) $M = 2.50.$

Figure 10.- Continued.



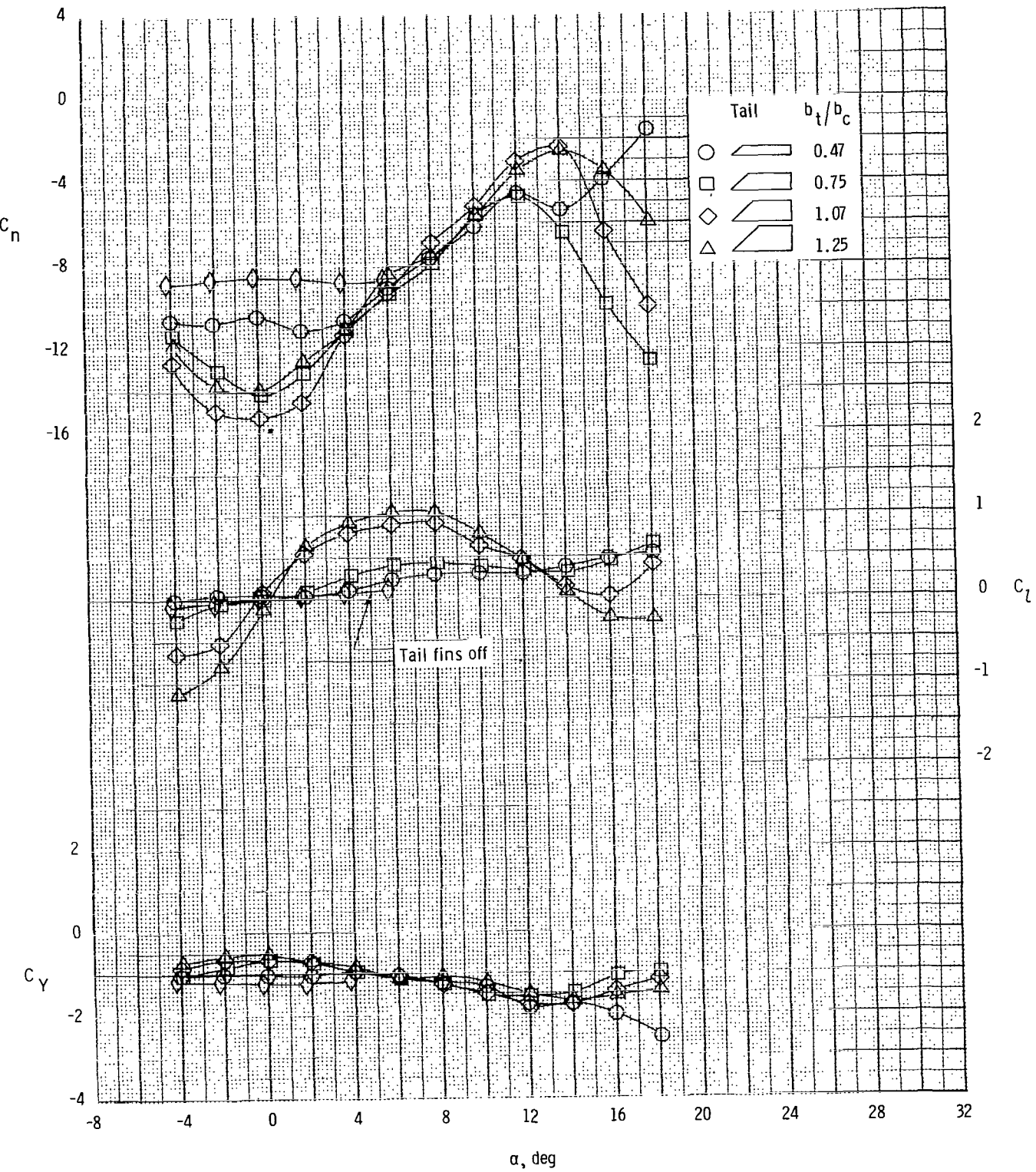
(c) $M = 3.00.$

Figure 10.- Continued.



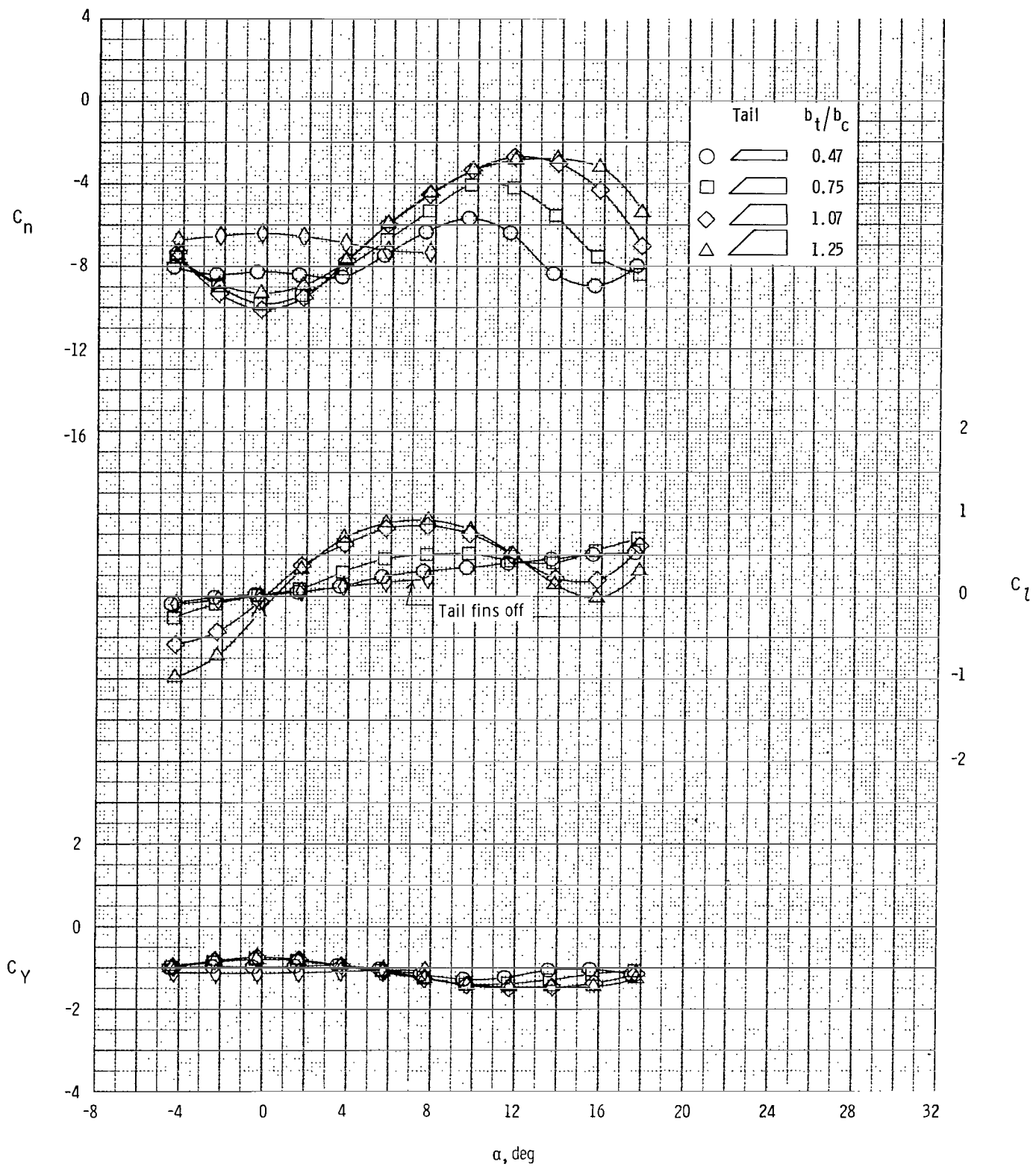
(d) $M = 3.50.$

Figure 10.- Concluded.



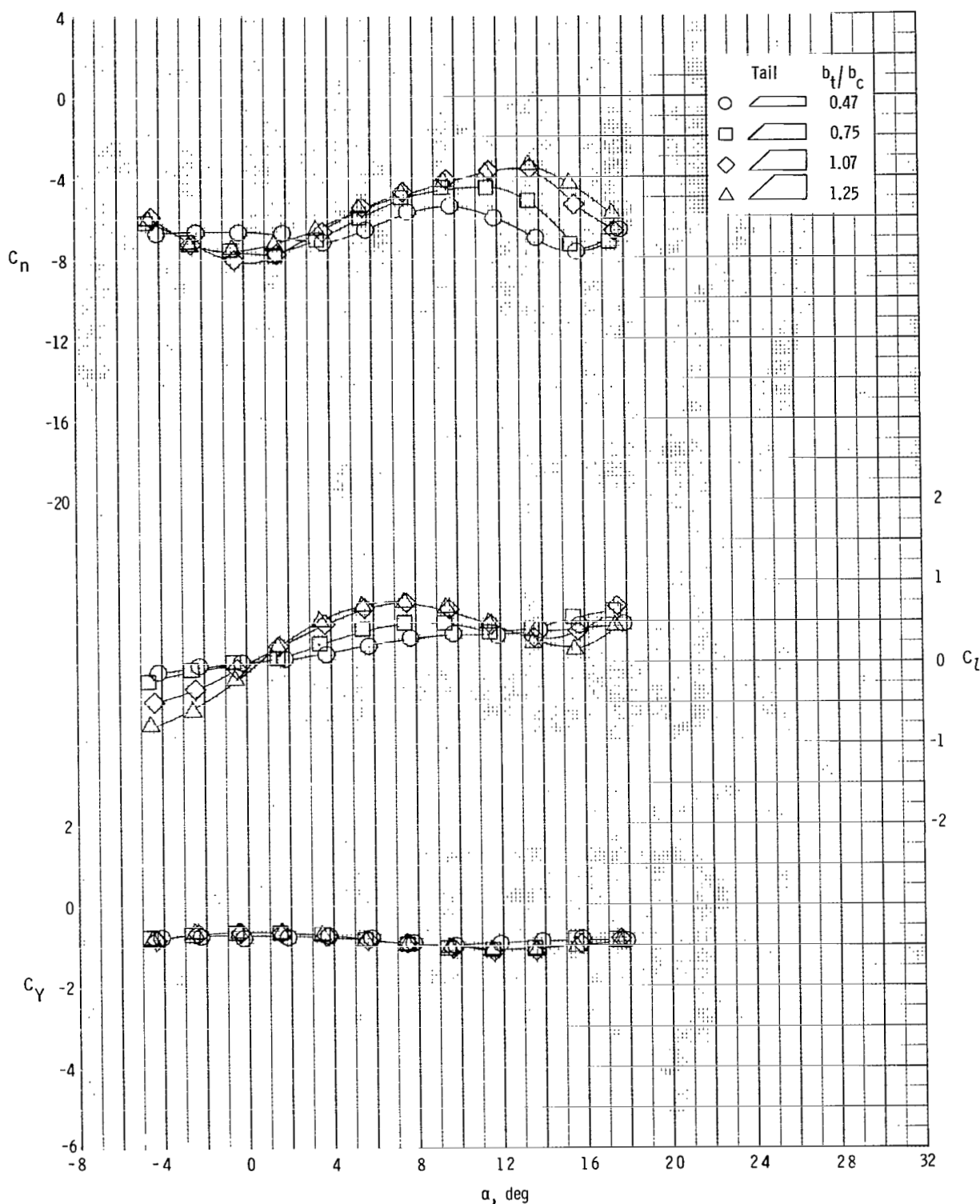
(a) $M = 2.50.$

Figure 11.- Effects of tail-fin span on yaw-control characteristics at $\phi = 0^\circ$.
 $\delta_{yaw} = -5^\circ$.



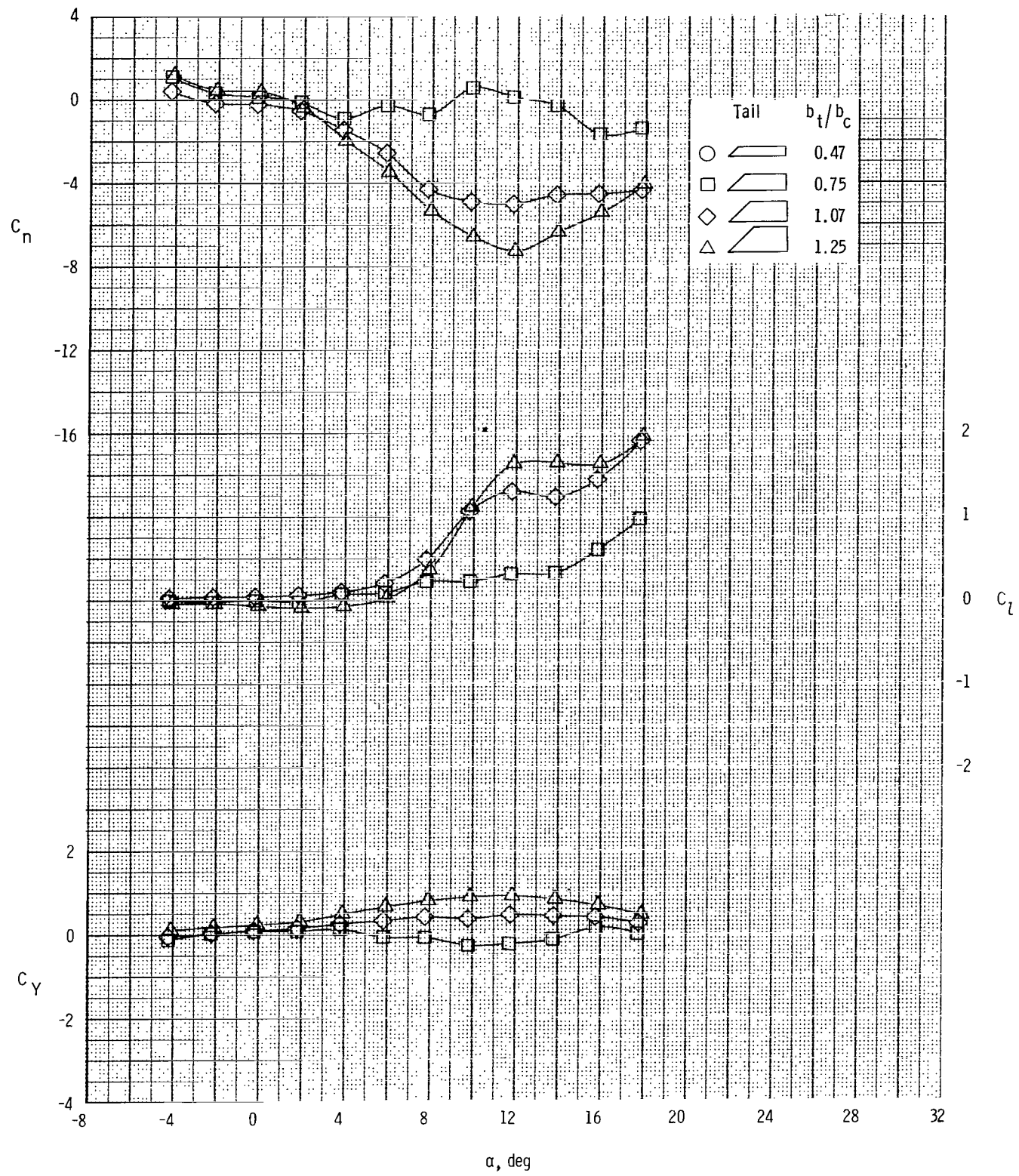
(b) $M = 3.00.$

Figure 11.- Continued.



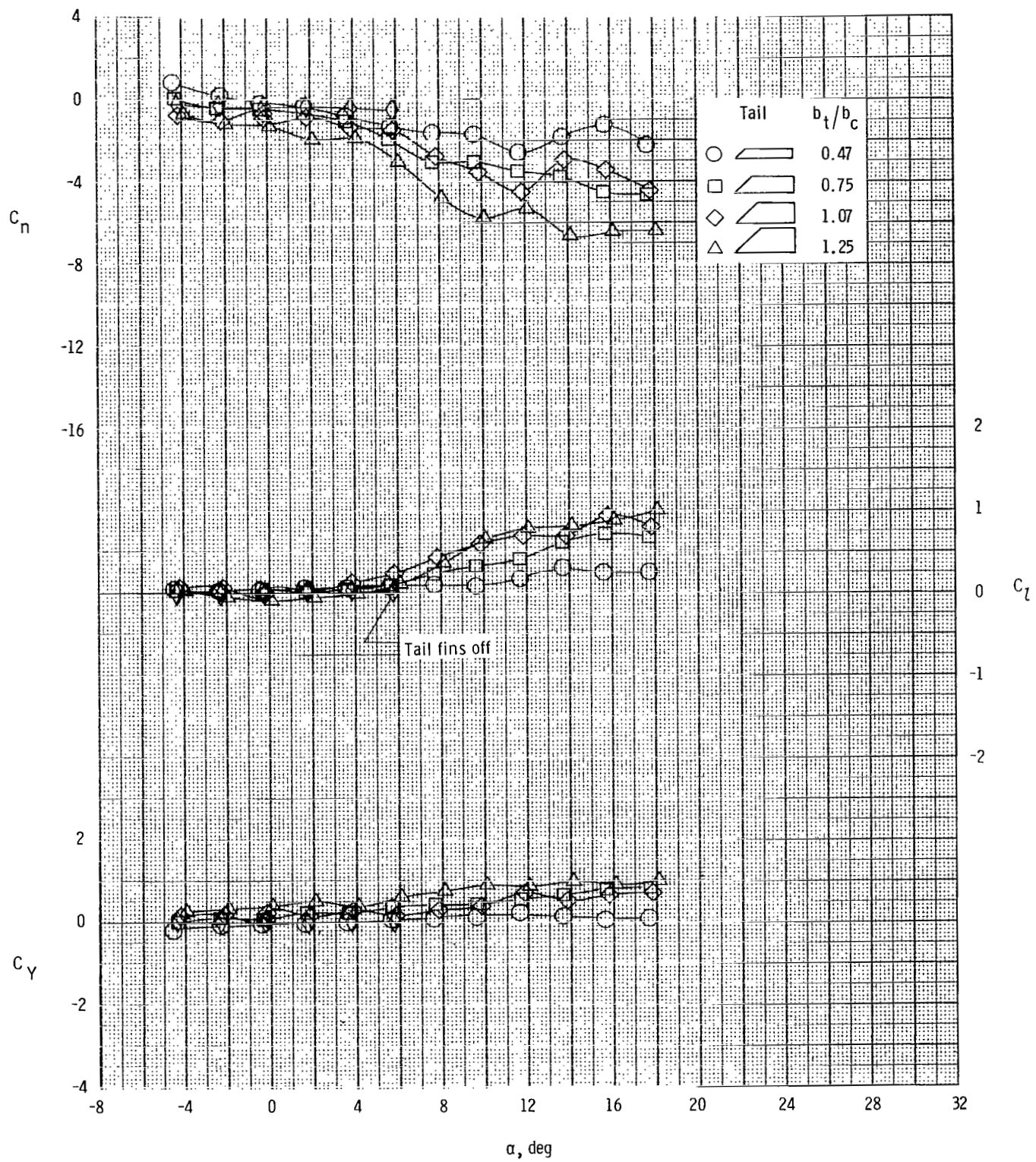
(c) $M = 3.50.$

Figure 11.- Concluded.



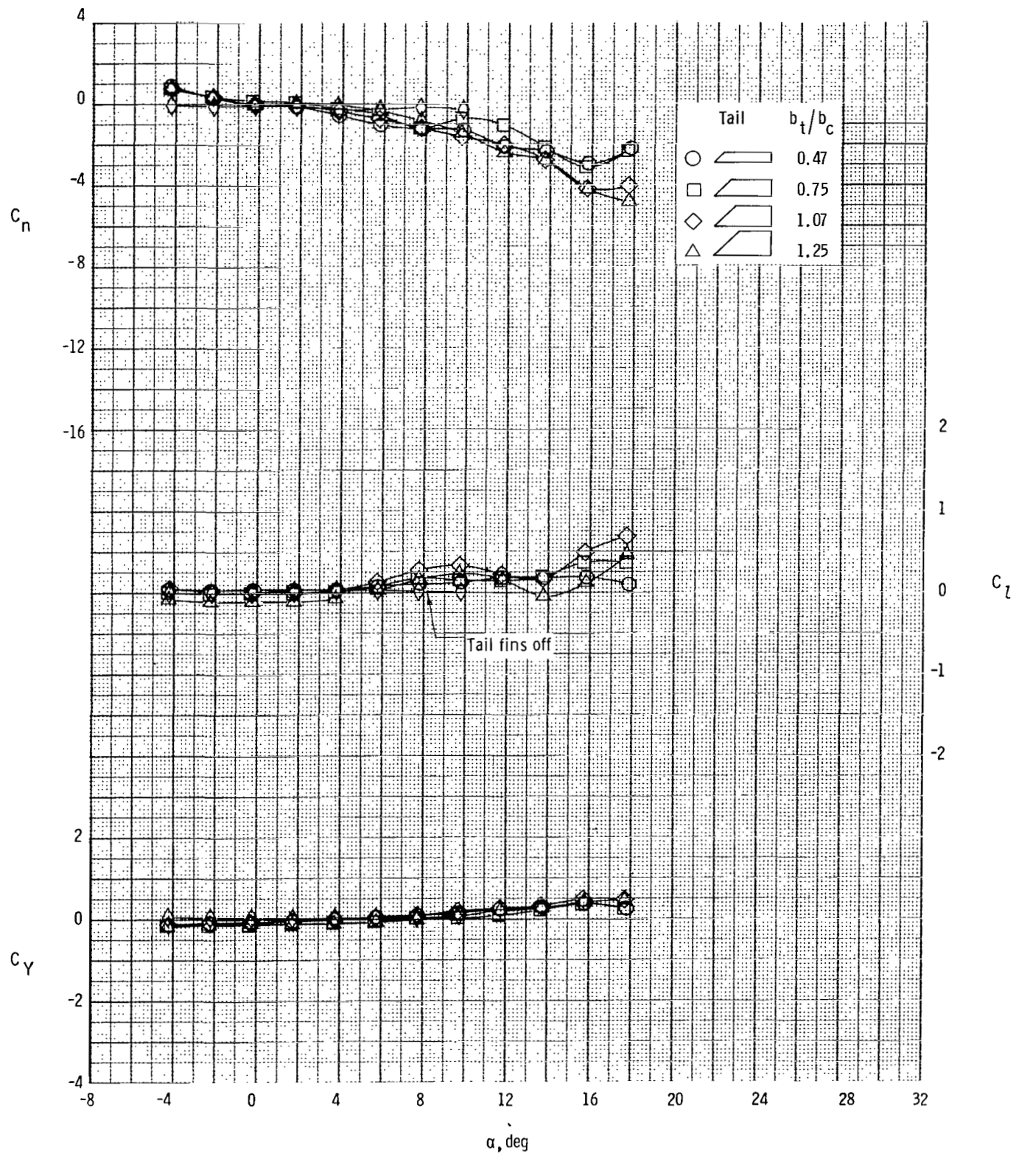
(a) $M = 1.75.$

Figure 12.- Effects of tail-fin span on lateral-directional aerodynamic characteristics at $\phi = 26.57^\circ$.



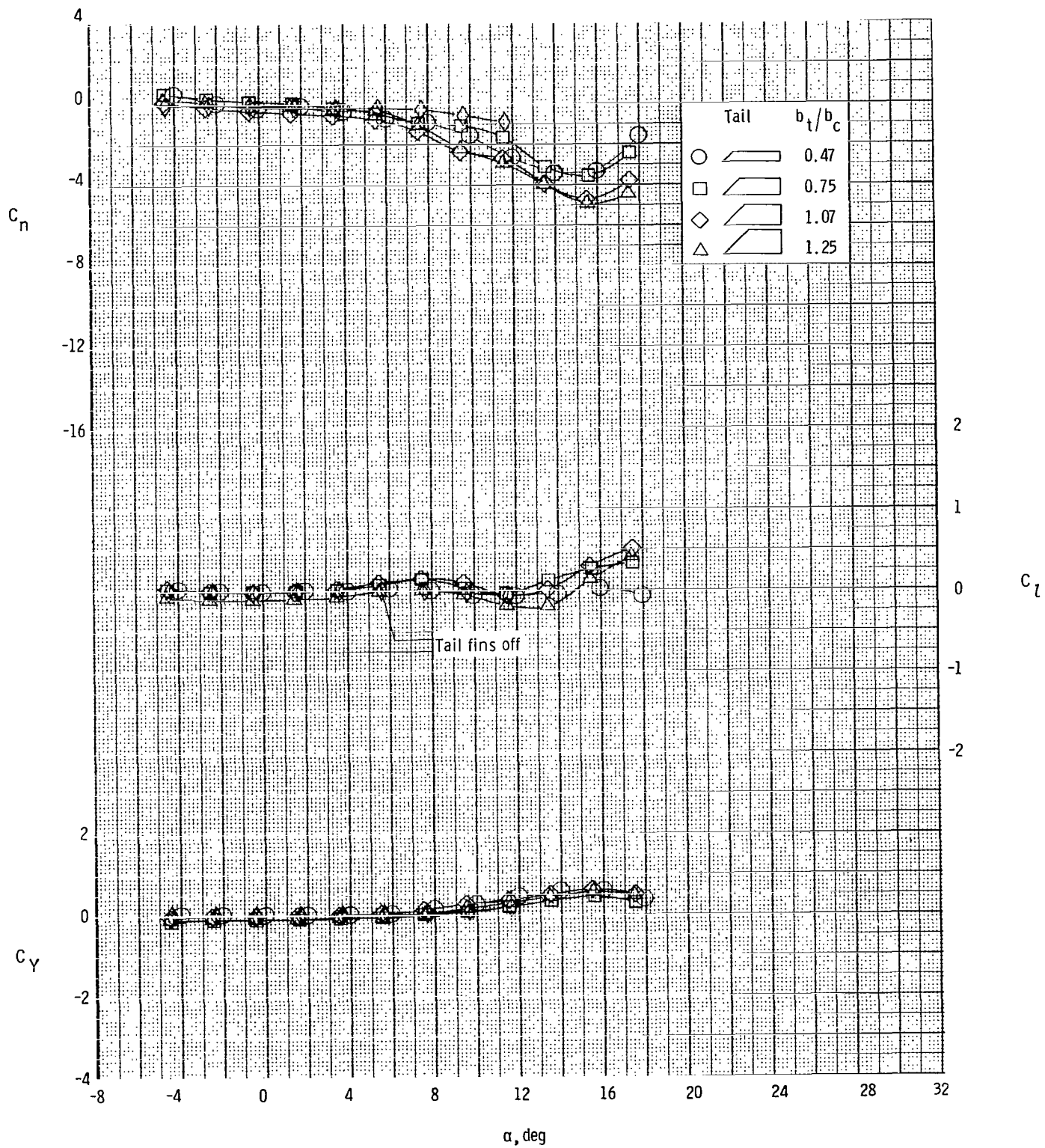
(b) $M = 2.50.$

Figure 12.- Continued.



(c) $M = 3.00.$

Figure 12.- Continued.



(d) $M = 3.50.$

Figure 12.- Concluded.

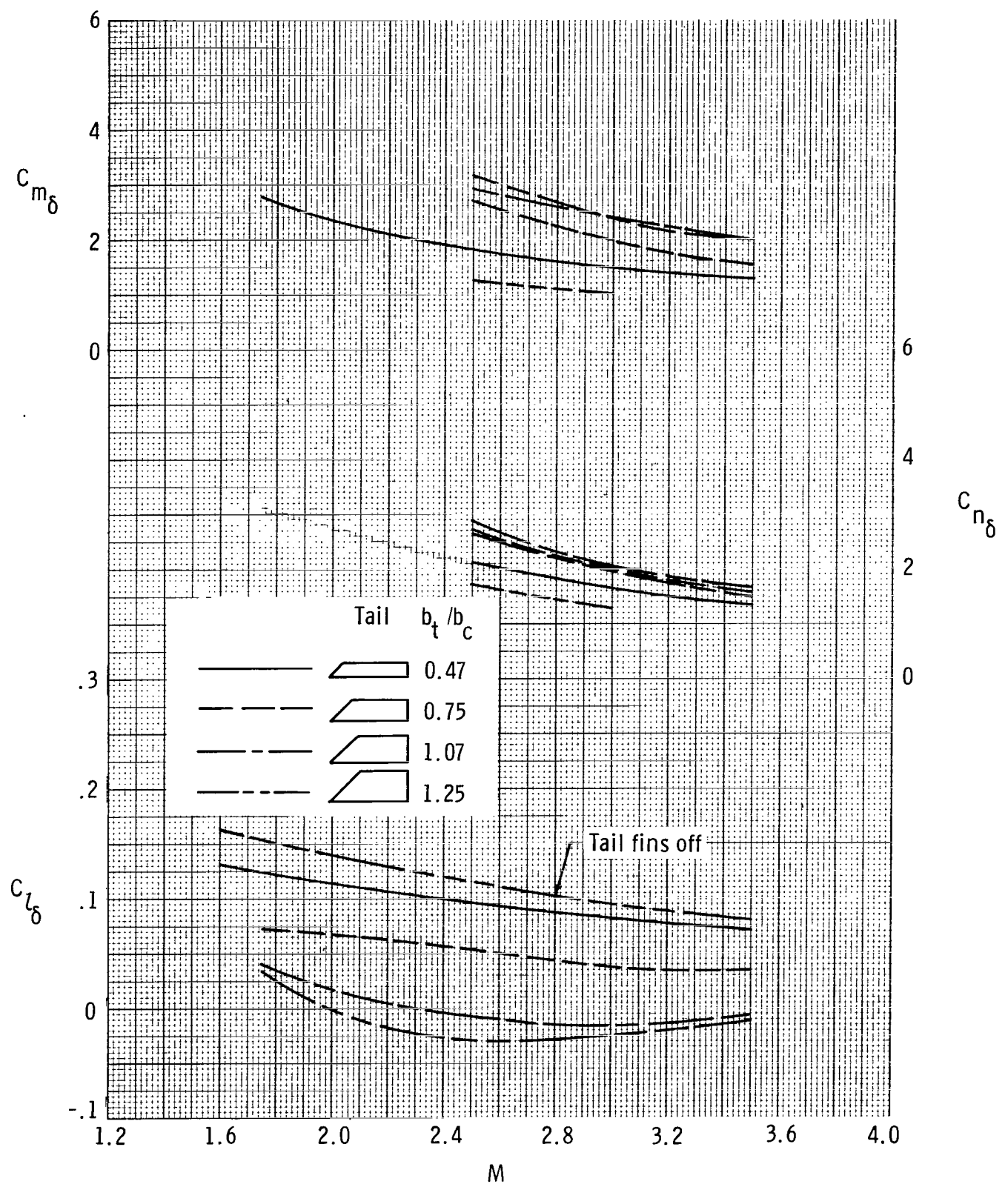


Figure 13.- Summary of canard control effectiveness of each tail-fin configuration
at $\phi = 0^\circ$. $\alpha = 0^\circ$.

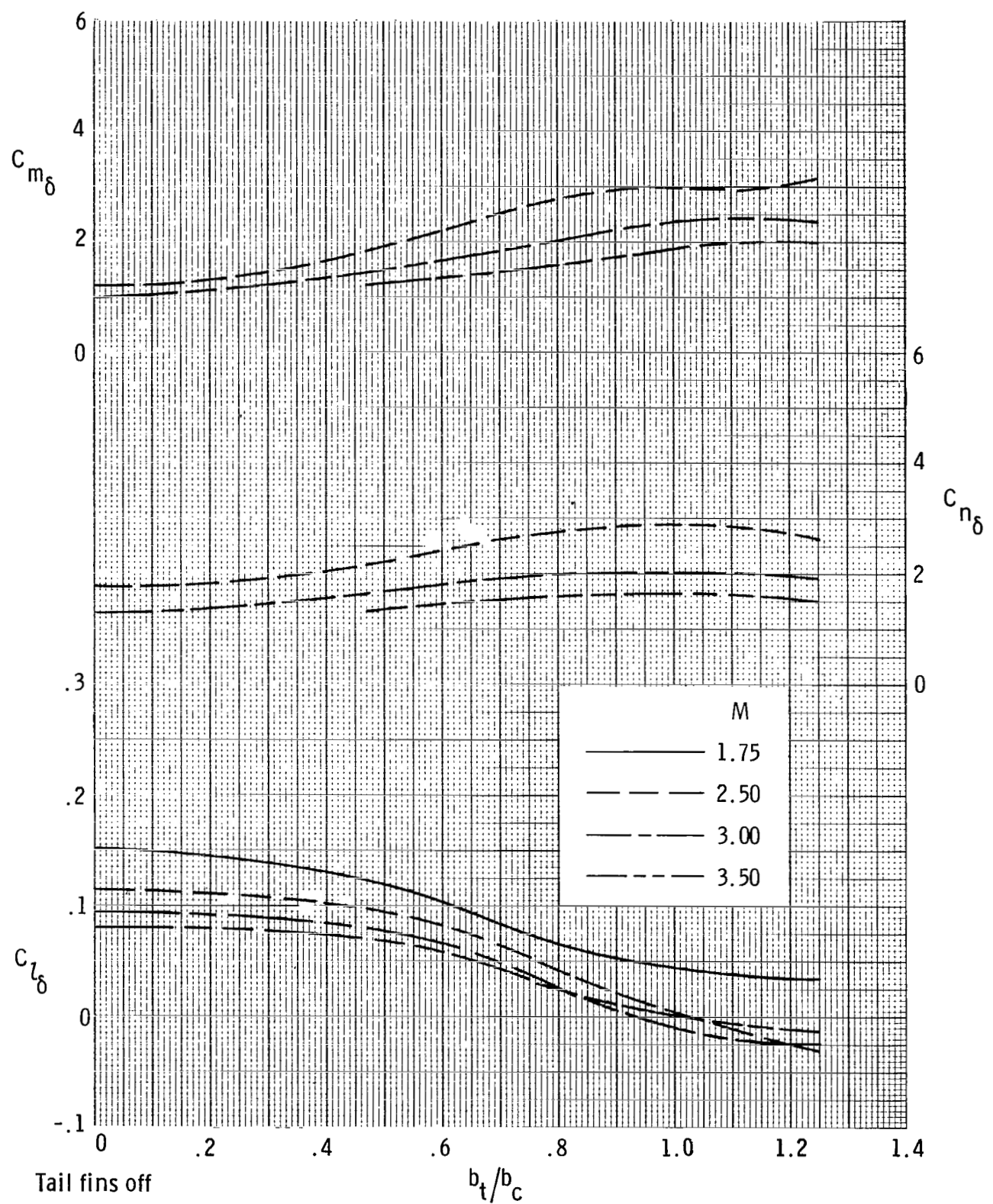
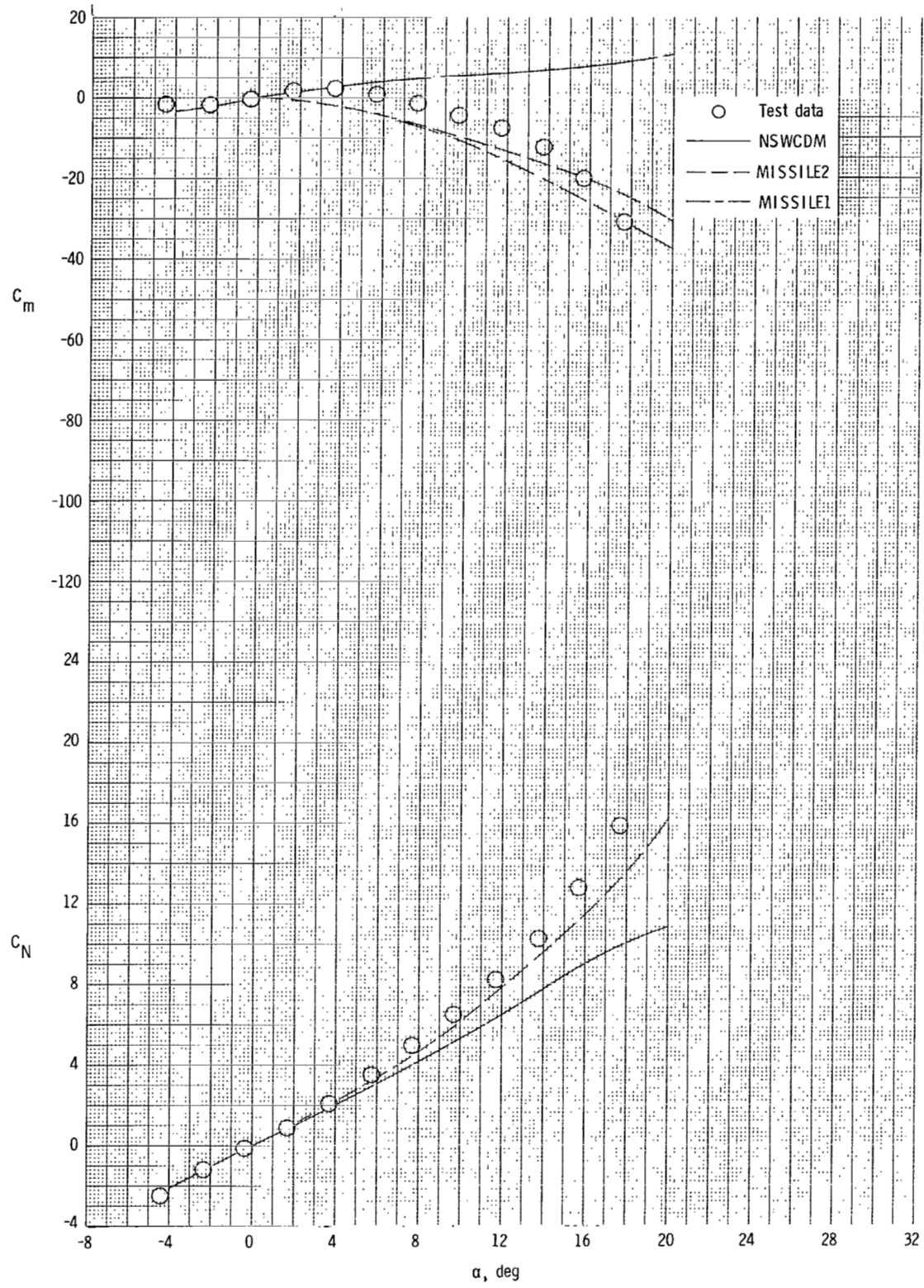
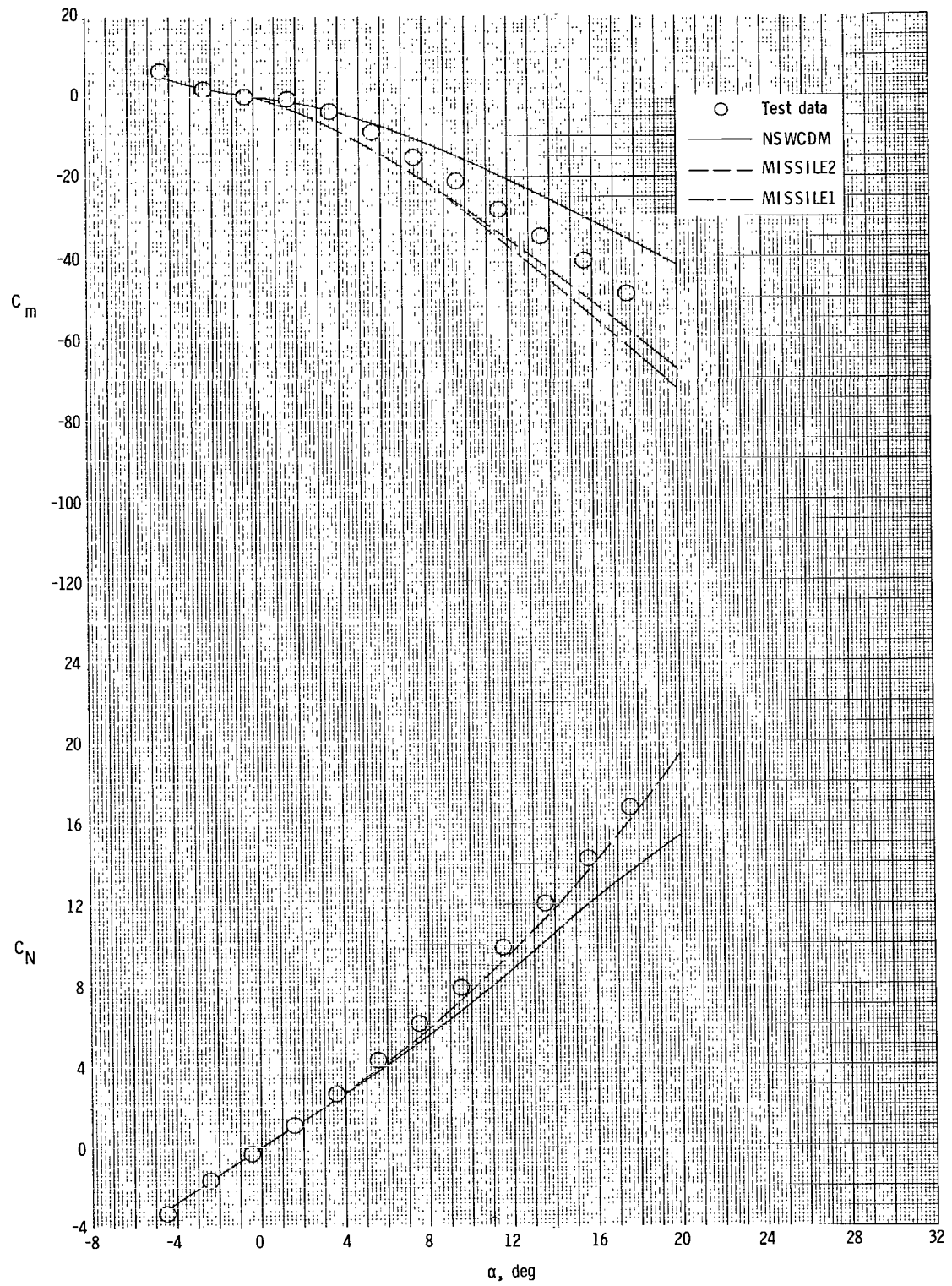


Figure 13.- Concluded.



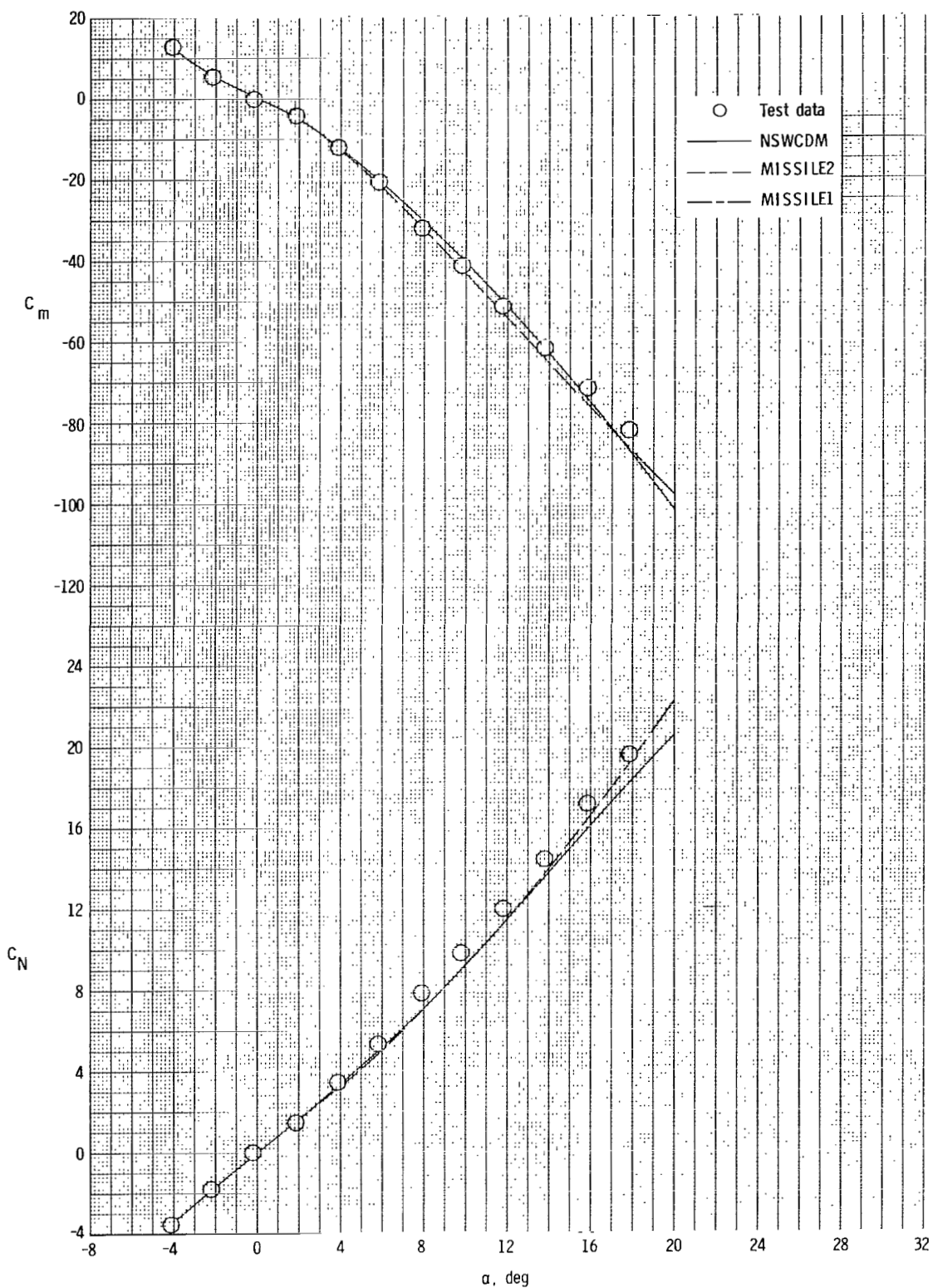
(a) $b_t/b_c = 0.47$.

Figure 14.- Comparison of experimental and analytical longitudinal aerodynamic characteristics of each tail-fin configuration at $\phi = 0^\circ$. $M = 2.50$.



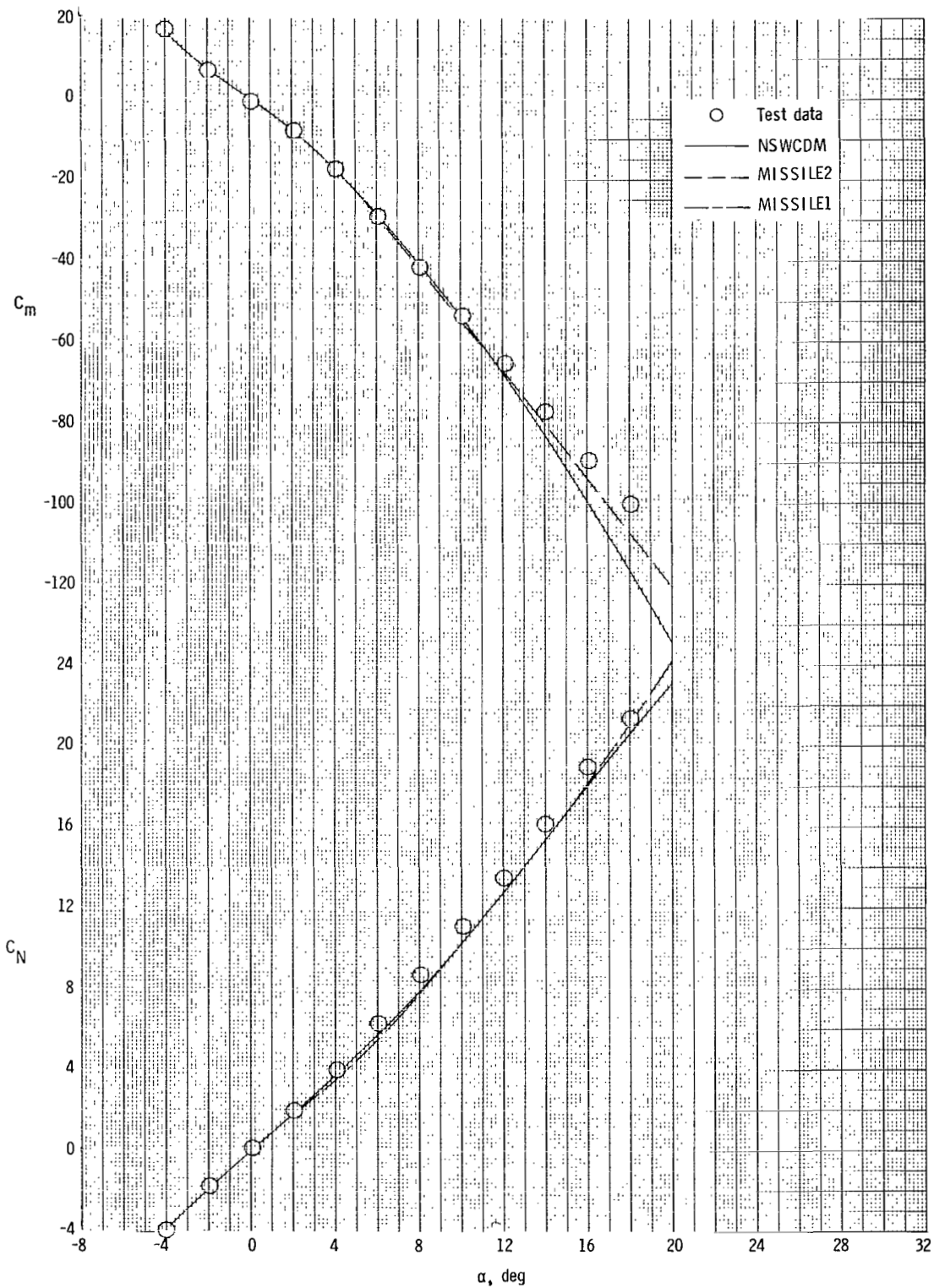
(b) $b_t/b_c = 0.75.$

Figure 14.- Continued.



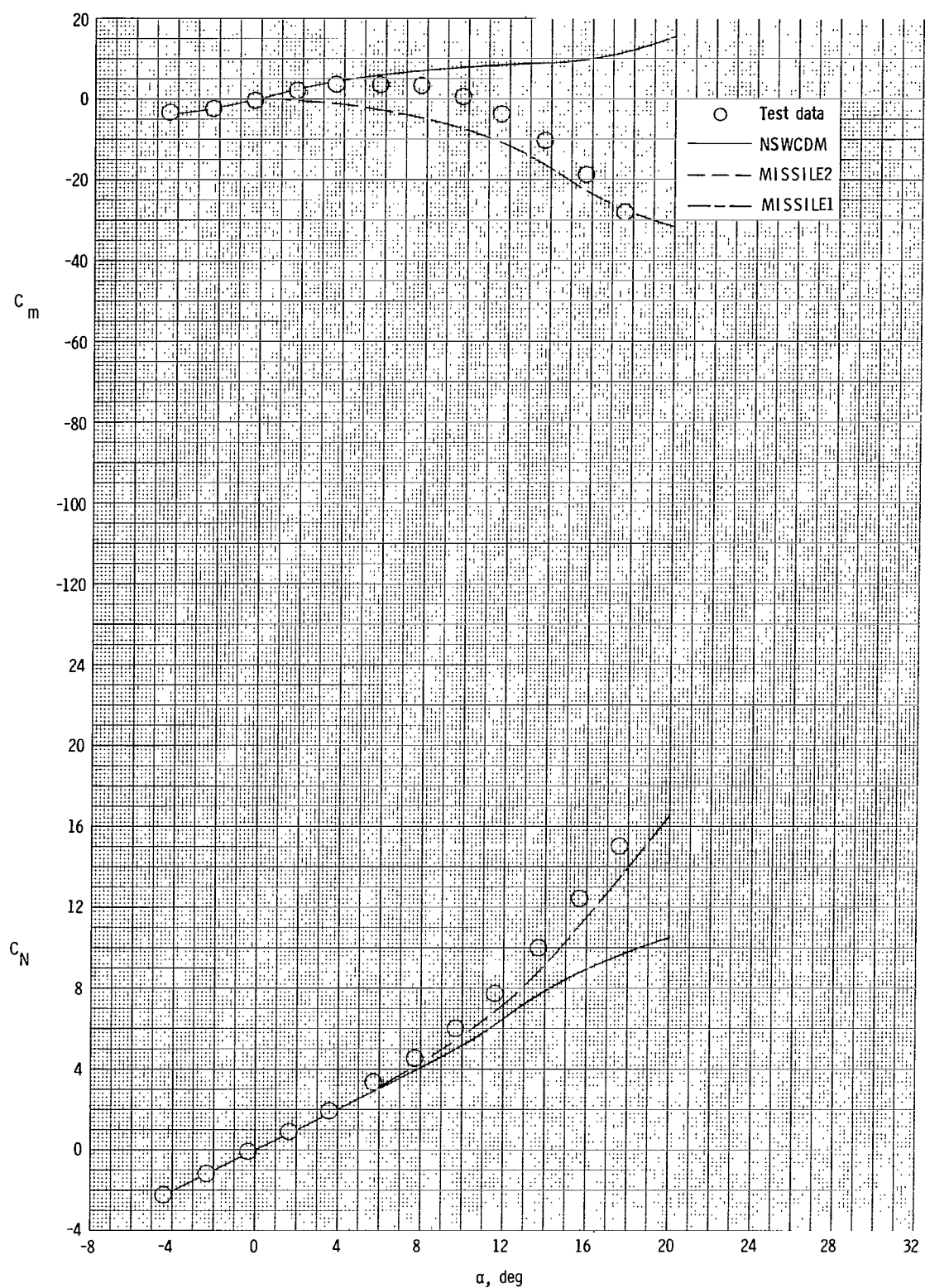
(c) $b_t/b_c = 1.07.$

Figure 14.- Continued.



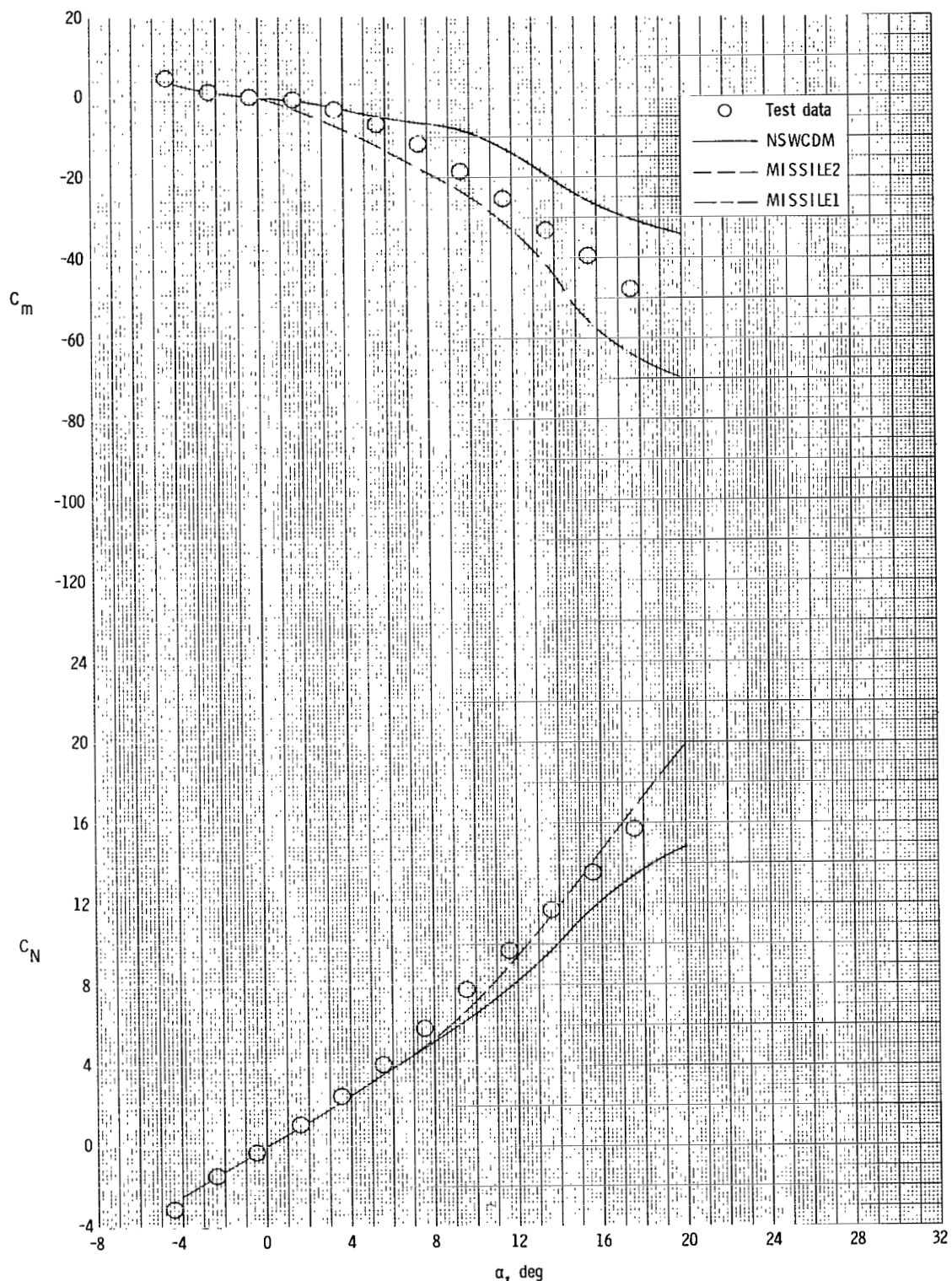
(d) $b_t/b_C = 1.25.$

Figure 14.- Concluded.



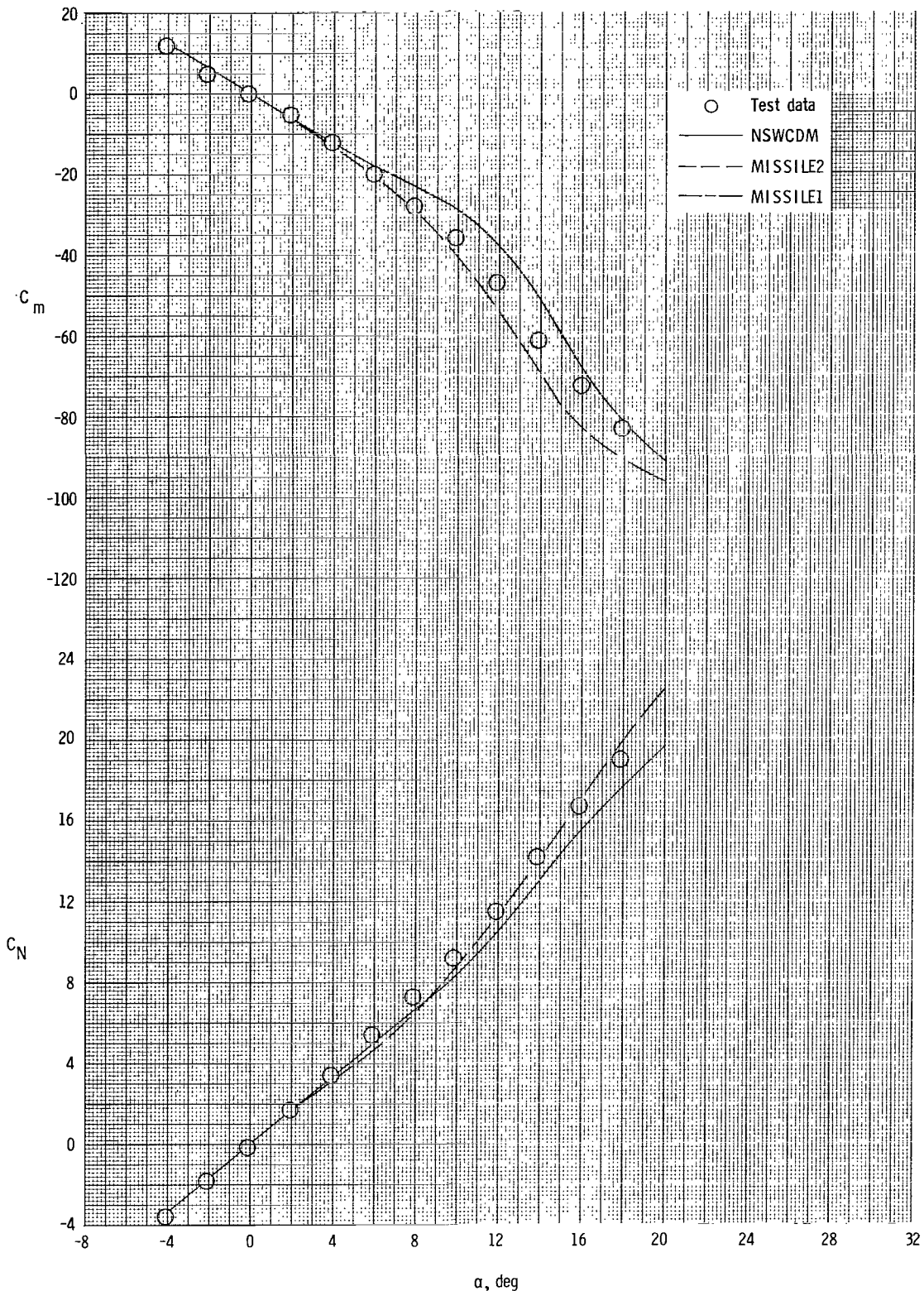
(a) $b_t/b_c = 0.47$.

Figure 15.-- Comparison of experimental and analytical longitudinal aerodynamic characteristics of each tail-fin configuration at $\phi = 45^\circ$. $M = 2.50$.



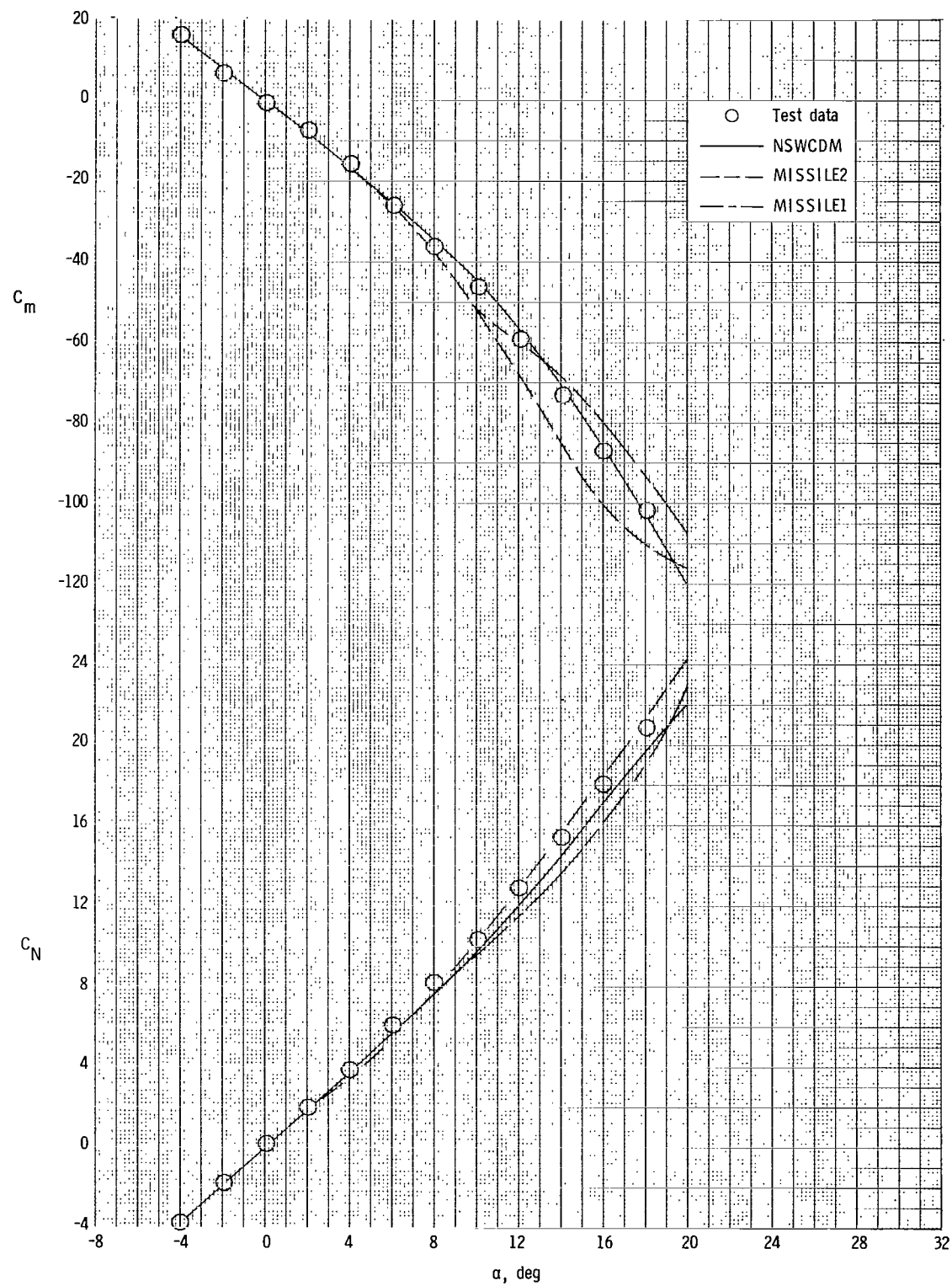
(b) $b_t/b_c = 0.75.$

Figure 15.- Continued.



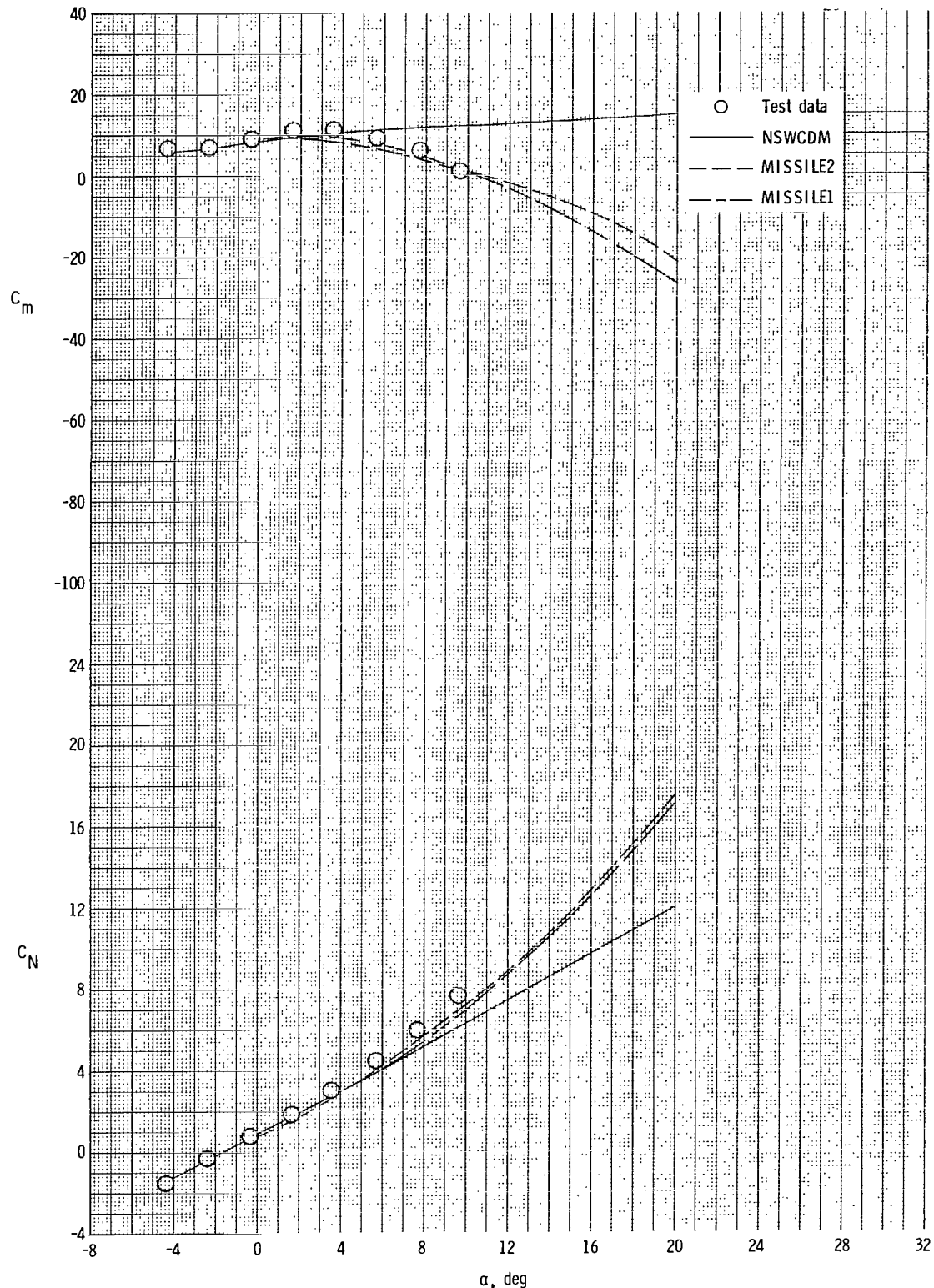
(c) $b_t/b_c = 1.07.$

Figure 15.- Continued.



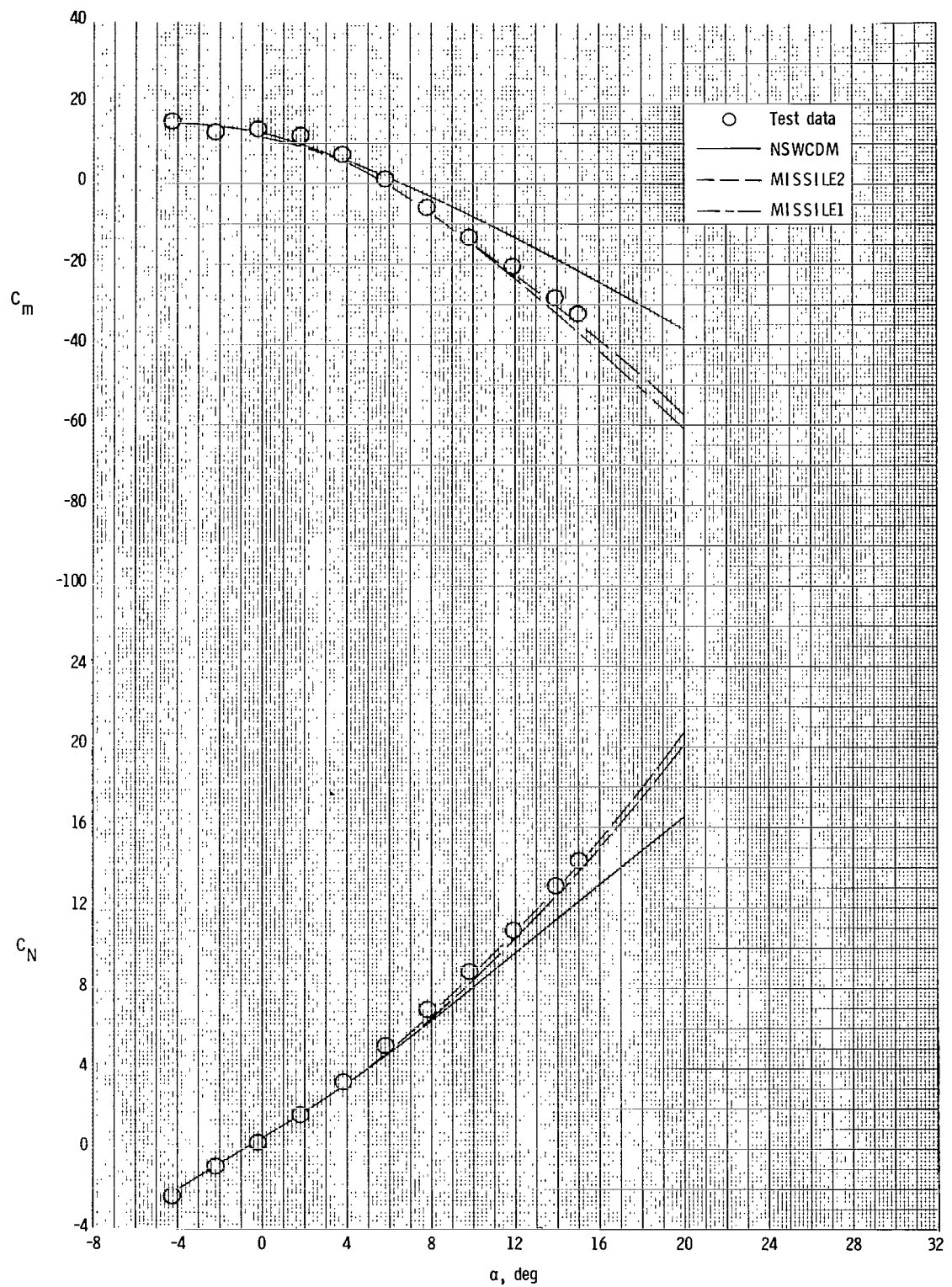
(d) $b_t/b_c = 1.25.$

Figure 15.- Concluded.



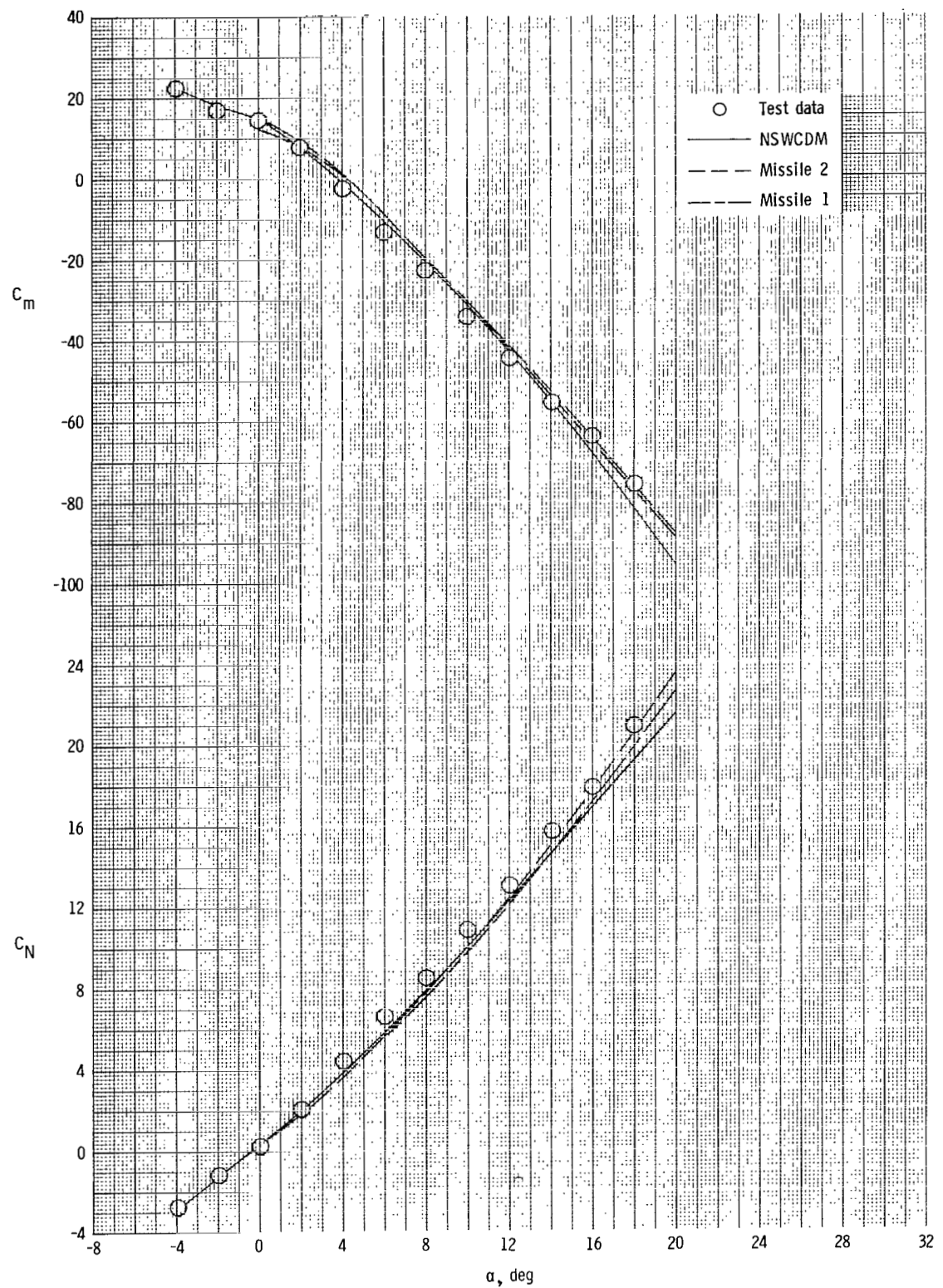
(a) $b_t/b_c = 0.47$.

Figure 16.- Comparison of experimental and analytical pitch-control characteristics of each tail-fin configuration at $\phi = 0^\circ$. $M = 2.50$; $\delta_{\text{pitch}} = 5^\circ$.



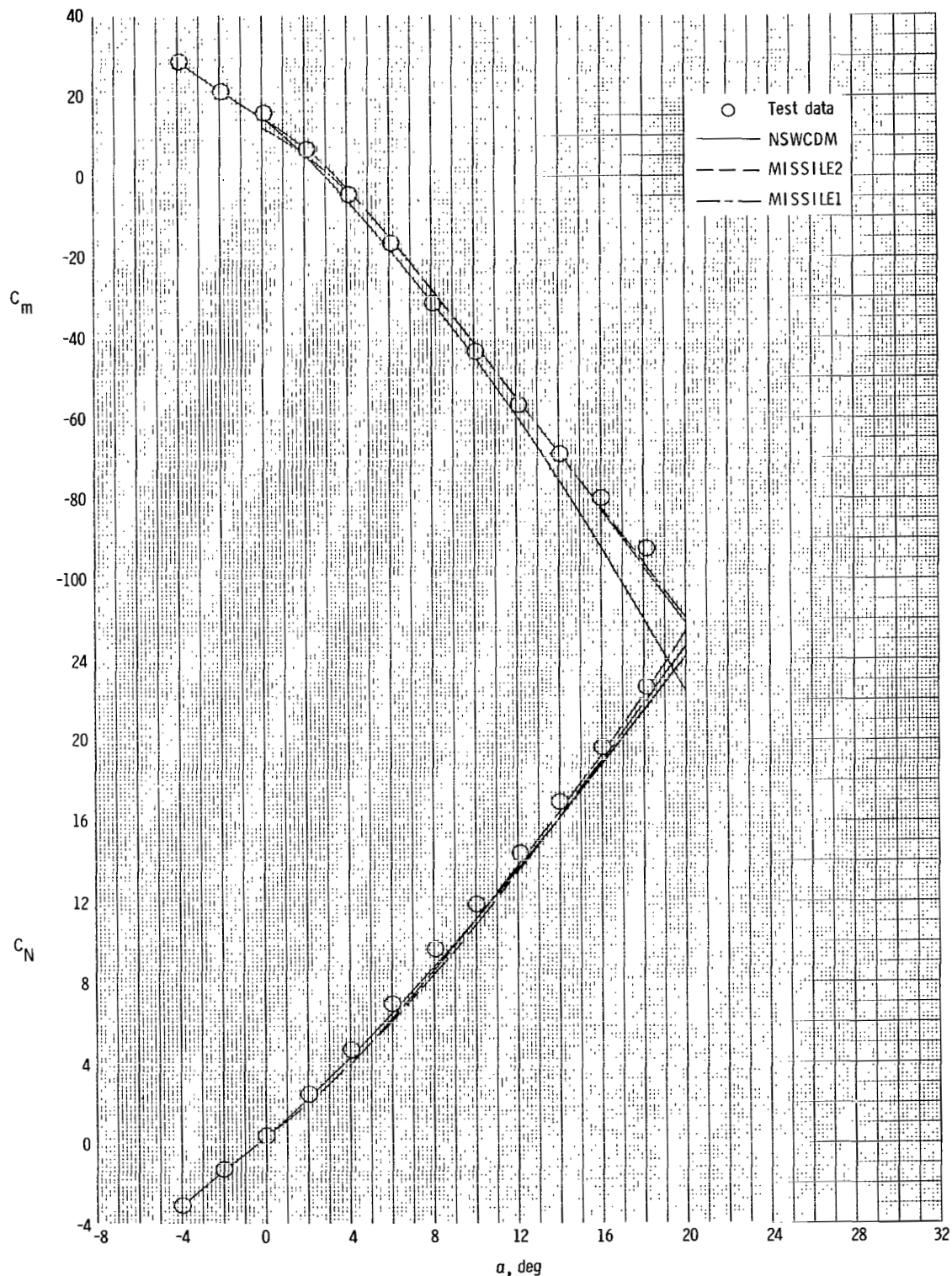
(b) $b_t/b_c = 0.75$.

Figure 16.- Continued.



(c) $b_t/b_c = 1.07.$

Figure 16.- Continued.



(d) $b_t/b_c = 1.25.$

Figure 16.- Concluded.

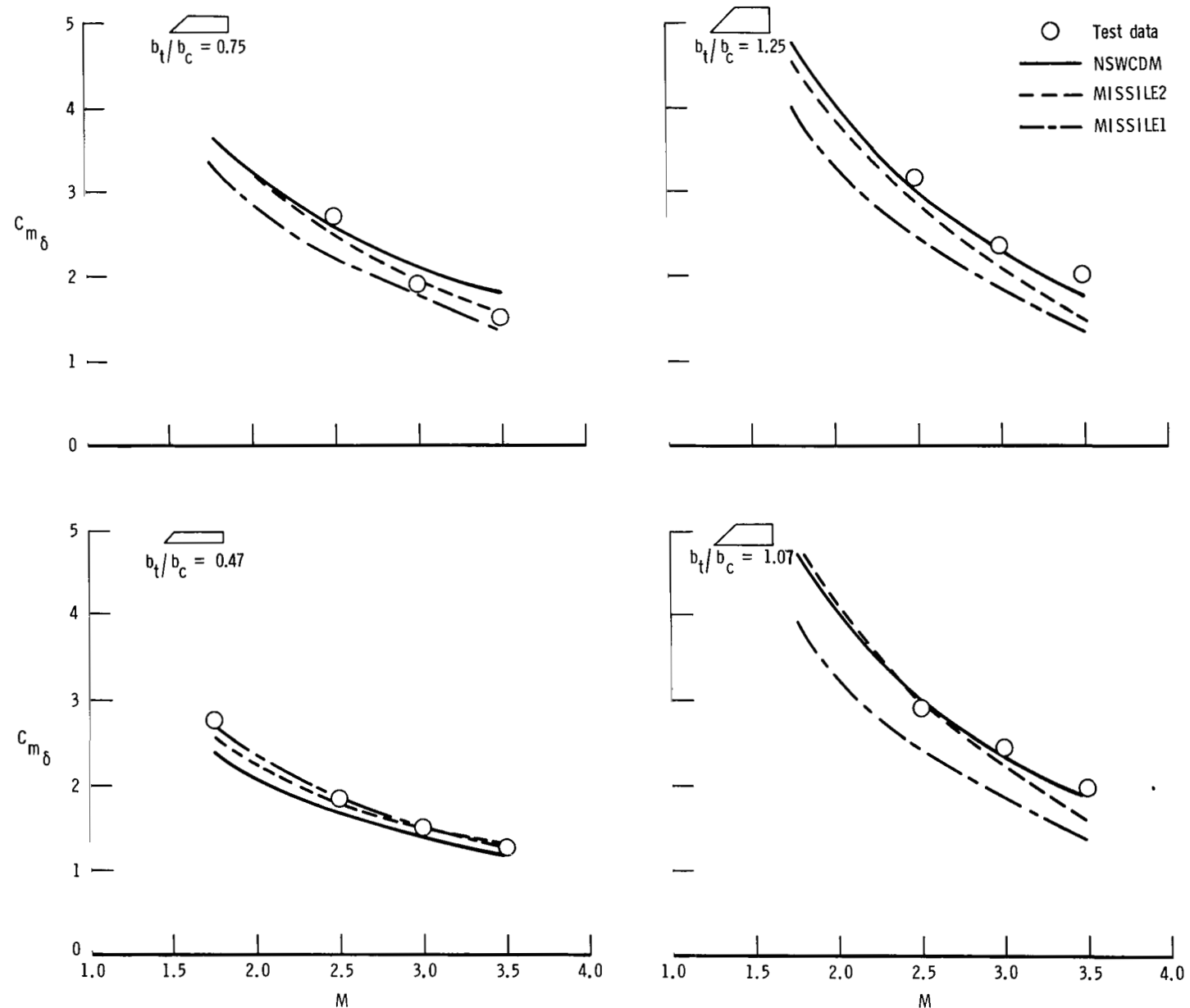
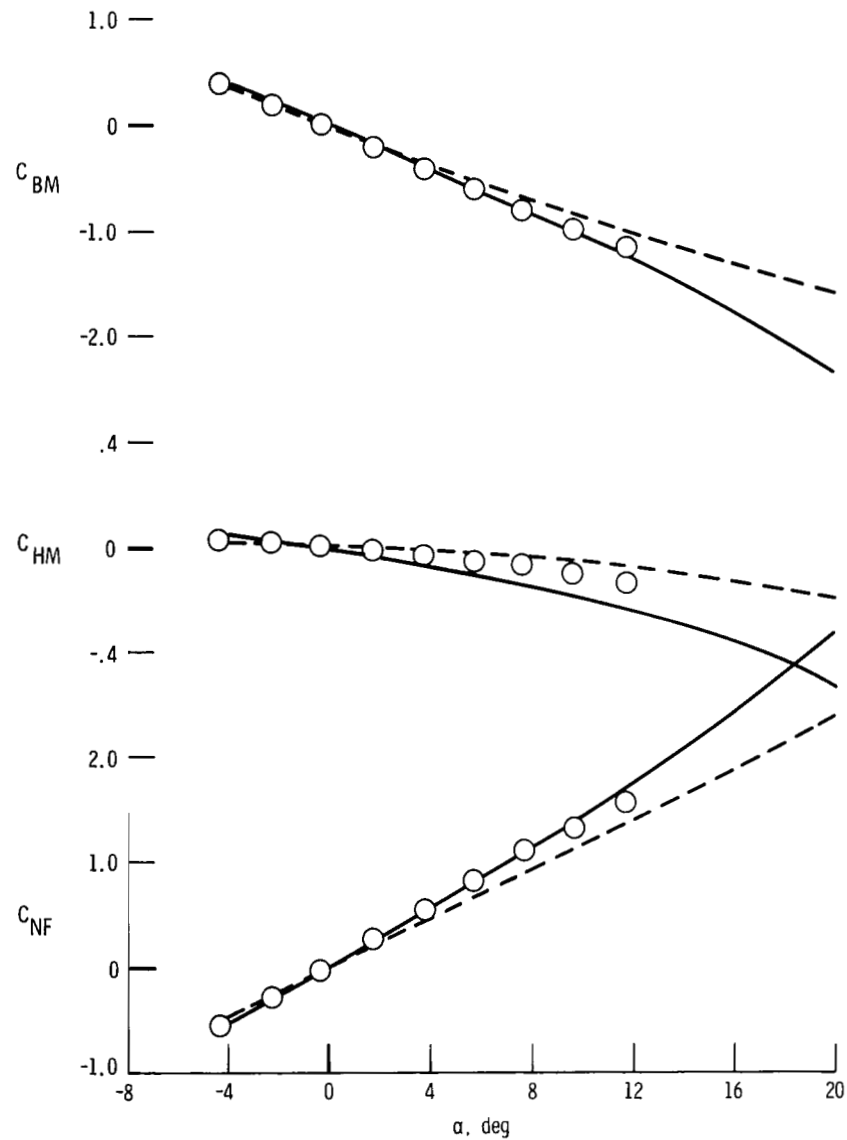
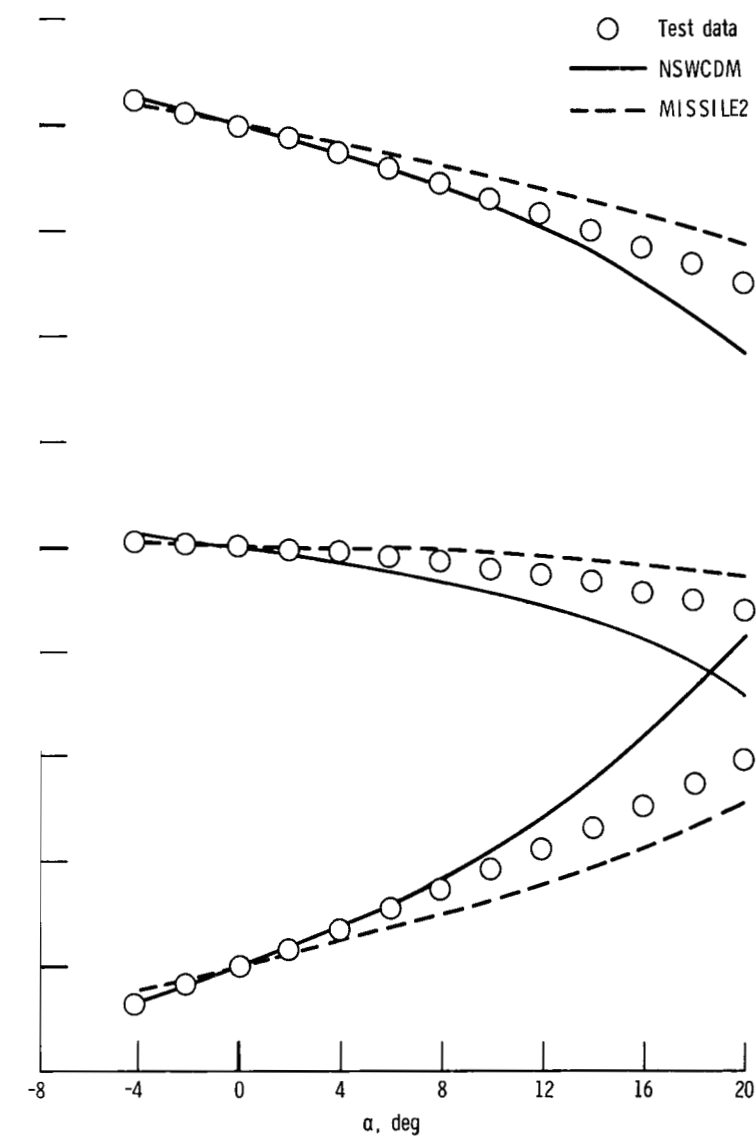


Figure 17.- Summary comparison of experimental and analytical canard pitch-control effectiveness of each tail-fin configuration at $\phi = 0^\circ$.



(a) $M = 2.50.$



(b) $M = 3.50.$

Figure 18.- Comparison of experimental and analytical canard loads (canard panel 2) in presence of body at $\phi = 0^\circ$. Zero control deflection.

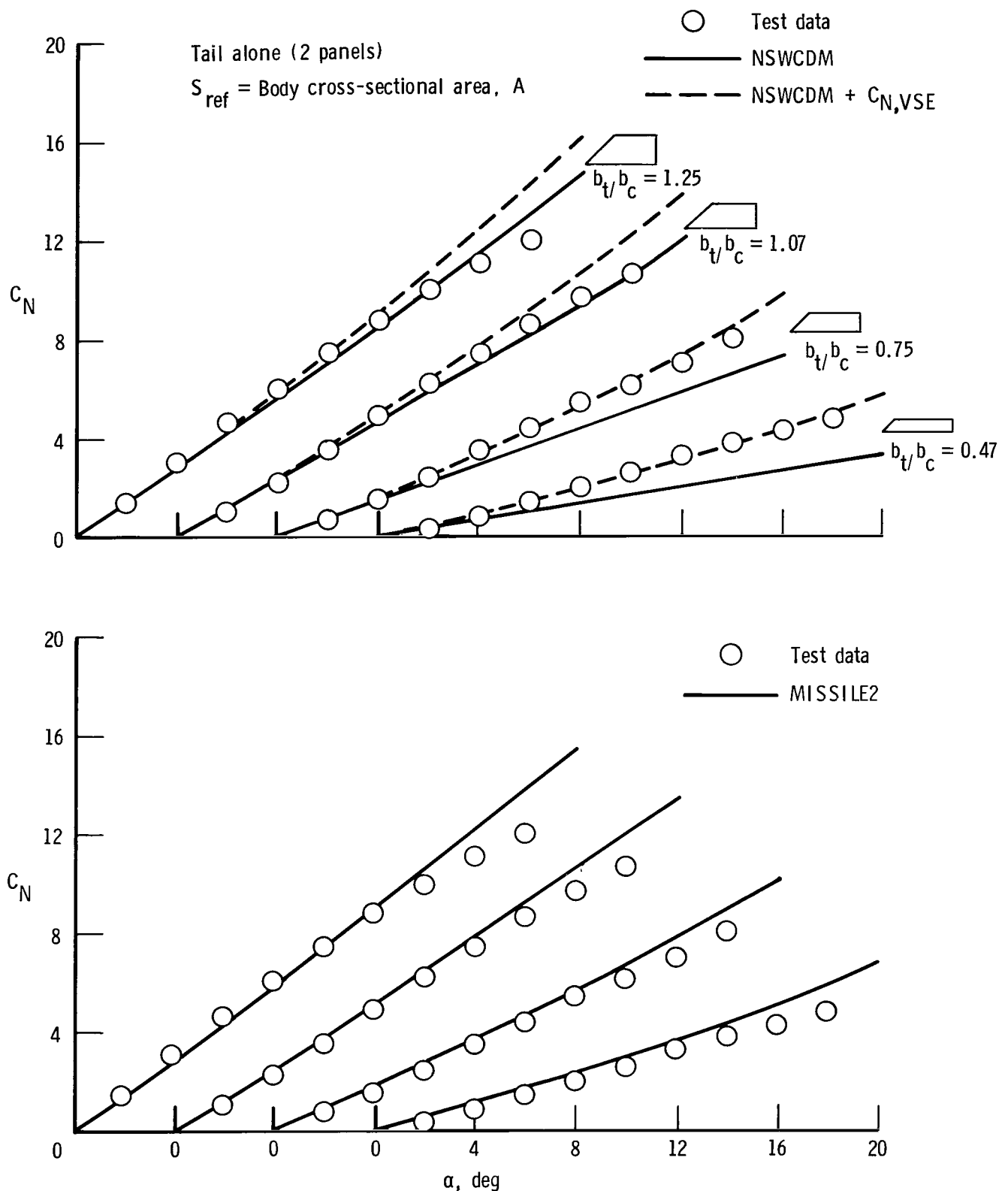
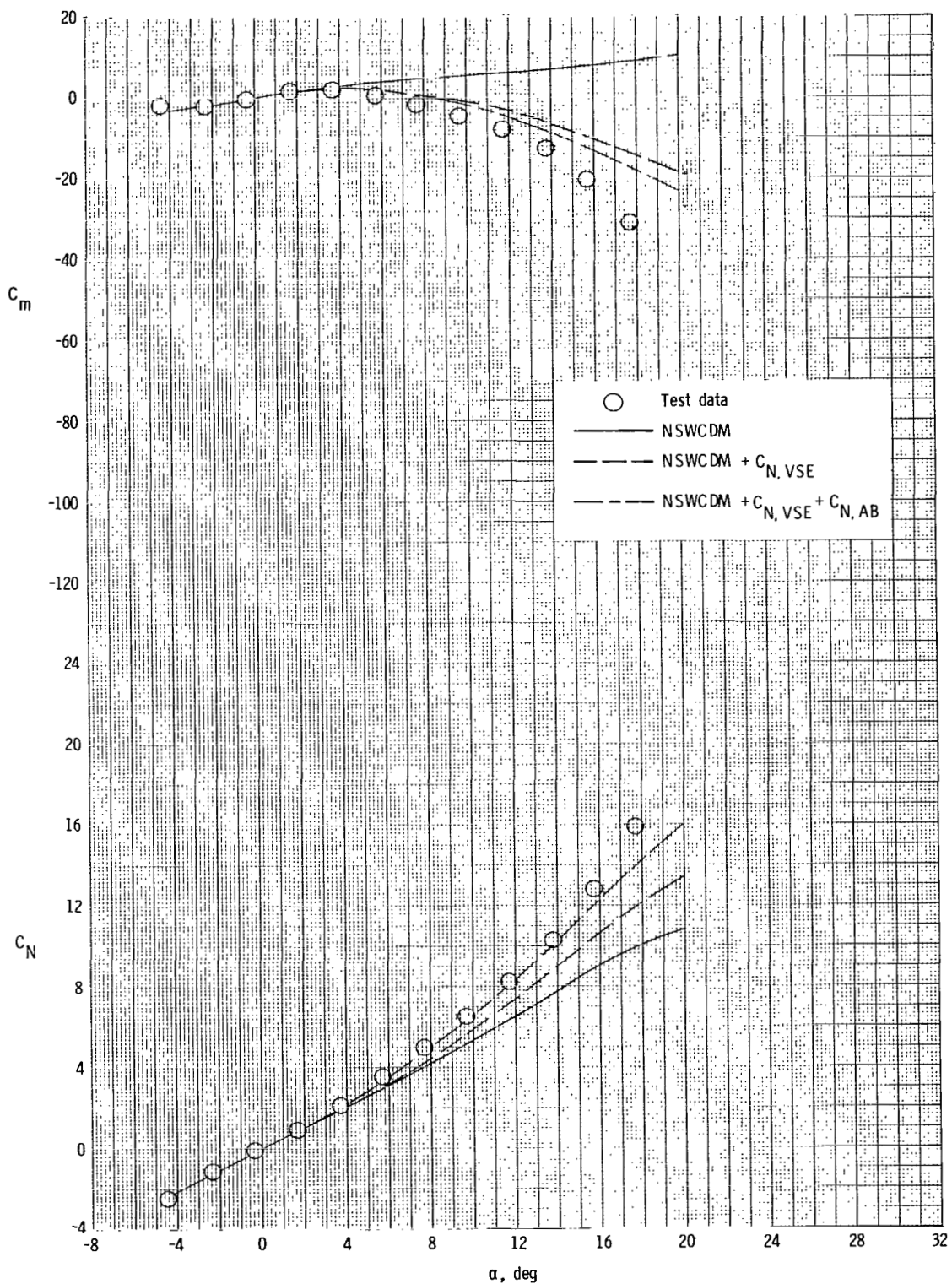
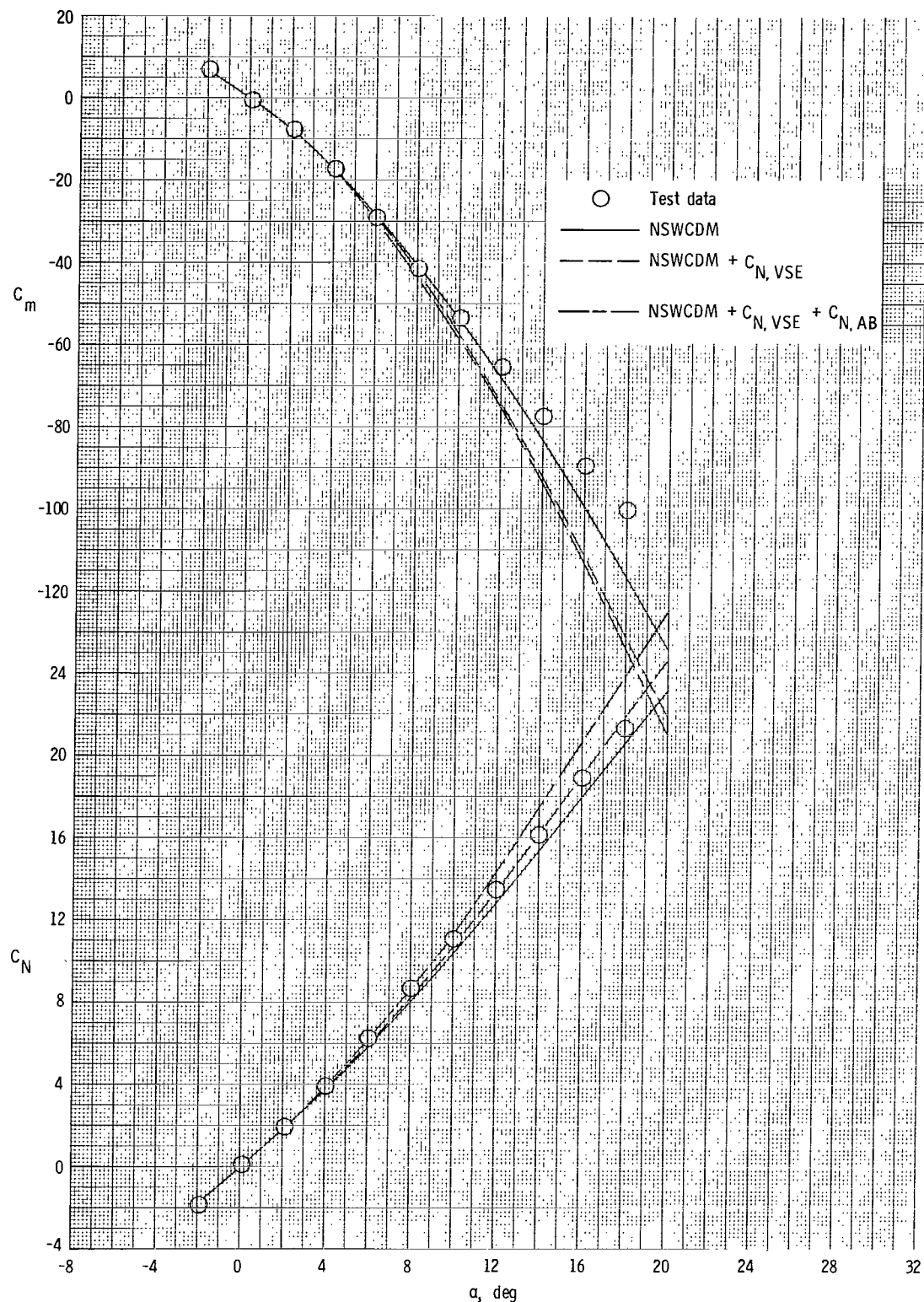


Figure 19.- Comparison of experimental and analytical normal-force coefficients for tail alone (two panels) in presence of body at $\phi = 0^\circ$. $M = 2.50$.



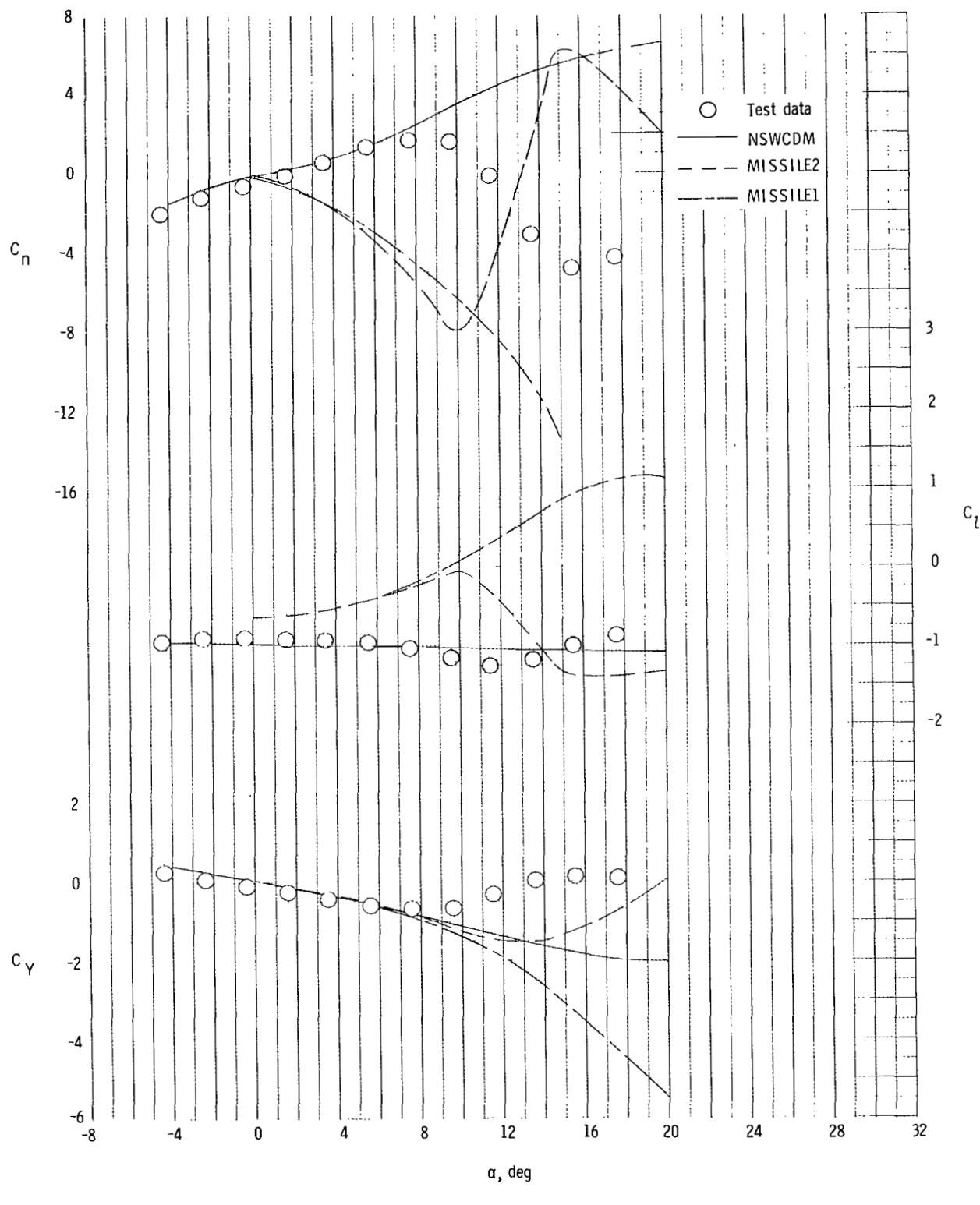
(a) $b_t/b_c = 0.47$.

Figure 20.- Comparison of experimental and analytical aerodynamic characteristics for complete model with $b_t/b_c = 0.47$ and 1.25 at $\phi = 0^\circ$. $M = 2.50$.



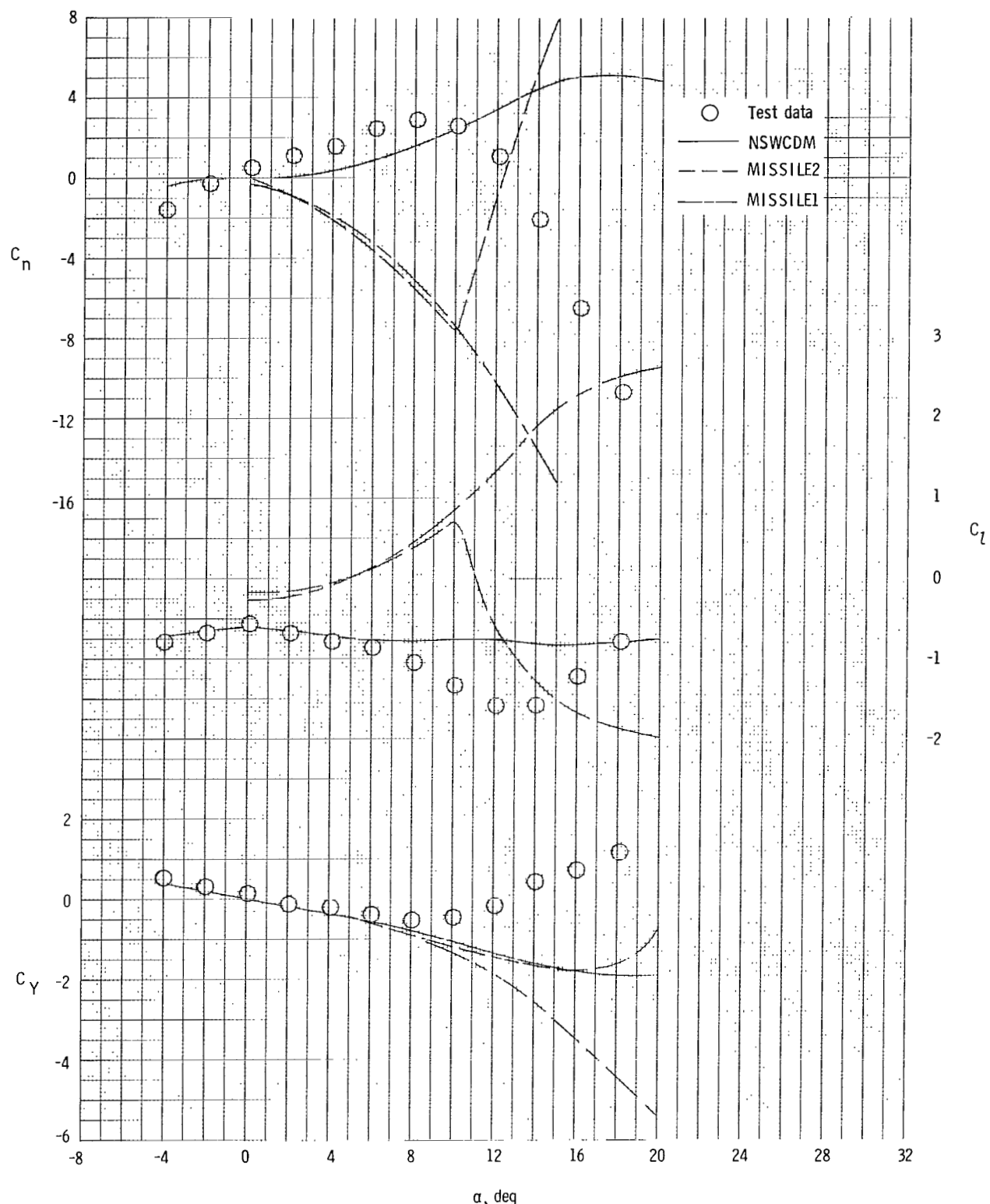
(b) $b_t/b_c = 1.25.$

Figure 20.- Concluded.



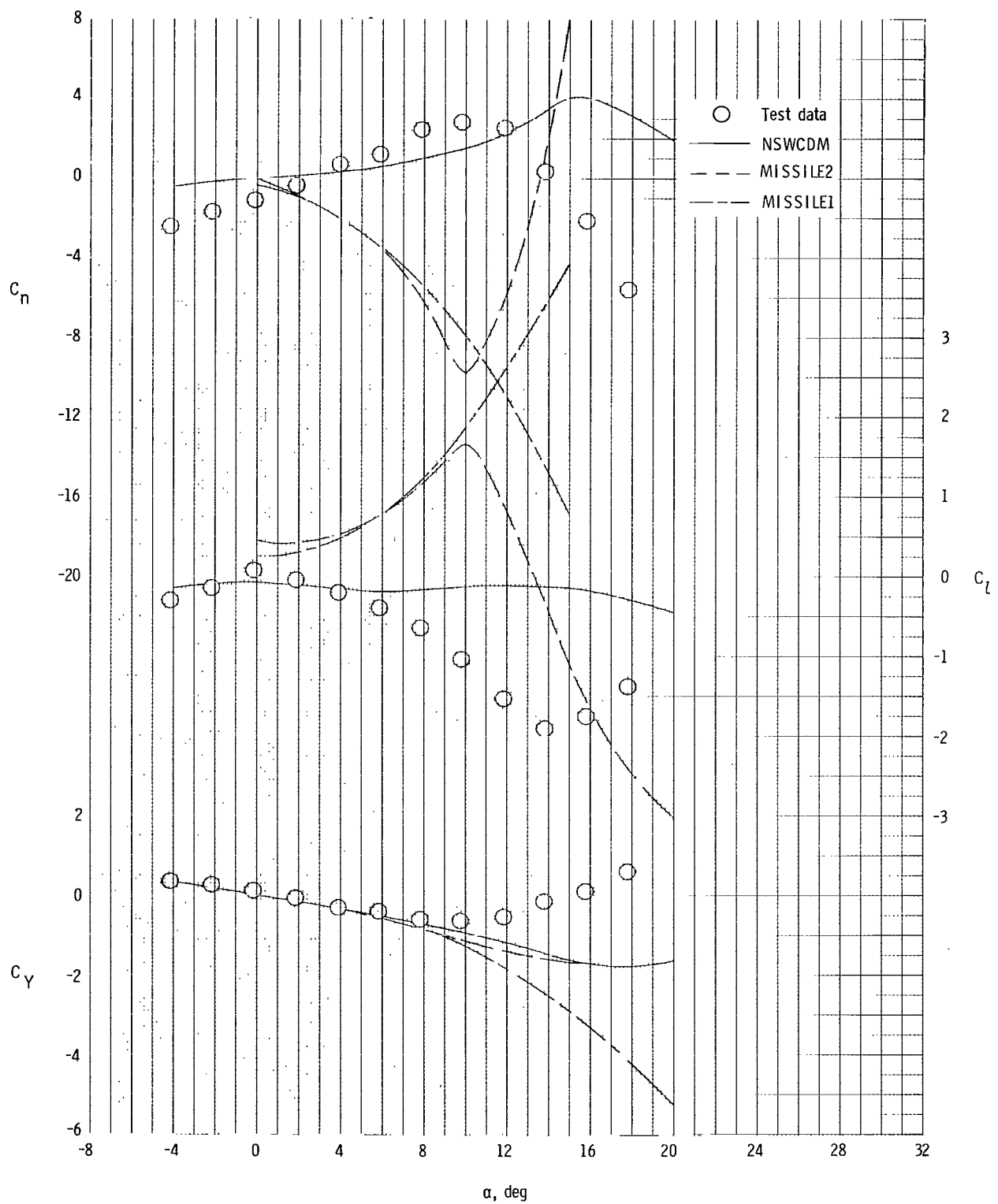
(a) $b_t/b_c = 0.47$.

Figure 21.- Comparison of experimental and analytical roll-control characteristics of each tail-fin configuration for $\delta_{roll} = -10^\circ$ at $\phi = 0^\circ$. $M = 2.50$.



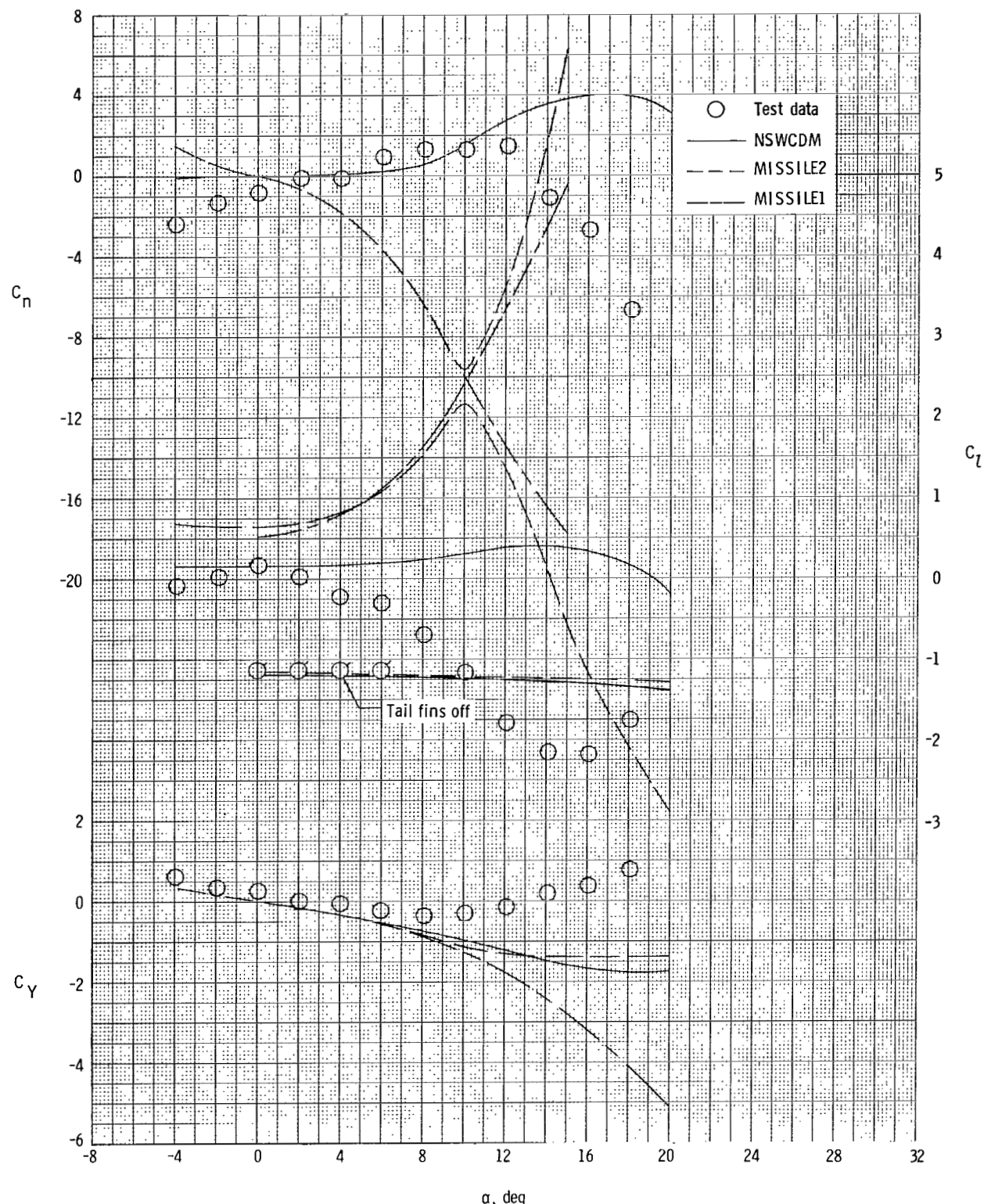
(b) $b_t/b_c = 0.75.$

Figure 21.- Continued.



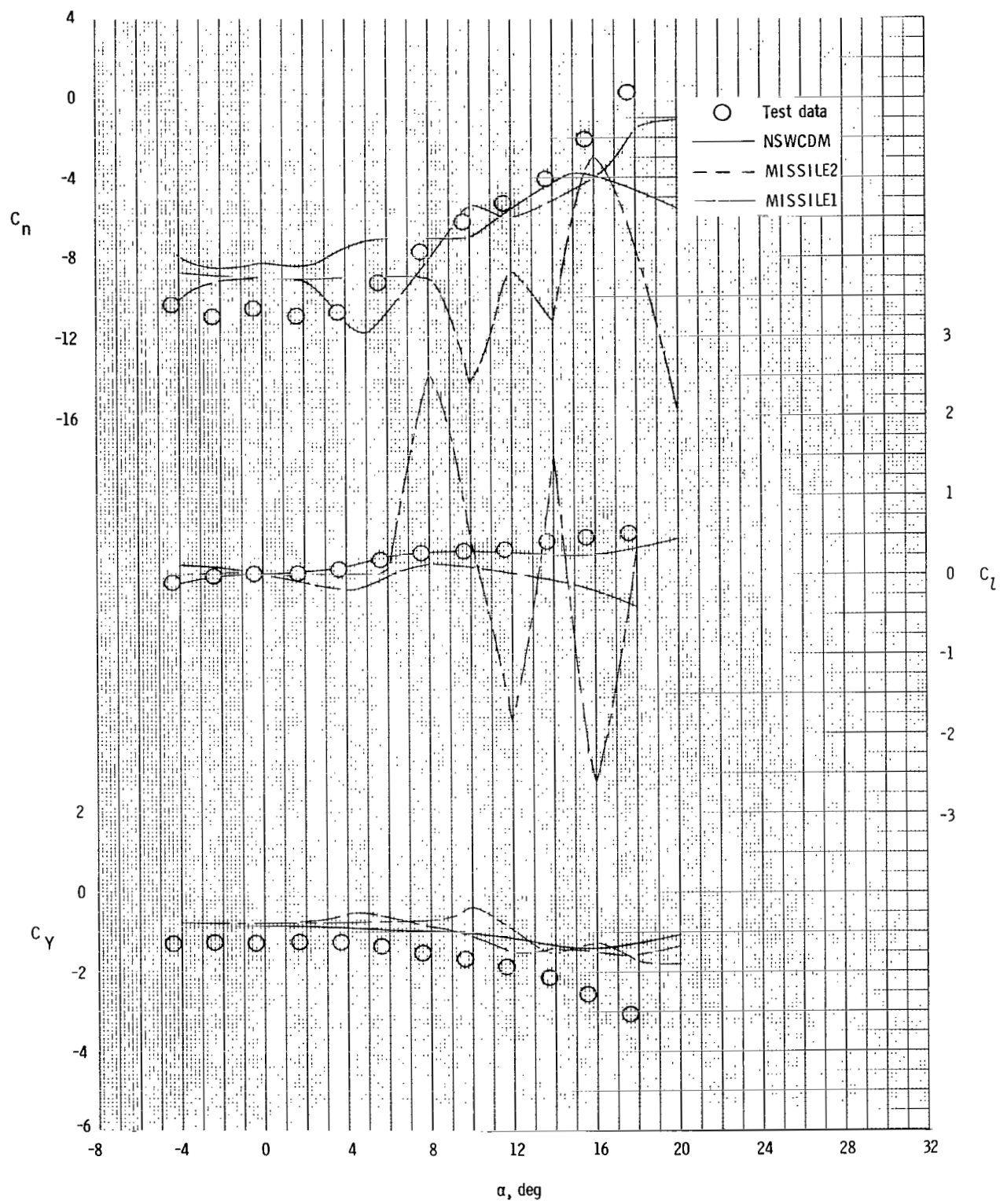
(c) $b_t/b_c = 1.07$.

Figure 21.- Continued.



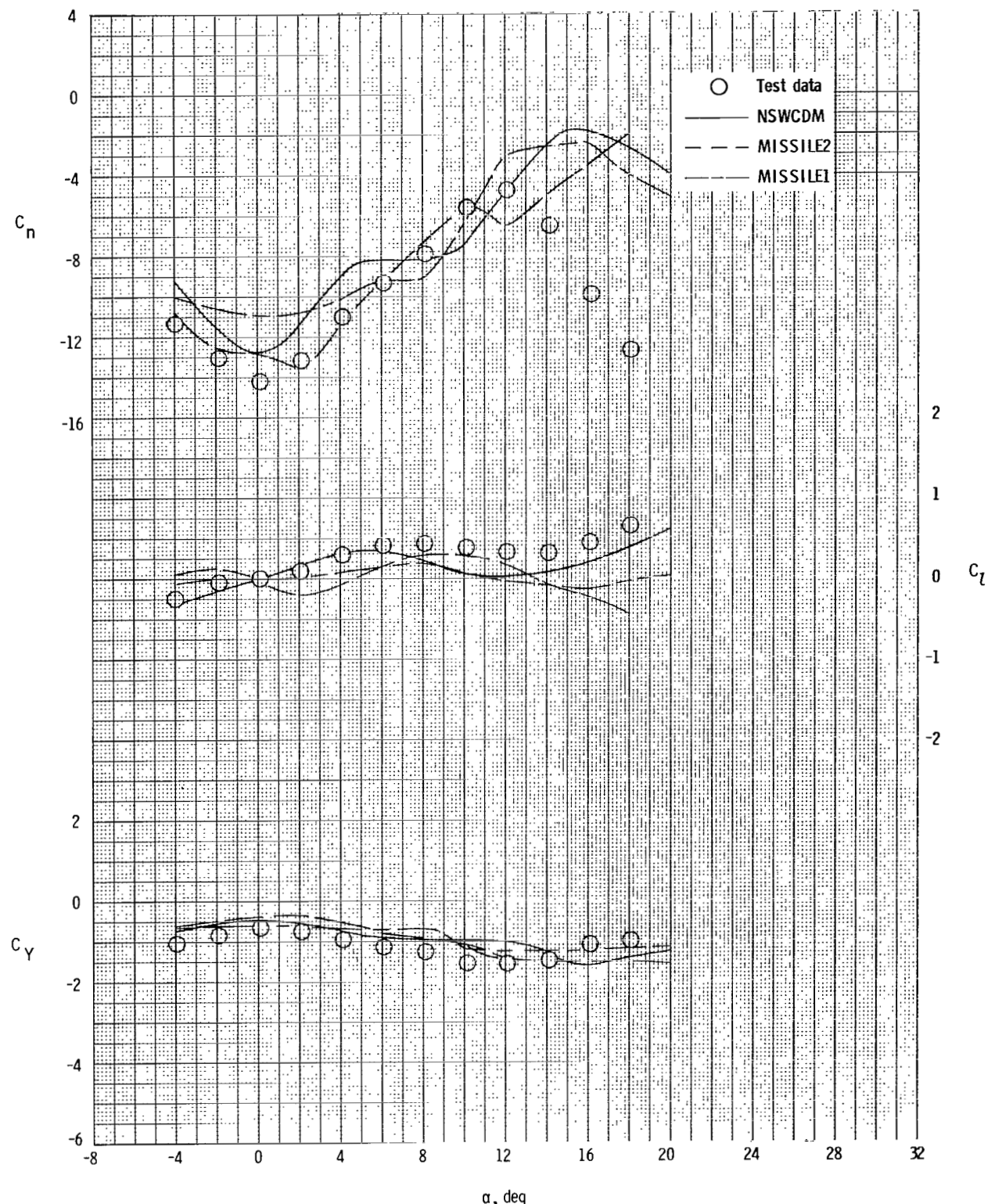
(d) $b_t/b_c = 1.25.$

Figure 21.- Concluded.



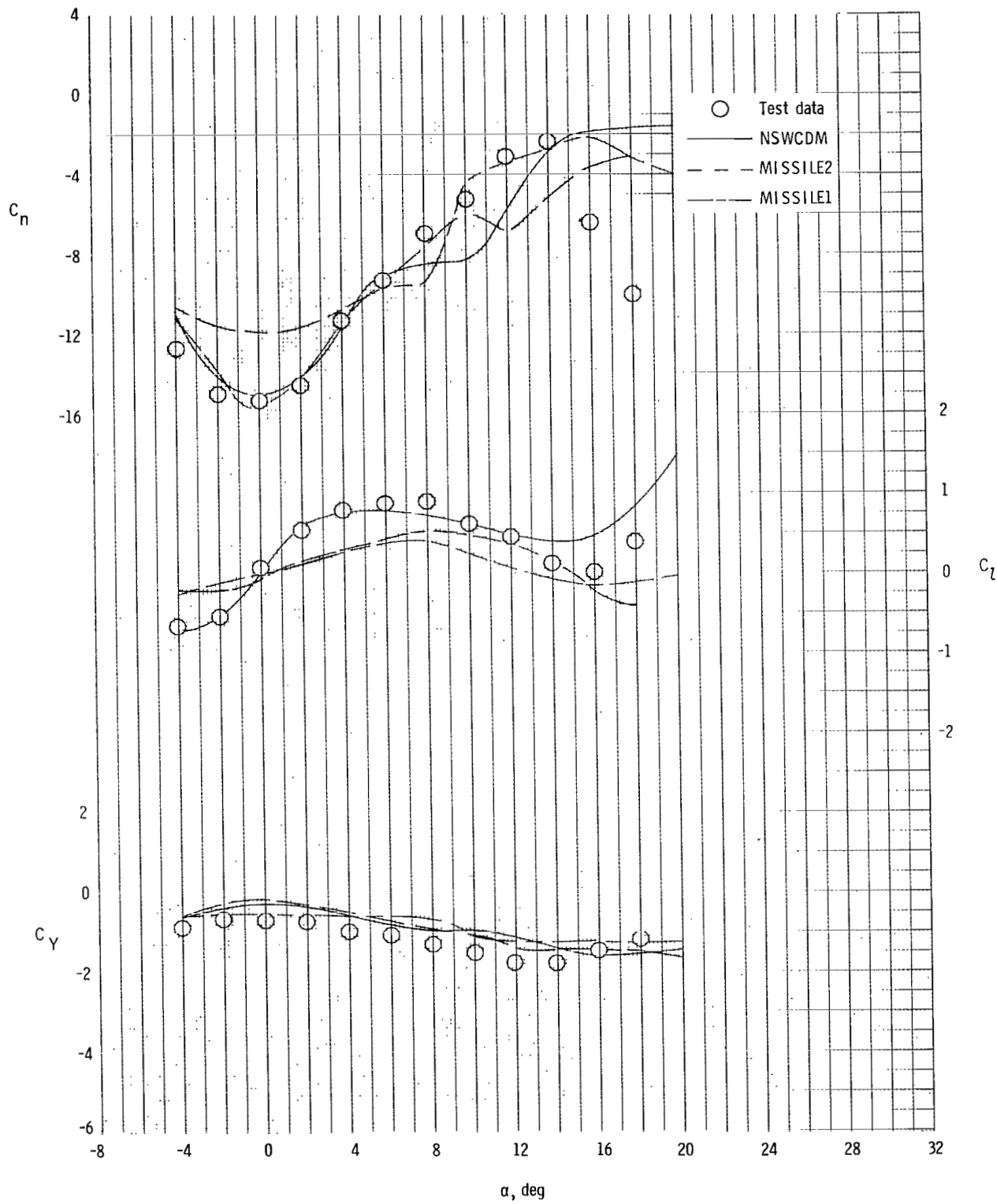
(a) $b_t/b_C = 0.47$.

Figure 22.- Comparison of experimental and analytical yaw-control characteristics of each tail-fin configuration for $\delta_{yaw} = -5^\circ$ at $\phi = 0^\circ$. $M = 2.50$.



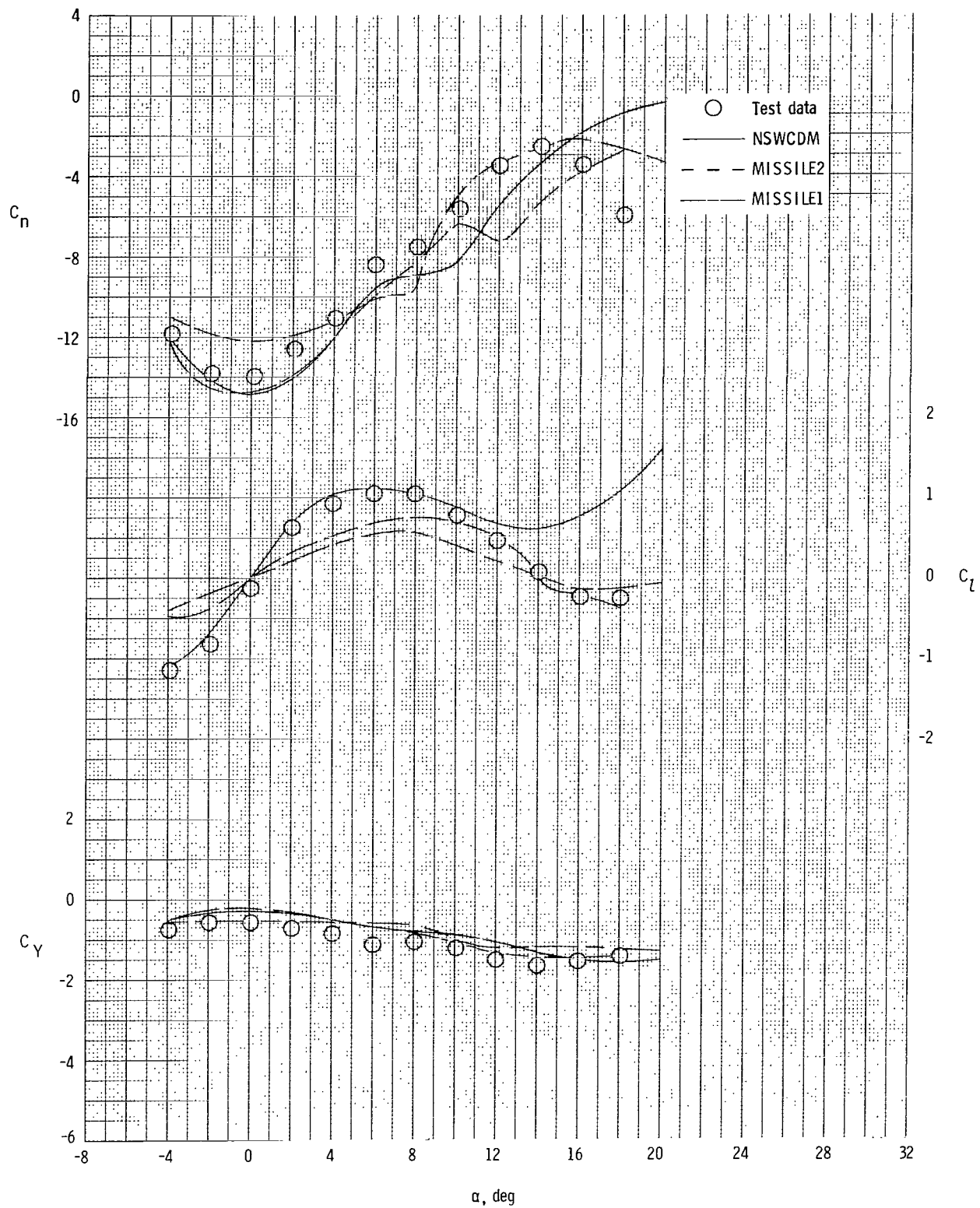
(b) $b_t/b_c = 0.75.$

Figure 22.- Continued.



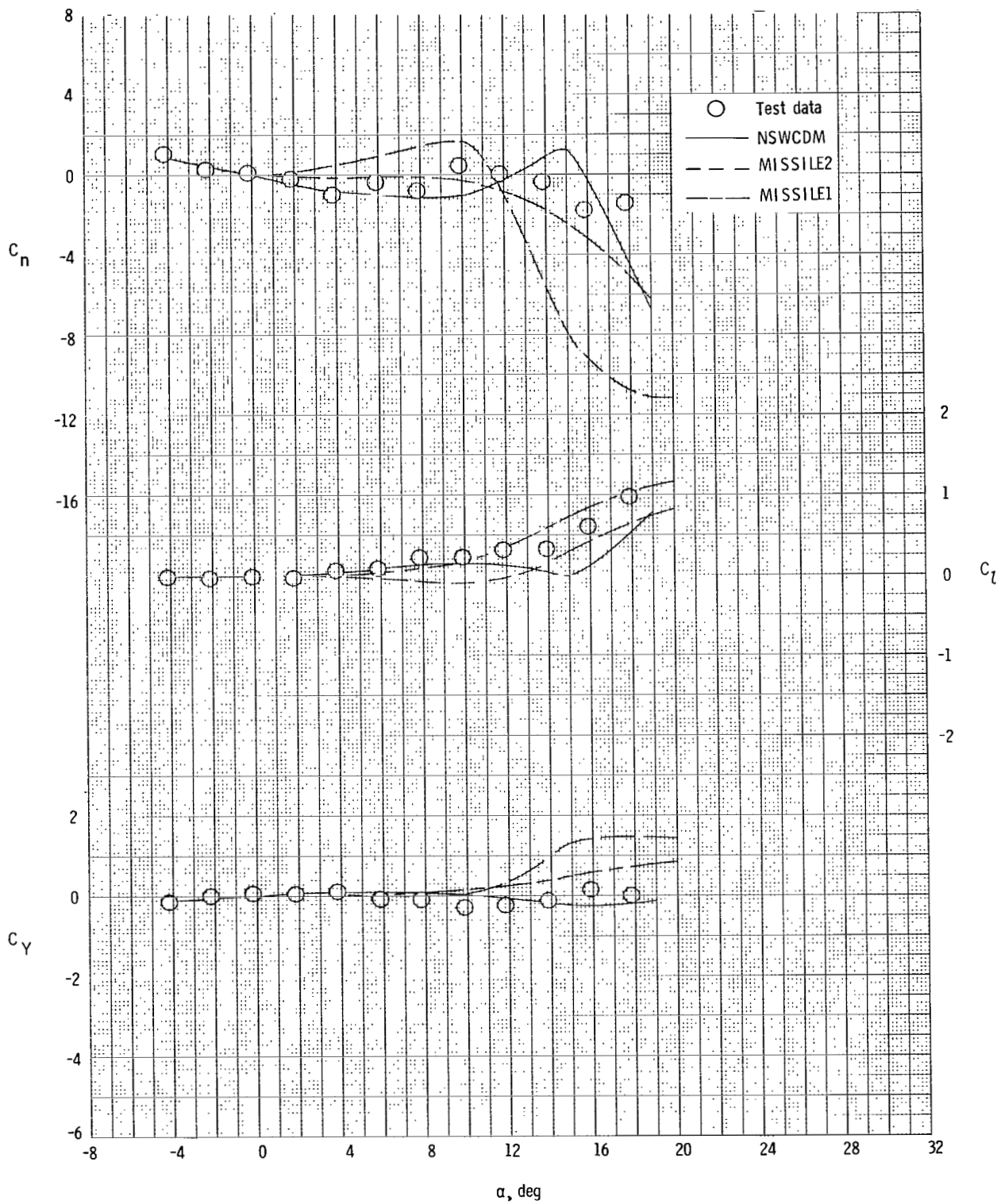
(c) $b_t/b_c = 1.07..$

Figure 22.- Continued.



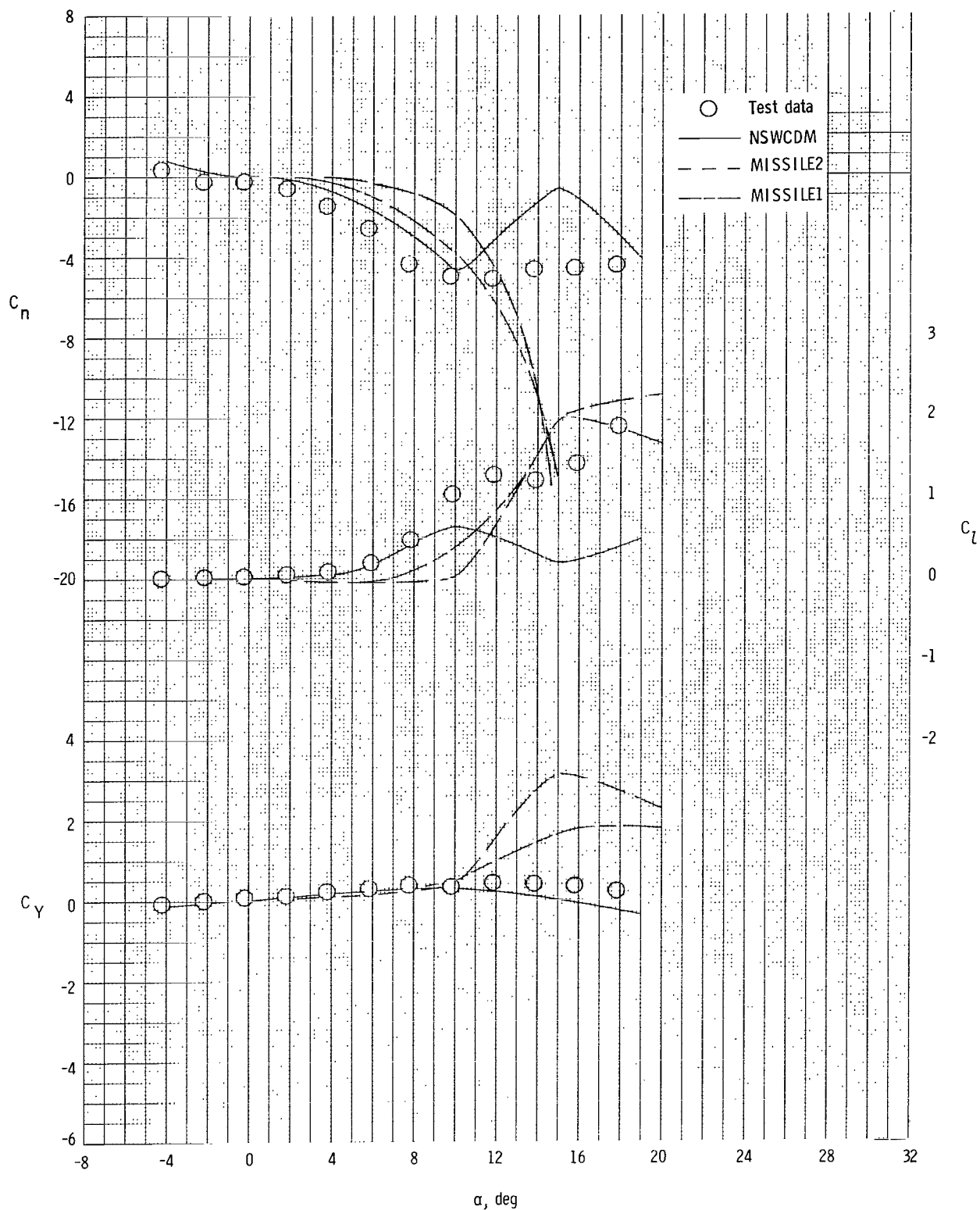
(d) $b_t/b_C = 1.25.$

Figure 22.- Concluded.



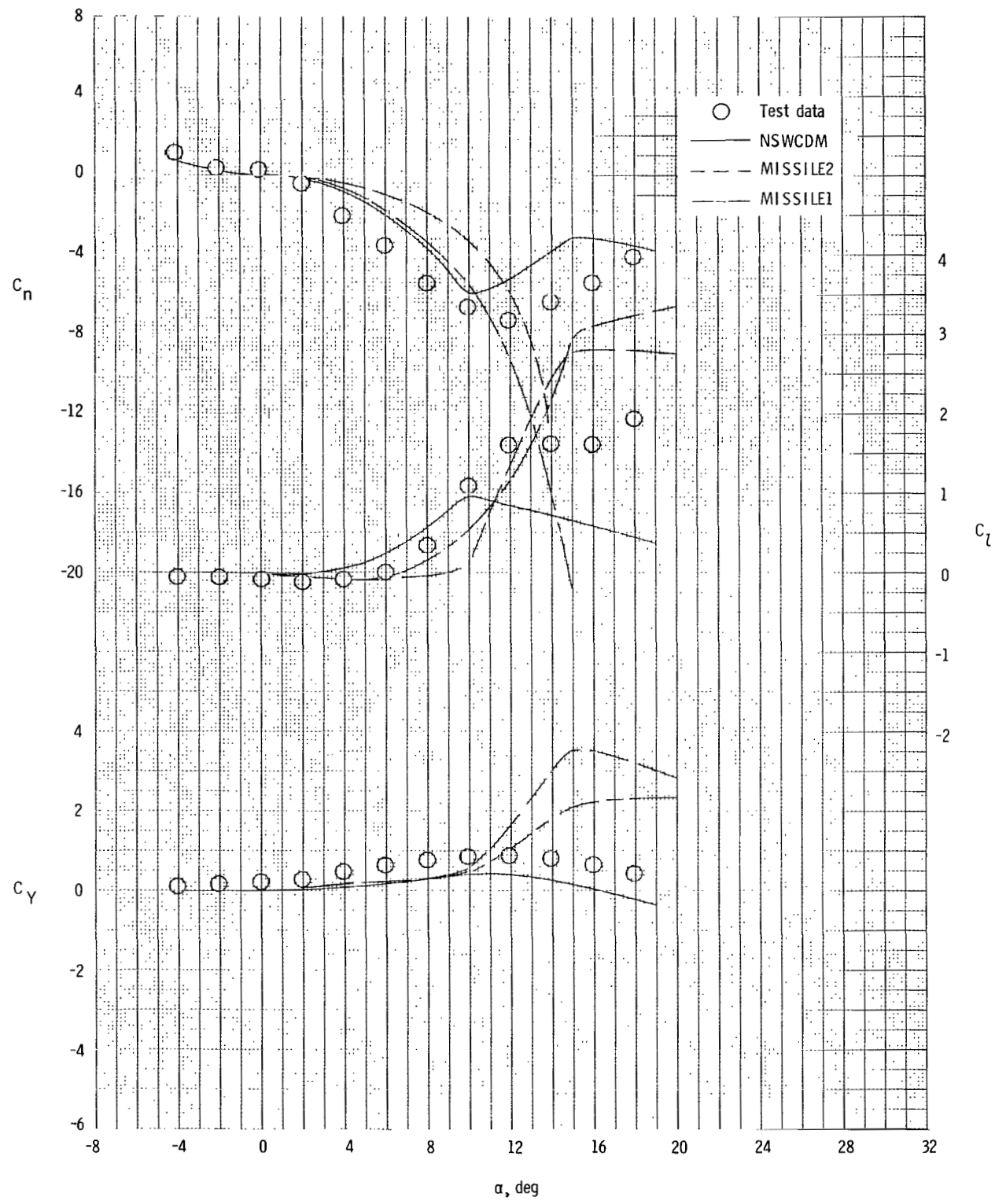
(a) $b_t/b_c = 0.75$.

Figure 23.- Comparison of experimental and analytical lateral-directional aerodynamic characteristics of selected tail-fin configurations at $\phi = 26.57^\circ$. $M = 1.75$.



(b) $b_t/b_c = 1.07.$

Figure 23.- Continued.



(c) $b_t/b_c = 1.25.$

Figure 23.- Concluded.

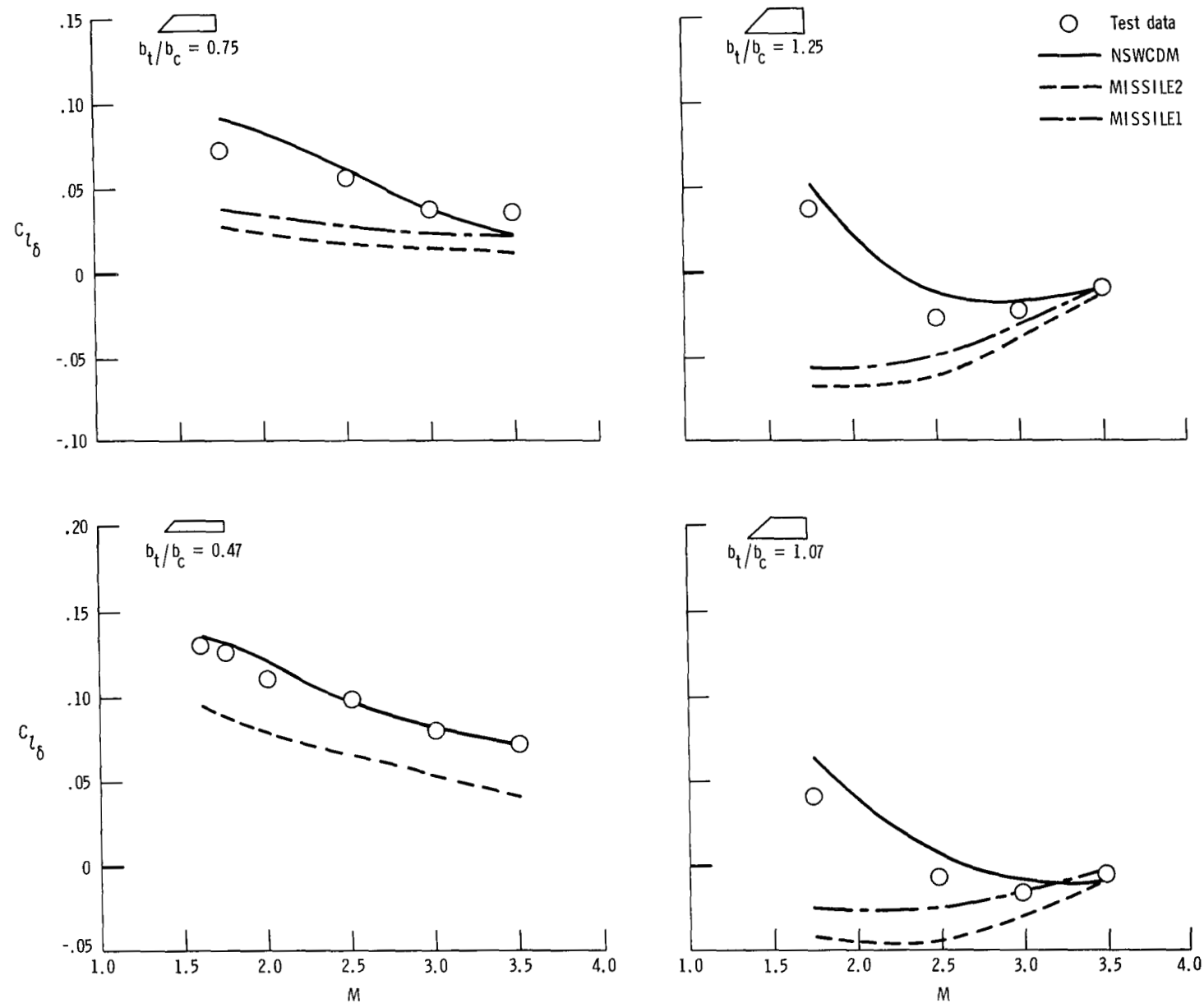


Figure 24.- Summary comparison of experimental and analytical canard roll-control effectiveness of each tail-fin configuration at $\phi = 0^\circ$. $\alpha = 0^\circ$.

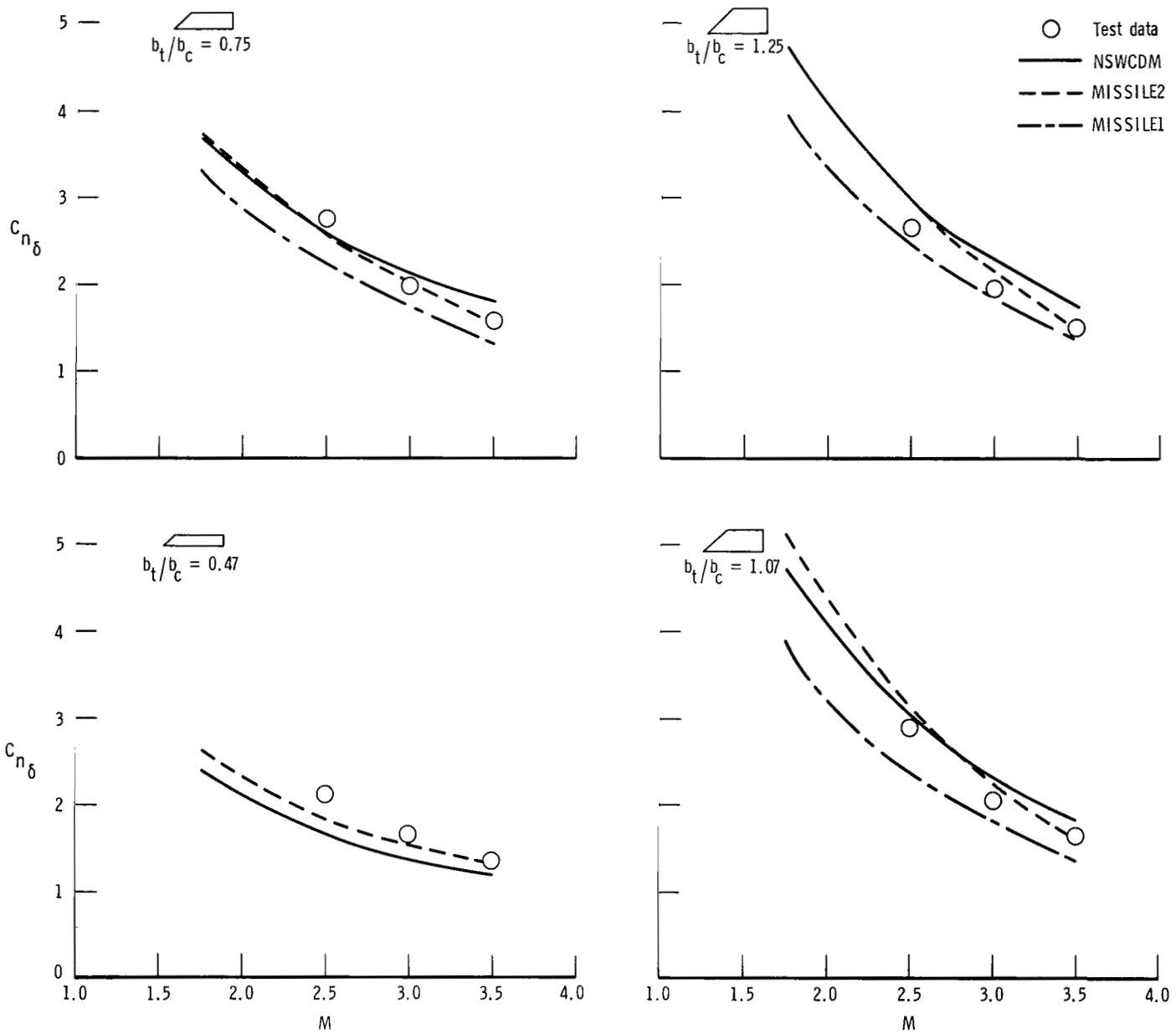
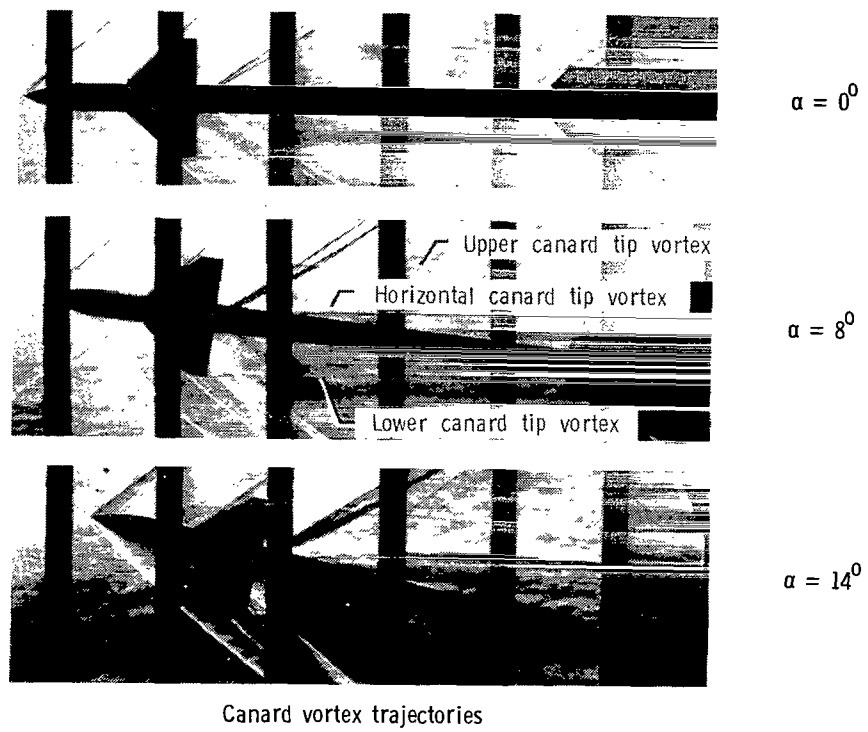
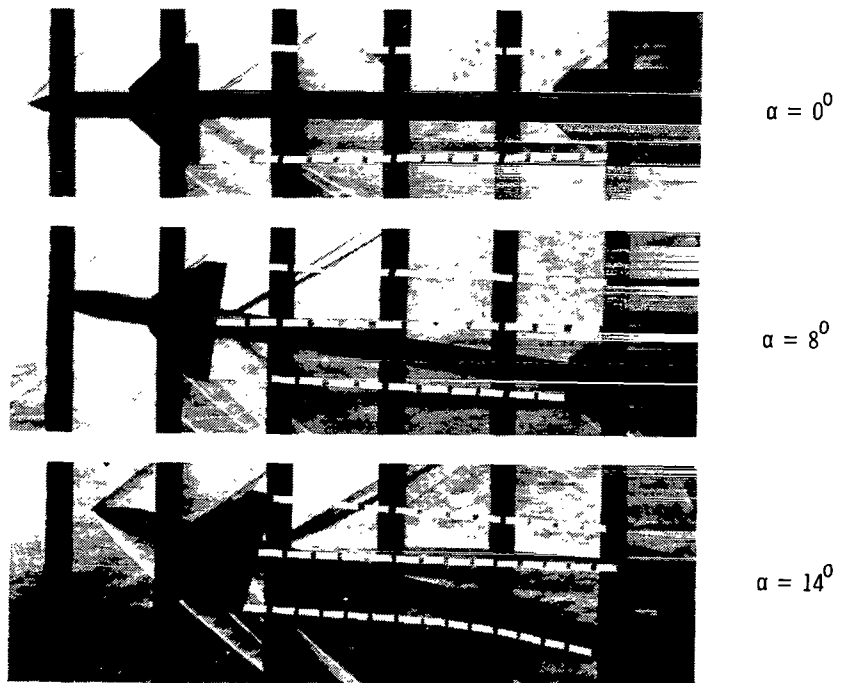


Figure 25.— Summary comparison of experimental and analytical canard yaw-control effectiveness of each tail-fin configuration at $\phi = 0^\circ$. $\alpha = 0^\circ$.



Canard vortex trajectories

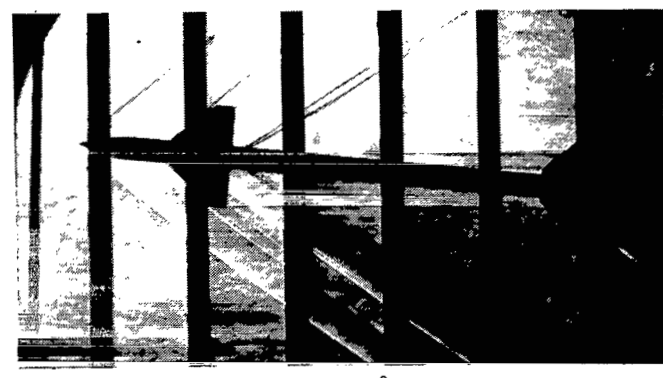
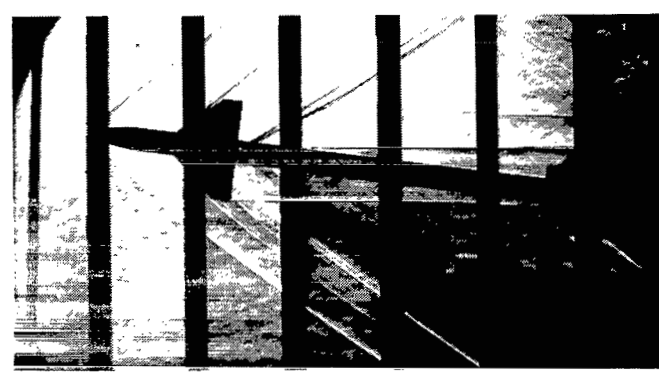
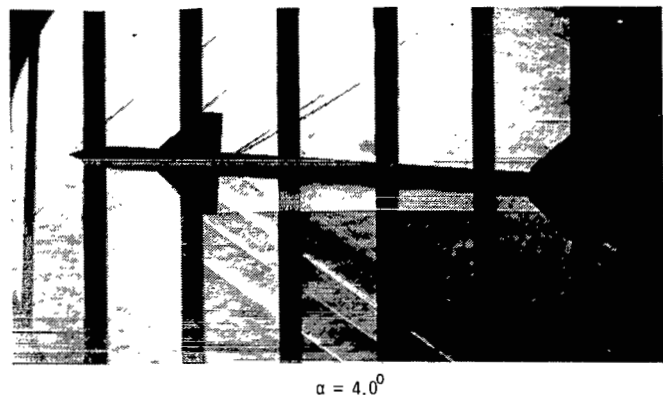
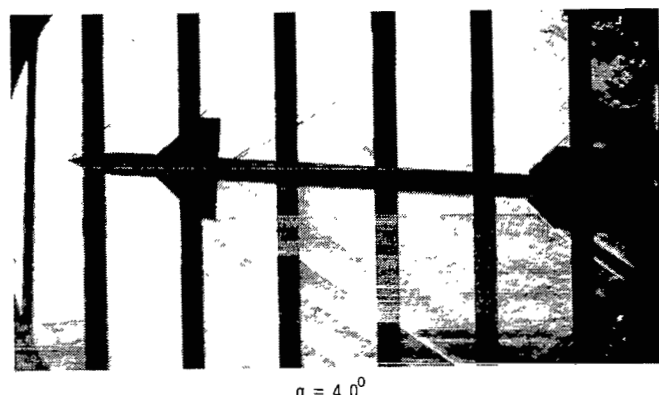
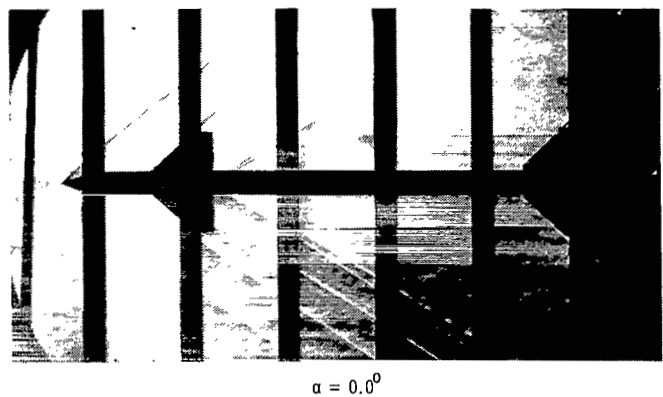
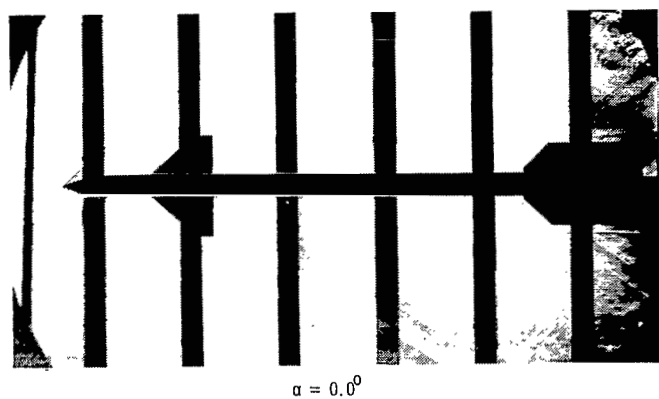


Predicted canard tip vortex trajectories (MISSILEI)

$$(a) \quad b_t/b_c = 0.47.$$

L-83-86

Figure 26.- Schlieren photographs of selected tail-fin configurations with canard yaw control. $\phi = 0^\circ$; $M = 1.75$; $\delta_{yaw} = -5^\circ$.



(b) $b_t/b_c = 0.75.$

(c) $b_t/b_c = 1.07.$

L-83-87

Figure 26.- Concluded.

1. Report No. NASA TP-2157	2. Government Accession No.	3. Recipient's Catalog No.	
4. Title and Subtitle EFFECT OF TAIL-FIN SPAN ON STABILITY AND CONTROL CHARACTERISTICS OF A CANARD-CONTROLLED MISSILE AT SUPERSONIC MACH NUMBERS		5. Report Date June 1983	
7. Author(s) A. B. Blair, Jr., Jerry M. Allen, and Gloria Hernandez		6. Performing Organization Code 505-43-23-02	
9. Performing Organization Name and Address NASA Langley Research Center Hampton, VA 23665		8. Performing Organization Report No. L-15586	
12. Sponsoring Agency Name and Address National Aeronautics and Space Administration Washington, DC 20546		10. Work Unit No.	
15. Supplementary Notes			
16. Abstract An experimental wind-tunnel investigation has been conducted at Mach numbers from 1.60 to 3.50 to obtain the longitudinal and lateral-directional aerodynamic characteristics of a circular, cruciform, canard-controlled missile with variations in tail-fin span. In addition, comparisons were made with the experimental aerodynamic characteristics using three missile aeroprediction programs: MISSILE1, MISSILE2, and NSWCDM. The results of the investigation indicate that for the test Mach number range, canard roll control at low angles of attack is feasible on tail-fin configurations with tail-to-canard span ratios of less than or equal to 0.75. The canards are effective pitch and yaw control devices on each tail-fin span configuration tested. Programs MISSILE1 and MISSILE2 provide very good predictions of longitudinal aerodynamic characteristics and fair predictions of lateral-directional aerodynamic characteristics at low angles of attack, with MISSILE2 predictions generally in better agreement with test data. Program NSWCDM provides good longitudinal and lateral-directional aerodynamic predictions that improve with increases in tail-fin span. Estimates of rolling-moment coefficient are in good agreement with test data at low angles of attack. Programs MISSILE1, MISSILE2, and NSWCDM appear to be acceptable engineering design tools for aeroprediction and, in general, make reasonable estimates of the test data; however, these programs need to be modified in order to better predict the lateral-directional aerodynamic characteristics at higher angles of attack (greater than 12°).			
17. Key Words (Suggested by Author(s)) Supersonic aerodynamics Missile aerodynamics Canard-controlled missiles Missile aeroprediction programs		18. Distribution Statement Unclassified - Unlimited	
Subject Category 02			
19. Security Classif. (of this report) Unclassified	20. Security Classif. (of this page) Unclassified	21. No. of Pages 84	22. Price A05

For sale by the National Technical Information Service, Springfield, Virginia 22161

NASA-Langley, 1983

National Aeronautics and
Space Administration

Washington, D.C.
20546

Official Business
Penalty for Private Use, \$300

THIRD-CLASS BULK RATE

Postage and Fees Paid
National Aeronautics and
Space Administration
NASA-451



2 1 10,A, 830624 500903DS
DEPT OF THE AIR FORCE
AF WEAPONS LABORATORY
ATTN: TECHNICAL LIBRARY (SJL)
KIRTLAND AFB NM 87117

NASA

S)

POSTMASTER: If Undeliverable (Section 158
Postal Manual) Do Not Return
